Bolted Joints Dynamic Simulation:

Improving the Computational Efficiency

by

Drithi Shetty

A dissertation submitted in partial fulfillment of the requirements for the degree of

DOCTOR OF PHILOSOPHY

(Mechanical Engineering)

at the

UNIVERSITY OF WISCONSIN-MADISON

2022

Date of final oral examination: 08/10/2022

The dissertation is approved by the following members of the Final Oral Committee:

Melih Eriten, Associate Professor, Mechanical Engineering
Matthew Allen, Professor, Mechanical Engineering, Brigham Young University
Dan Negrut, Professor, Mechanical Engineering
Jacob Notbohm, Assistant Professor, Engineering Physics
Daniel Segalman, Professor, Mechanical Engineering, Michigan State University
Ramathasan Thevamaran, Assistant Professor, Engineering Physics
Michael Zinn, Associate Professor, Mechanical Engineering

Abstract

Friction is ubiquitous and a significant source of nonlinearity in mechanical structures. Even before complete slip occurs, the edges of contact surfaces experience slip at the microscale when tangential loads are applied, due to non-uniform contact pressure. This impacts the macroscale dynamics of the system. While one could create a high-fidelity finite-element model to simulate the interfacial mechanics, the orders-of-magnitude difference in the length scales makes dynamic analyses of the FE model computationally expensive. An alternative is to replace the contact interface with a constitutive, hysteretic model capable of simulating the observed nonlinear dynamic behavior due to friction. In case of jointed structures, the focus of this dissertation, the nonlinear behavior is characterized by small changes in frequency and orders-of-magnitude shift in damping with respect to response amplitude. This work aims at improving the accuracy and computational efficiency of constitutive models for simulating the dynamics of jointed structures.

The first contribution of this dissertation is a novel integration approach for simulating the dynamic behavior of a commonly used hysteretic model, the four-parameter Iwan model. A quasi-linear form of the equation-of-motion is presented that can be integrated using explicit methods with larger time steps, resulting in faster dynamic simulations. The case studies included show that the proposed integration method solves the differential equations at a fraction of the computational cost, without significant loss of accuracy.

The second contribution is a parametric analysis of the amplitude-dependent frequency and damping behavior of another hysteretic model, known as the Bouc-Wen model. The

dynamic simulation of this model is known to be significantly faster than that of the Iwan model. However, existing literature does not analyze the Bouc-Wen model's ability to simulate power-law damping behavior that is characteristic of bolted joint dynamics. This dissertation shows the limitations of the Bouc-Wen model in simulating power-law damping at low amplitudes.

Thirdly, this dissertation includes a new, non-parametric form of the Iwan model that can directly be derived from quasi-static force-displacement data. This model form provides more flexibility in fitting the nonlinear hysteretic behavior compared to existing parametric Iwan models. Additionally, it does not utilize computationally intensive optimization schemes that are typically required to identify the parameters of the existing Iwan models. The dissertation includes two case studies analyzing the accuracy of the non-parametric Iwan model.

Thin panels are commonly used in the design of lightweight, high-speed structures that are assembled together using mechanical fasteners. These panels exhibit nonlinear behavior due to large deformations. The final contribution of this dissertation is a novel approach to predict the dynamic behavior of the mode of a structure that comprises both geometric and friction nonlinearity. This approach can be used to simulate the dynamic behavior of the nonlinear mode at a fraction of the computational cost of performing a finite-element analysis of a high-fidelity model. Two case studies highlighting the advantages and limitations of the approach have been presented.

Acknowledgments

Thank you to my advisor, Prof. Matt Allen, for being patient, supportive and available whenever needed.

Thank you to my Ph.D. committee for their time and valuable feedback on the dissertation materials.

Thank you to all my peers in the Structural Dynamics group over the past five years for their support, feedback, and for providing a collegial work environment.

Thank you to my family and friends for being very supportive and encouraging, despite not comprehending why it would take someone so long to figure out how bolts work :) I probably shouldn't tell them I have more questions now than I did when I started.

Part of this dissertation is based on work supported by the National Science Foundation under Grant No. CMMI-1561810. Any opinions, findings, and conclusions or recommendations expressed in this material are those of the author and do not necessarily reflect the views of the National Science Foundation.

Dissertation

This dissertation consists of an executive summary (Part I), and the following appended papers (Part II):

Paper I	D. Shetty, and M.S. Allen, "Fast Simulation of a Single Degree-of-Freedom System Consisting of An Iwan Element Using the Method of Averaging," in Journal of Vibration and Acoustics, 142(5), 2020.
Paper II	D. Shetty, and M.S. Allen, "A Parametric Study of the Bouc-Wen Model for Bolted Joint Dynamics," in Journal of Vibration and Acoustics (submitted, 2022).
Paper III	D. Shetty, and M.S. Allen, " Non-Parametric Iwan Model Derived from Quasi-Static Force-Displacement Data," in Journal of Vibration and Acoustics (in preparation).
Paper IV	D. Shetty, M.S. Allen, and K. Park, "A New Approach to Model a System with Both Friction and Geometric Nonlinearity", in Journal of Sound and Vibration (submitted, 2022).

Contents

Part I

Executive Summary

Chapter 1

Introduction and Motivation

Mechanical structures experience different forms of loads during their lifetime that they must be designed to withstand. Finite element analysis techniques are typically used to simulate the structure's response to different types and amplitudes of excitation. Most structures exhibit some form of nonlinearity due to different factors - material damping due to slip between the internal planes [1], bending-stretching coupling at large deformations [2, 3], frictional energy dissipation due to mechanical fasteners [4, 5], fluid-structure interactions [6], and so on. This work primarily focuses on the nonlinearity arising from friction due to fasteners. The industry standard is often to make linear approximations to create a computationally efficient finite element model. In case of bolted connections, the friction at the contact surfaces is ignored and the bolt is modeled as a high-stiffness linear spring that can approximate the dynamic behavior.

Such simplifications lead to conservative designs that can have consequences beyond just the life and performance of the system. For example, accounting for friction due to bolted connections in aircraft and spacecraft results in more lightweight and fuel-efficient designs. Consider the casing of a typical jet engine, held together using hundreds of bolts, as shown in Fig. 1.1. The casing is designed to fit closely to the turbine blades of the engine, with lower spacing resulting in higher fuel efficiency. On the other hand, the casing will vibrate with

large amplitudes at its natural frequencies and if this amplitude is not accurately controlled, it can result in erosion of the blades. Moreover, the rubbing can excite the modes of the blades causing them to fail. In a dynamic environment, the vibration amplitude of the casing is impacted by loss of energy due to friction at the interfaces that are bolted together. If this is accounted for, the fuel efficiency of the engine can be improved by designing for tighter tolerances. This makes it possible to create more lightweight aircraft designs. For every 100 kg of mass added to an aircraft, approximately 2.5 kg of additional aviation fuel is consumed per hour of flight [7] resulting in about 8 kg of additional CO_2 emissions per hour, or nearly 70 metric tons of CO_2 emissions per year. Thus, lightweight aircraft, designed as a result of accounting for the nonlinearity due to friction, can play a significant role in limiting CO_2 emissions. This applies to more than just airplanes; any built-up, fuel-powered structure that experiences dynamic loads, such as automobiles, drilling rigs and cargo ships, would benefit from an improved understanding of friction.

Figure 1.1: Turbine engine, consisting of different components fastened together using numerous bolts

Including the effect of contact when simulating the dynamics of any structure is expected to reduce the cost of prototyping and dynamic testing. One approach to do so could be to create a high-fidelity finite element (FE) model that can capture the dissipation of energy

at the interfaces and hence simulate the dynamic response of the structure [8, 9]. However, this method is limited by how accurately the chosen friction model emulates the specific interactions that would be observed experimentally. Friction is known to be notoriously difficult to accurately model and predict. One reason for this is the different phenomena that occur at various length scales. Interactions between the materials occur at the nanoscale, the effects of surface roughness are observed at the microscale, and all these phenomena affect the overall force and stresses in the structure at the macroscale. Additionally, many different mechanisms can be involved in interface interaction, such as plasticity, generation of heat, formation of new surfaces by breaking of bonds, and so on. The effect of these mechanisms is difficult to understand or quantify since they cannot be easily isolated. Some literature exists that tackles these challenges [10–13], and this is an area of active research that is gaining importance within the bolted joints community.

Moreover, there is orders-of-magnitude difference in the length scales associated with micro-level displacements occurring at the interacting surfaces and that of the whole model, which makes analysis of a high-fidelity FE model computationally expensive [14]. The contact pressure at the interface is not uniform, with higher pressure closer to the bolted joint and lower pressure further away [15]. Therefore, at lower amplitudes, the edges of the jointed surfaces slip while the region closer to the bolt hole remains mostly stuck. This is called microslip. Jewell et al. [9] observed that a very fine mesh is needed around the contact region to effectively capture microslip nonlinearity, as shown in Fig. 1.2.

An alternative is to replace the contact interface with a constitutive, reduced-order model that can simulate the dynamics that is characteristic of bolted joints. There are two interconnected quantities that are useful in characterizing bolted joint dynamics - the amplitude dependence of damping and stiffness, and the hysteretic nature of the force-displacement backbone curve. Both stiffness and energy dissipation (and hence damping) have been found to show amplitude-dependent behavior [16], that is the amount of slip that occurs is dependent on the amplitude of the force applied (illustrated in Fig. 1.3a, 1.3b). In the

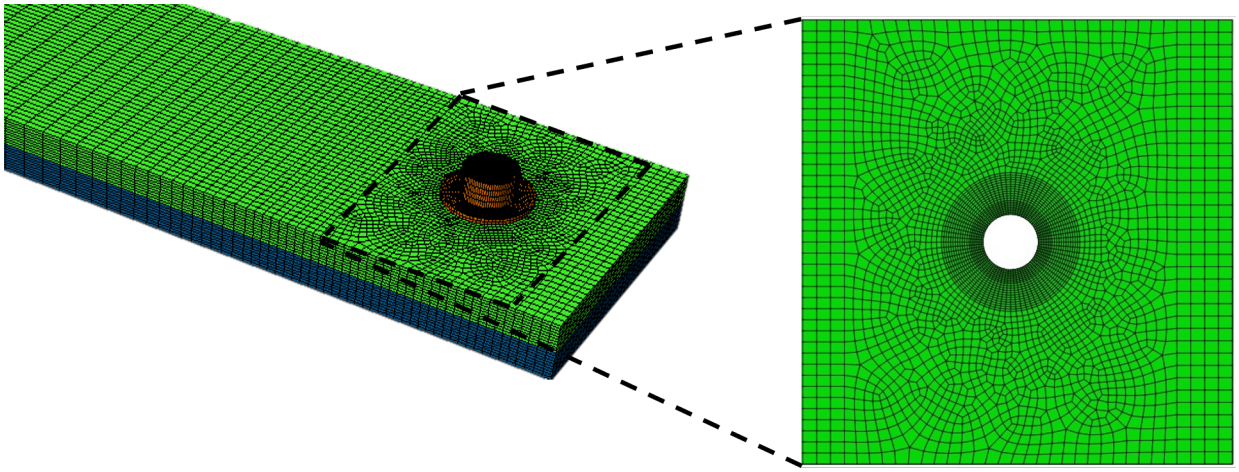

Figure 1.2: 3D beam assembly FE model with fine mesh around contact region to capture microslip [9]

microslip regime, the stiffness of the joint decreases slightly, whereas the damping increases by orders of magnitude [17], as seen in Fig. 1.3b. This behavior has been observed in numerous experimental studies [18–20]. The response of a structure at resonance, and, as a result, to random excitation, depends on the damping [21]. As the force amplitude increases, the slip region gradually expands until macroslip occurs, which is characterized by relative motion between the surfaces and significant decrease in joint stiffness. Apart from this, the force-displacement curve for frictional contact is hysteretic in nature, as seen in Fig. 1.3c. The area enclosed by the hysteresis loop equals the energy dissipated during the oscillation cycle and the slope of the hysteresis curve represents the varying stiffness of the system. Thus, the constitutive model must be able to accurately capture the hysteretic and amplitude-dependent behavior associated with friction at contact surfaces.

This dissertation focuses on improving the accuracy and computational efficiency of the dynamic simulation of jointed structures using constitutive hysteretic models. Two hysteretic models have been considered in this study - the Iwan model [22] and the Bouc-Wen model [23, 24]. The following section provides an overview of these models. There are different approaches available to incorporate the constitutive model into the analysis of the rest of the structure. Two main ones - the whole-joint modeling approach [16] and the

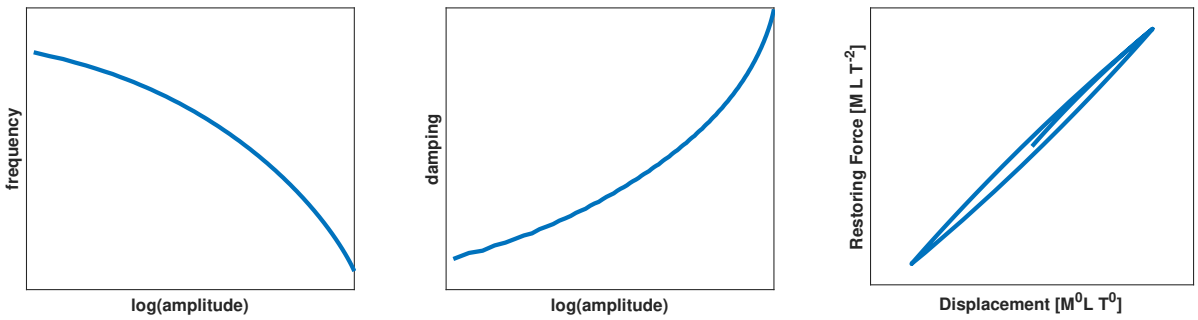

(a) (b) (c)

Figure 1.3: Example of (a) amplitude-dependent frequency, (b) amplitude-dependent damping and (c) hysteretic force-displacement relationship of bolted joints

modal modeling approach [25] are briefly discussed in Sec. 1.2. The modal modeling approach has been extensively used in this work due to the computational advantage it offers. Section 1.3 describes the method of quasi-static modal analysis (QSMA) that is commonly used to identify the parameters of constitutive models [26]. Lastly, many real-world structures, especially in the aircraft, spacecraft and automobile industries, consist of assemblies with thin, curved panels. Therefore, these structures exhibit geometric nonlinearity due to bending-stretching coupling of the panels as well as friction nonlinearity due to the mechanical fasteners holding the different parts together. Part of this dissertation presents a new reduced-order modeling approach to simulate such nonlinear systems using QSMA and the modal modeling approach. Section 1.4 provides an overview of the existing reduced-order models for geometrically nonlinear structures.

1.1 Hysteretic Models

Different constitutive hysteretic models have been developed for various nonlinear systems. The development of hysteretic models predates bolted joints research. In fact, some of the models used for bolts were originally developed for elastoplasticity [22, 27, 28]. Gaul and Nitsche [29] reviewed different friction models that could be used to describe joint dynamics. More recently, Mathis et al. [30] presented an extensive review of the different damping

models that can be used to simulate bolted joint structures and discussed the relation between them. The Iwan model [22] and the Bouc-Wen model [23] have been the main focus of this work.

The Distributed Element model [22,31] , or the Iwan model, is a lumped, hysteretic model that is widely popular in bolted joints research. It consists of an arrangement of linear spring and slider units. Two possible arrangements were studied by Iwan - the parallel-series arrangement and the series-parallel arrangement. The parallel-series arrangement consists of Jenkins elements (unit of spring and slider in series) that are arranged in parallel whereas the series-parallel arrangement consists of Prager elements (unit of spring and slider in parallel) that are arranged in series. Apart from this, Quinn and Segalman [32] also studied a series-series arrangement. The Iwan model was originally developed to characterize metal elastoplasticity. Researchers have since developed the Iwan model for bolted joints applications [33–35]. Of the different arrangements possible, the parallel-series Iwan model comprising Jenkins elements, illustrated in Fig. 1.4a, is most commonly used when modeling joints. Figure 1.4b shows the force-displacement relationship of a single Jenkins element, showing elastic-perfectly plastic behavior. Even though each element is bi-linear, the slider strength, written as f_i^*/N in the figure, of the Jenkins elements that constitute the Iwan model varies. This is similar to the edges of the contact slipping while the region close to the bolt remaining stuck in the microslip regime. As a result, the overall force-displacement relationship of the Iwan model is nonlinear in microslip. On the other hand, the system is in macroslip when all the sliders have slipped.

The constitutive form of the Iwan model is given by Eq. 1.1,

$$F_{\text{nl,Iwan}}(x,t,\phi) = \int_0^\infty \rho(\phi)[x(t) - u(t,\phi)]d\phi \tag{1.1}$$

where $F_{\text{nl,Iwan}}(x,t,\phi)$ is the nonlinear restoring force, $x(t)$ is the imposed displacement, $u(t)$ is the displacement of the Jenkins elements that constitute the Iwan joint, ϕ is the displacement

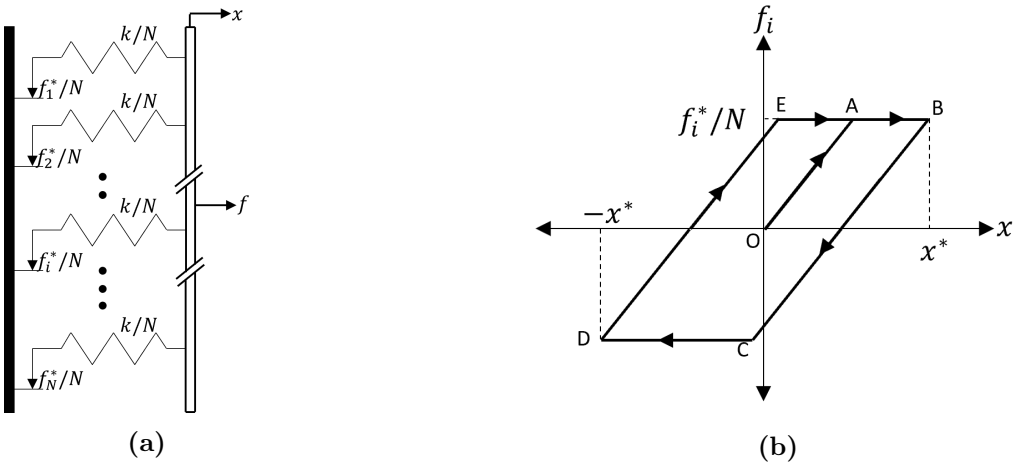

Figure 1.4: (a) Illustration of the parallel-series Iwan Model, and (b) The bi-linear force-displacement relationship of a Jenkins element

at which $\rho(\phi)$ number of sliders slip. Thus, $\rho(\phi)$, also referred to as the distribution function, can be understood as the population density of the sliders. The derivation for Eq. 1.1 can be found in [22]. The definition of the distribution function determines the nonlinear behavior of the Iwan model. Segalman's four-parameter Iwan model [35] is most prevalent in bolted joints research since it can effectively capture the power-law dissipation behavior - a behavior in which the log of the energy dissipated (or effective modal damping ratio) increases linearly with the log of the vibration amplitude, and the natural frequency of the system decreases with increase in response amplitude. Segalman used this experimental observation to define the distribution function as follows:

$$\rho(\phi) = R\phi^{\chi}[\mathrm{H}(\phi) - \mathrm{H}(\phi - \phi_{\max})] + S\delta(\phi - \phi_{\max}) \tag{1.2}$$

where $H(.)$ and $\delta(.)$ are Heaviside and Dirac-delta functions respectively.

Segalman's four-parameter model can thus be represented by the parameter set [$\phi_{\max}$, χ, R, S], where $\phi_{\max}$ is the displacement at which all sliders slip (i.e. macroslip occurs), χ is a dimensionless quantity that measures the power-law energy dissipation, and R and S can be understood as the stiffness of the power-law portion of the distribution and the

delta function portion of the distribution respectively. Since the parameters R and S have fractional dimension, Segalman proposed using another set of more intuitive parameters, $[F_{\mathrm{S}}, K_{\mathrm{T}}, \chi, \beta]$, with F_{S} being the force required to cause macroslip, K_{T} being the tangential stiffness of the joint at small applied loads, and χ and β being dimensionless parameters that measure the energy dissipation. It must be noted here that the parameter χ is identical in both parameter sets. Further details about the model formulation and conversion from one set of parameters to another can be found in [16].

There have been various adaptations of the four-parameter model. Brake [36] presented a reduced formulation of the Iwan model that makes it possible to derive an analytical expression for the nonlinear Iwan force. Mignolet et al. [37] presented a five-parameter Iwan-type model that uses the same distribution function as in Eq. 1.2 but included different coefficients of static and dynamic friction in the sliders. Lacayo and Allen [38], however, found that this model did not provide a significant advantage in estimating the amplitude-dependent frequency and damping. Li and Hao [39] proposed a six-parameter Iwan model with a distribution function having the same power-law form as the four-parameter model but consisting of two Dirac-delta functions instead of just one. The second Dirac-delta function results in a residual stiffness being added to the macroslip region of the backbone curve. Segalman also proposed adding a parameter to the four-parameter model that would replace the Dirac-delta function with a more gradual change in stiffness [30, 36]. However, this model has not yet been experimentally characterized.

A limitation of the Iwan model is that implicit integration schemes are required to simulate the dynamic behavior of this model, with the state of the sliders being evaluated at each time step. White the distribution of Jenkins elements is theoretically continuous, a discrete form of Eq. 1.2 is used for numerical integration, with 100 discretization points typically being a good approximation. The larger the number of discretization points, the greater the integration time is expected to be. Several implicit integration methods exist [40–43]. Of these, the Newmark-β method [40, 44] has been implemented in this work. Note that the

Hilber-Hughes-Taylor (HHT) method is an extension of the Newmark method that has the same order of accuracy with additional numerical dissipation. While there are applications in which the added high-frequency dissipation is desirable, the Newmark method has been used in this work to avoid contamination of the damping estimate due to numerical damping.

Another model that can capture hysteretic behavior is the Bouc-Wen model [23, 24, 45]. This formulation is intended for any form of hysteresis and was originally applied to force – deflection and flux– current diagrams of mechanical and ferromagnetic hysteresis. In particular, it has been used experimentally to model piezoelectric elements [46], magnetorheological dampers [47], wood joints [48] and so on.

The nonlinear restoring force due to the Bouc-Wen model is given as

$$F_{\text{nl,BW}}(x, z) = (1 - \alpha)K_0 z \tag{1.3}$$

where K_0 is the initial low-amplitude stiffness and α is defined as the ratio of the macroslip stiffness, K_∞, to the initial stiffness. The hysteretic state variable, $z(t)$ is defined by the following ODE:

$$\dot{z} = A\dot{x} - \beta|\dot{x}||z|^{n-1}z - \gamma\dot{x}|z|^n \tag{1.4}$$

where A, n, β and γ are the Bouc-Wen parameters that can be tuned to fit a force-displacement hysteresis loop. This formulation provides a computational advantage over the four-parameter Iwan model since the state variable is given by a nonlinear, first-order ODE that can easily and quickly be integrated using explicit ODE solvers. For $n = [1, 2]$, closed-form solutions for z can be obtained [45]. For non-integer values, however, no further simplifications to the ODE can be made. It is preferable to allow non-integer values of n so there is more flexibility when calibrating the model.

In the context of structural dynamics, the Bouc-Wen model is considered semi-physical in nature since unlike the spring-slider units in Iwan models, the state variable $z(t)$ does not have any known physical interpretation. Guo et al. [49] proposed an equivalent normal-

ized Bouc-Wen model with parameters that can be qualitatively linked to the shape of the hysteresis curve. The existing literature predominantly focuses on applying the Bouc-Wen model to capture the steady-state hysteretic behavior of various nonlinear systems [50–52].

1.2 Whole-Joint and Modal Modeling Approach

The hysteretic model can be incorporated into an FE model using the whole-joint modeling approach [16]. In this approach, each side of the contact interface is treated as rigid and all its nodes are tied together to a single representative node. The appropriate hysteretic model is then applied between the representative nodes of the surfaces in contact. Consider the FE model of a jointed structure with each bolted joint represented by a constitutive model. The resulting equation of motion (EoM) is given by Eq. 1.5,

$$\mathbf{M}\ddot{\mathbf{x}} + \mathbf{C}\dot{\mathbf{x}} + \mathbf{K}_{\infty}\mathbf{x} + \mathbf{f}_{\text{nl}}(x, t, h) = \mathbf{f}_{\text{ext}}(t) \tag{1.5}$$

where $\mathbf{M}$ is the mass matrix, $\mathbf{C}$ is the linear damping matrix, $\mathbf{K}_{\infty}$ is the linear stiffness matrix if all the joints were disconnected, and $\mathbf{f}_{\text{nl}}(x, t, h)$ is the vector of nonlinear joint forces given by a hysteretic model, that depend on the nodal displacement x, time t and previous state of the system h. The definition of h varies for different hysteretic models. For example, it corresponds to the slider state ϕ for the Iwan model and the hysteretic variable z for the Bouc-Wen model.

This approach is less computationally expensive that including a friction element between every pair on nodes in contact. However, the whole-joint model does have some drawbacks [25]. While this approach is computationally more efficient than creating a high-fidelity FE model, it is difficult to isolate the effect of each joint on the overall system dynamics. Therefore, computationally intensive optimization schemes are required to calibrate the constitutive models [53]. Firstly, as seen in section 1.1, the parameters of these constitutive models are not very intuitive. For example, the parameters $[A, \beta, \gamma]$ for the

Bouc-Wen model are chosen such that the model best fits experimental data, not based on any observable physics. Similar observations can be made about other semi-physical constitutive models. The parameters of the four-parameter Iwan model, on the other hand, are somewhat physical. For example, F_S is the force at which macroslip occurs, and so on. However, in a structure with multiple joints, it is difficult to isolate the effect each joint has on the overall system dynamics, making the estimation of these parameters non-trivial.

As an alternative, Segalman [25] proposed a modal modeling approach, where each nonlinear mode of the structure is represented by a single degree-of-freedom (SDOF) system with a parallel arrangement of a linear spring, linear damper and a nonlinear hysteretic element. This approach makes two important assumptions. Firstly, it assumes that there is no coupling, or energy transfer, between the modes. This assumption holds true if the external force results in excitation of a single, dominant mode. Eriten et al. [54] showed that in a weakly nonlinear structure, the interaction between modes is not significant if their natural frequencies, or harmonics of the frequencies, are sufficiently spaced. On the other hand, Moldenhauer et al. [55] and Wall et al. [56] showed the presence of modal coupling in two different jointed structures. Therefore, ther are limitations to the applicability of this method. In this paper, however, the modal modeling approach has been applied to a case that does not exhibit modal coupling. The second assumption is that the low-amplitude, linear mode shapes of the system are preserved and hence applicable in the amplitude range being analyzed. For weakly nonlinear structures like the ones under consideration, this is a reasonable assumption to make.

Under these assumptions, Eq. 1.5 is transformed to the modal domain using $\mathbf{x} = \mathbf{\Phi}_0\mathbf{q}$, where $\mathbf{\Phi}_0$ is the low-amplitude, linear mode shape matrix and $\mathbf{q}$ is the vector of modal displacements. If there is no modal coupling, the modal transformation results in the nonlinear joint force $\mathbf{f}_{\text{nl}}$ being projected onto each mode and being a function of the corresponding

modal displacement, i.e. $\mathbf{\Phi}_{0r}^T \mathbf{f}_{\text{nl}}(x,h) = \hat{f}_{\text{nl}}(q_r, \hat{h})$. As a result, Eq. 1.5 reduces to

$$\ddot{q}_r + 2\zeta_{0r}\omega_{0r}\dot{q} + \omega_{\infty r}^2 q + \hat{f}_{\text{nl}}(q_r, \hat{h}) = \mathbf{\Phi}_{0r}^T \mathbf{f}_{\text{ext}} \tag{1.6}$$

for the r^{th} mode. Here, ω_{0r} is the linear frequency of the r^{th} mode at low amplitudes, when there is no slip occurring, whereas $\omega_{\infty r}$ is the frequency at macroslip. It is also assumed that the modal transformation results in a diagonal linear damping matrix, with ζ_{0r} being the low-amplitude damping ratio of the r^{th} mode. Each nonlinear mode can be independently analyzed using a suitable hysteretic model to represent the modal joint force, $\hat{f}_{\text{nl}}(q_r, h)$. Figure 1.5 provides a schematic of the modal model.

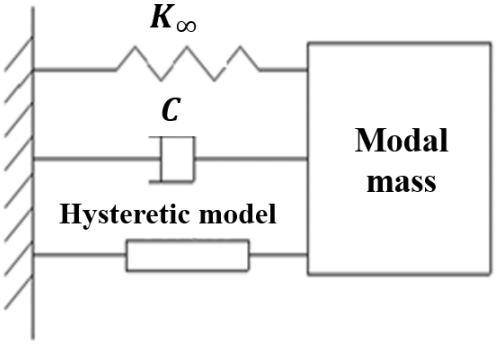

Figure 1.5: Modal model: SDOF system with a linear spring, damper and nonlinear element in parallel

Modal models significantly reduce the computation cost of dynamic simulations. Deaner et al. [19] and Roettgen and Allen [20] showed that the modal Iwan model is capable of describing the nonlinearity in various bolted structures. Further, Lacayo et al. [57] found that this approach can accurately capture the nonlinear response to an impulse-type excitation (that excites different modes of the structure to varying extents) if it consists of one dominant mode, and may still be fairly acceptable in cases of more than one dominant mode, provided the mode being studied is a dominant one.

1.3 Overview of Quasi-Static Modal Analysis

The force-displacement hysteresis loop is required to estimate the parameters of the constitutive model being used. In the modal modeling approach, this would be the hysteresis loop of the nonlinear mode of the structure that is being analyzed. Various quasi-static methods have been developed for estimating the force-displacement data. In these methods, quasi-static simulations are performed on the high-fidelity FE model to extract the force-displacement relationship. Since quasi-static simulations are significantly faster than dynamic analyses, such methods are computationally feasible.

Festjens et al. [58] presented a method to study the nonlinearity due to bolted joints, in which a quasi-static distributed load was applied such that it represented the inertial loading when the structure vibrates in the mode of interest. The corresponding displacement can then be calculated using any finite element package. This was done over a range of load amplitudes to obtain the force-displacement curve. While Festjens et al. allowed the change of mode shapes in the nonlinear domain of the structure (i.e. near the bolted joints), Lacayo and Allen [26] proposed a simplification where they assumed the linear mode shape to be valid over the entire structure. This is called the method of Quasi-Static Modal Analysis, or QSMA. Its efficacy has been tested on various systems consisting of friction nonlinearity [12,59,60]. Further, Park and Allen [61] showed how QSMA could be successfully applied to estimate the force-displacement relationship for the nonlinear mode of a structure with geometric nonlinearity. Balaji and Brake [62] proposed a variation of QSMA, known as Rayleigh-Quotient based Nonlinear Modal Analysis (RQNMA), where they extended the concept of Rayleigh quotients to both conservative and non-conservative nonlinear systems, updating the mode shapes, and hence the applied static load, at each amplitude level. In this work, the method of QSMA presented by Lacayo and Allen [26] has been used.

To understand how the method of QSMA is applied, consider the FE model of a structure, the Equations of Motion (EoM) for which can be given by Eq. 1.5. The equations can be linearized about some state of interest, to capture the behavior for small vibrations about

that state. Without loss of generality, the equations above are assumed to be linearized about $x = 0$ to estimate the low-amplitude modal frequencies, $\boldsymbol{\omega}_0$, and linear mode-shapes, $\boldsymbol{\Phi}$, by performing an eigen-value analysis. Then, a static load is applied such that it excites only the r^{th} mode of the system. The applied load must be $f_{\text{ext}} = \mathbf{M}\boldsymbol{\Phi}_r$, where $\boldsymbol{\Phi}_r$ is the low-amplitude linear mode shape of the r^{th} mode of interest [26]. This results in the following quasi-static problem:

$$\mathbf{K}\mathbf{x} + \mathbf{f}_{\text{nl}}(\mathbf{x}, \mathbf{h}) = \boldsymbol{\alpha}\mathbf{M}\boldsymbol{\Phi}_\mathbf{r}. \tag{1.7}$$

Equation 1.7 can be solved to obtain $\mathbf{x}$ for different force amplitude levels, $\boldsymbol{\alpha}$. Typically, the structure starts in equilibrium and $\boldsymbol{\alpha}$ is chosen to be monotonically increasing. This gives the initial loading behavior, also known as the backbone curve. To compute the full hysteresis loop, the initial loading is followed by unloading to the negative maximum amplitude and then reloading back to the positive maximum amplitude. Now, to retrieve the force-displacement relation of the r^{th} mode, the force applied to the structure and the displacement calculated need to be converted from the physical to the modal domain, using Eqs. 1.8 and 1.9.

$$\mathbf{f}_{\text{modal}} = \boldsymbol{\Phi}_r^{\text{T}}\boldsymbol{\alpha}\mathbf{M}\boldsymbol{\Phi}_r = \boldsymbol{\alpha} \tag{1.8}$$

$$q_r(\alpha) = \boldsymbol{\Phi}_r^T\mathbf{M}x(\alpha) \tag{1.9}$$

In this way, the force-displacement relation for the nonlinear mode of a structure, α versus $q_r(\alpha)$, can be calculated by solving a quasi-static problem.

1.4 Redued-order Models for Geometric Nonlinearity

Simulating the dynamic response of a geometrically nonlinear structure using a high-fidelity Finite Element (FE) model is highly computationally expensive. Therefore, several reduced-order models have been developed as an alternative. A reduced-order model equation of motion for geometric nonlinearity will typically contain linear mass and stiffness terms along

with additional higher-order polynomial stiffness terms, usually limited to quadratic and cubic terms. The polynomial coefficients can be estimated using static nonlinear solutions, as described in [63]. The methods that use static solutions can be classified as indirect, or non-intrusive evaluation methods, since they do not require manipulation of the nonlinear stiffness matrices in the FE package [64, 65]. Murayov and Rizzi [66] developed one such method, known as the Enforced Displacement (ED) procedure. Here, the nonlinear FE model is constrained to take the shape of the linear mode of interest, and the reaction forces needed to do so are calculated by a static analysis. This is done over a range of displacement amplitudes, with the resultant force-displacement backbone curve being used to estimate the polynomial coefficients. In this method, both bending and stretching (i.e. axial or dual [64]) modes need to be included when defining the modal basis in order to capture the bending-stretching coupling. Alternatively, McEwan et al. [67] presented the Implicit Condensation (IC) method where a static force is applied in the shape of the mode of interest and the resulting displacement field is estimated using the nonlinear FE model. The displacement data is transformed from the physical to the modal space. Similar to the ED method, this can be done over a range of force amplitudes to estimate the nonlinear coefficients. In the IC method, however, the bending-stretching coupling is implicitly captured by applying a force instead of displacement. Thus, the axial modes do not need to be included in the basis. Hollkamp and Gordon [68] presented the Implicit Condensation and Expansion (ICE) method to recover the axial displacements or the corresponding stresses from the IC method. In both the ED and ICE methods, multiple modes can be considered simultaneously to account for modal coupling. Park and Allen [61] presented a single degree-of freedom ICE method, dubbed the SICE-ROM, where the nonlinear restoring force is approximated by a single, dominant mode. This ROM requires polynomial terms higher than just the third order, presumably to capture quasi-static coupling between the mode under consideration and all other modes. Park and Allen showed that the dynamics near a single mode of strongly nonlinear structures can often be represented by the SICE-ROM with minimal loss

of accuracy.

The undamped SDOF EoM of the r^{th} mode was assumed to have the following form,

$$\ddot{q}_r + \omega_r^2 q_r + \theta_{\text{gnl}}(q_r) = \mathbf{\Phi}_r^{\text{T}} \mathbf{f}_{\text{ext}} \tag{1.10}$$

where $\theta_{\text{gnl}}(q_r)$ is the nonlinear restoring force approximated by the r^{th} mode only. This restoring force can be obtained from the quasi-static solution calculated using QSMA, described in Sec. 1.3. Next, a polynomial can be used to approximate this restoring force function, given by Eq. 1.11,

$$\theta_{\text{gnl}}(q_r) = \sum_{j=2}^{m} k_j q_r^j, \tag{1.11}$$

where k_j is the j^{th} nonlinear stiffness coefficient and m is the highest order of the polynomial. Higher order polynomials are required for modes that exhibit strong static coupling. The coefficients, k_j, can be estimated from the quasi-static force-displacement data by applying the method of least squares, as elaborated in [61]. This approach minimizes the cost function, J, given by Eq. 1.12,

$$\min_{k_j} J = \frac{1}{S} \sum_{l=1}^{S} \frac{\left(\omega_r^2 q_{r,l} + \sum_{j=2}^{m} k_j (q_{r,l})^j - \alpha_l\right)^2}{\alpha_l^2} \tag{1.12}$$

where S is the number of sample points in the QSMA analysis, i.e. the length of the vector α. The resulting ROM is called the Single degree-of-freedom Implicit Condensation and Expansion, or SICE-ROM. Park and Allen also showed three different case studies, where the SICE-ROM was used to successfully characterize the geometric nonlinearity of structures with varying complexity, thus verifying the method's capabilities. It must be noted that this ROM only accounts for static coupling between modes. In case of dynamic coupling, the SICE-ROM is unable to simulate the dynamic response accurately even when higher-order polynomials are used. In such a case the single-mode quasi-static backbone curve cannot be used to accurately predict the dynamic response.

Nonlinear normal modes (NNMs) are commonly used to represent how the resonant frequencies and mode shapes change as a function of amplitude in a strongly nonlinear system (such as due to geometric nonlinearity) [69]. NNMs can be understood as an extension of linear normal modes to nonlinear systems. They can be determined experimentally [70, 71] or computed efficiently for the ROMs [72] of the nonlinear system of interest. Thus, NNMs can be used to characterize the amplitude (or energy) dependent frequency behavior of the geometrically nonlinear system using the ROM that has been fit to its backbone curve.

Chapter 2

Scope of the Dissertation

2.1 Paper I: Fast Simulation of a Single Degree-of-Freedom system consisting of an Iwan Element using the Method of Averaging

This paper presents a new method to simulate the dynamic response of an SDOF system (or the nonlinear mode of a system) consisting of the four-parameter Iwan model. Taking advantage of the weakly nonlinear behavior of the Iwan model, its EoM is written in quasi-linear form, where the frequency and damping are functions of the response amplitude that is assumed to be constant at each vibration cycle. Closed-form expressions for the amplitude-dependent frequency and damping that are applicable in the microslip regime are used. The resulting ODE can be solved using explicit solvers such as the Runge-Kutta methods. On the other hand, the original EOM of the Iwan model uses implicit integration schemes since the past state of the sliders is required to calculate their current state. The paper shows that the proposed integration method is much faster since it requires fewer times steps. When the external force on the system goes to zero, the simulation speed is further improved by changing the state variables from the fast–varying displacement and velocity to the slowly–

varying amplitude and phase of oscillation. Since the amplitude and phase vary slowly, even fewer time steps are required to simulate the response.

The paper presents two different case studies. First, an SDOF system with an Iwan element is considered. The integration algorithm is used to simulate the response to three different types of excitation - an impulse, a sine beat, and a bandlimited random force. The Newmark-β integration method is used as a benchmark for comparison. The proposed algorithm gives accurate results for all three force inputs at a fraction of the computational effort required by the Newmark-β method. Next, a modal model of a jointed benchmark structure is considered. In this case, too, the proposed method gives results that closely match the Newmark-β solution. They both show some deviation from the whole-joint modeling approach. This can be attributed to inaccuracies in the modal Iwan model and not due to the integration approach used.

2.2 Paper II: A Parametric Study of the Bouc-Wen Model for Bolted Joint Dynamics

Existing literature shows the applicability of the Bouc-Wen model in simulating steady-state hysteretic behavior of nonlinear systems. However, the nonlinearity in bolted joints is also characterized by the amplitude-dependent frequency and damping behavior, specifically the power-law dissipation in the microslip regime. This paper studies the ability of the Bouc-Wen model to capture this amplitude-dependent behavior by comparing it with the four-parameter modal Iwan model. A method to identify the Bouc-Wen parameters that best fit the hysteresis loop from an Iwan model is presented. Then, the nonlinear frequency and damping are estimated by simulating the response of the model to an impulsive force.

The paper shows that the Bouc-Wen parameter n, the exponent term in the nonlinear ODE of the model, affects the amplitude-dependent frequency and damping estimated by the model, even though it does not significantly affect the hysteretic behavior. Additionally,

a single Bouc-Wen model cannot be used to characterize both microslip and macroslip level behavior. The paper also studies the effect of each Bouc-Wen parameter on the overall nonlinear damping. It shows that none of the Bouc-Wen model parameters can capture the microslip level power-law dissipation behavior associated with bolted joint nonlinearity. The parameter β causes the damping curve to shift vertically upwards, while increasing n results in a horizontal shift. On the other hand, the parameter γ changes the slope of the curve near macroslip. However, the damping at lower-amplitudes remains largely unaffected. Thus, the Bouc-Wen model may not be suitable for simulating the power-law dissipation observed in the microslip regime in jointed structures.

2.3 Paper III: A Non-Parametric Iwan Model Derived from Quasi-Static Force-Displacement Data

This paper proposes a new, non-parametric form of the Iwan model that can be used to simulate the dynamic response of a nonlinear mode of a jointed structure. QSMA is used to estimate the force-displacement backbone curve of the nonlinear mode of interest. The distribution function of the Iwan model can then be obtained directly from the backbone curve by calculating the second derivative of the force as a function of the displacement, using a method described in the paper. The distribution function is calculated in discrete form as opposed to a continuous function form. Thus, the model obtained is not limited to a finite set of parameters. This provides more flexibility in capturing the hysteretic behavior. Moreover, it eliminates the need for expensive optimization schemes typically used to identify the parameters.

Two case studies have been presented in the paper. First, a 2D FE model of two cantilever beams with a single bolt at the free end is considered. In the second case study, the cantilever beam assembly is modified to include two bolts with different preload at the free end. The paper shows that the non-parametric Iwan model is able to capture the observed interface slip

behavior better than existing parametric Iwan models. The amplitude-dependent behavior also closely matches the results obtained by simulating the full FE model.

2.4 Paper IV: A New Approach to Model a System with Both Friction and Geometric Nonlinearity

This paper presents a novel reduced-order modeling approach to predict the amplitude-dependent frequency and damping of a system comprising both geometric and friction nonlinearity. A new ROM, referred to here as the Iwan Model with Geometric Nonlinearity, or the IGNL model, is presented. It consists of the conventional Iwan model, with an added element that is composed of a slider of infinite strength and nonlinear spring. The spring corresponds to a SICE-ROM that represents the geometric nonlinearity of the system, while the Iwan model captures the hysteretic behavior. The paper also shows how the IGNL model for a nonlinear mode can be identified using QSMA. Two case studies testing the effectiveness of the proposed modeling approach have also been included.

For the numerical case study of an SDOF system with a cubic spring and Iwan element in parallel, the proposed approach estimates the frequency and damping at an acceptable level of accuracy, and is nearly 30 times faster than simulating the dynamic response of the system. The computational efficiency of the model is even more beneficial when analyzing more complex FE models, such as the second case study of a benchmark structure comprising a curved panel clamped at the ends using bolts. However, as shown in the paper, the hysteretic behavior of the nonlinear mode being studied must obey Masing's rules for the proposed approach to be accurate.

Chapter 3

Concluding Remarks and Future Work

This dissertation presented numerical methods to improve the speed and accuracy of the nonlinear dynamic simulation of built-up structures using hysteretic models. A novel approach to speed up the numerical integration of the four-parameter Iwan model, most commonly used to simulate the microslip-level behavior of joints was presented. Parametric studies performed on another hysteretic model, the Bouc-Wen model, showed the limitations of this model in simulating power-law dissipation behavior. This work also presented a new, non-parametric form of the Iwan model that is more accurate in capturing the slip behavior at the contact interface than the existing parametric Iwan models. Finally, the Iwan model with geometric nonlinearity, or the IGNL model, was developed to predict the dynamic behavior of a structure with both geometric and joint nonlinearity.

While significant work has been done to advance constitutive modeling of bolted joints, the numerical methods presented make certain approximations due to the existing limitations in the understanding of joint dynamics. The methods presented rely on the modes of the structure being uncoupled. This may not always be the case, as has been observed experimentally [55,56]. While there has been some effort to characterize modal coupling [73], it is a

complex phenomenon that is not yet well understood. Additionally, the models presented are phenomenological in nature. This means that they simulate the overall nonlinear dynamics of the behavior without a clear understanding of the various physical phenomena occurring at the different length scales. Therefore, the accuracy of the model depends on the method used to identify it. Using an FE model to identify the hysteretic model, as shown in this work, gives a priori estimates of the nonlinear dynamics. However, the accuracy of the results is limited by the level of detail of the FE model used. Factors such as lubrication, residual stresses, topology and surface roughness can impact the dynamic behavior due to friction, but cannot be accurately estimated without experimentation. Experimental data can be used to update the constitutive model parameters and improve the accuracy of the ROM for further dynamic simulations. However, doing so results in added cost of prototyping and experimentation. To create a truly predictive model, a multiscale and multidisciplinary approach needs to be considered that bridges the gap between phenomenological and physical models.

The lumped hysteretic model provides a more realistic estimate of the dynamic behavior of jointed structures than approximating the joint as a linear spring. Moreover, it does so at a lower computational cost than analyzing high-fidelity FE models for different types of excitation. However, the reliance on uncertainty quantification and on model updating through experimentation indicates that further research is needed to improve the accuracy of friction prediction.

Part II

Appended Papers I–IV

Paper I: Fast Simulation of a Single Degree-of-Freedom System Consisting of an Iwan Element using the Method of Averaging

While Iwan elements have been used to effectively model the stiffness and energy dissipation in bolted joints, integrating the equations of motion of these elements is fairly expensive since implicit schemes, such as Newmark's methods, need to be used. This paper presents a method of simulating dynamic systems containing nonlinear Iwan elements that significantly reduces the computation cost by using closed form expressions for stiffness and damping in the microslip regime and an averaging method for regions of time in which no external force is applied. The proposed algorithm is demonstrated on a single degree-of-freedom (SDOF) system to evaluate the range over which it retains accuracy and the improvement in performance it offers. Although the current implementation is limited to SDOF systems, it can be used to simulate the response of each mode in structures exhibiting weak nonlinearity that can be modeled using the modal Iwan approach. To verify this, the dynamic response of a finite element model of a beam assembly, integrated using the Newmark-β method, has been compared with its equivalent modal model integrated using the proposed algorithm. The results show that the algorithm accurately predicts the response in a fraction of the time taken by implicit integration schemes, so long as the modes remain uncoupled and weakly nonlinear.

1 Introduction

Mechanical fasteners have long been known to be a source of stiffness and energy dissipation in built-up structures [5,15]. Bolted joints allow slip between contact interfaces, which leads to frictional energy dissipation and changes in stiffness. Both stiffness and energy dissipation (and hence damping) have been found to show amplitude-dependent behavior [16], that is the amount of slip that occurs is dependent on the amplitude of the force applied. At lower amplitudes, the edges of the joint surfaces slip while a majority of the joint remains clamped due to the bolt pre-load. This is known as microslip. In the microslip regime, the stiffness of the joint decreases only slightly with increase in vibration amplitude, but there is significant energy loss which leads to a large increase in damping. This behavior has been observed in numerous experimental studies [18–20]. As the force amplitude increases, the slip region gradually expands until macroslip occurs, which is characterized by relative motion between the surfaces and significant decrease in joint stiffness. Joints are typically designed to maintain their integrity and are hence expected to predominantly show microslip behavior in most realistic structures. In fact, Deaner et al. [19] experimentally observed that very high force levels are required to cause a bolted structure to go into macroslip, making it difficult to even fully characterize this behavior, unless the bolt torques were unrealistically low.

Modeling the above-explained phenomena in detail would make dynamic analysis highly computationally expensive. An alternative is to replace the contact interface with a lumped, hysteretic model capable of simulating the microslip and macroslip behavior observed. One such model is the Iwan model [22], initially used for metal elasto-plasticity. The Iwan model consists of a parallel system of spring-slider units known as Jenkins elements. There have been many adaptations of the Iwan model to capture joint mechanics. The most widely used among them is Segalman's four-parameter Iwan model [35], with the four parameters accounting for the joint stiffness, the macroslip force, the transition to macroslip, and the power law energy dissipation that many joints have been found to exhibit in microslip.

While this is less expensive than modeling the contact in detail, the computational burden is significant in structures with multiple joints or when performing parametric studies. As an alternative, Segalman [25] proposed a modal approach, stating that each nonlinear mode can be represented as an SDOF system with an Iwan element to account for the nonlinearity, provided the modes are uncoupled and weakly nonlinear. Deaner et al. [19] and Roettgen and Allen [20] showed that the modal Iwan model is capable of describing the nonlinearity in various bolted structures. Further, Lacayo et al. [57] found that this approach can accurately capture the nonlinear response to an impulse-type excitation (that excites different modes of the structure to varying extents) if it consists of one dominant mode, and may still be fairly acceptable in cases of more than one dominant mode, provided the mode being studied is a dominant one.

While these developments have helped speed up nonlinear dynamic response analysis, one bottleneck that remains is the time integration. Currently, implicit numerical integration techniques like Newmark's methods need to be used with Newton-Raphson iteration schemes to account for the nonlinear force in the Iwan model. These methods are robust and effective but require a small time step, making the integration computationally expensive. In an effort to reduce integration costs, Brake [36] presented a reduced formulation of the Iwan model that makes it possible to derive an analytical expression for the nonlinear Iwan force. This paper presents another alternative that exploits the weakly nonlinear behavior of bolted joints in the microslip regime to significantly speed up the integration. Using the modal Iwan approach [25], the response of the uncoupled modes can be computed using closed-form expressions for the energy dissipation and joint stiffness, applicable in the microslip regime. Additionally, the averaging method can be used, taking advantage of the fact that the amplitude and phase of the decaying response vary slowly with time in comparison to the response itself [74]. The simulation method presented in this paper also provides the benefit of calculating the amplitude-dependent damping and natural frequency of the system in the course of the time integration, without requiring further post-processing (like the Hilbert

transform [75]). Krack et al. [76] presented a similar approach to compute the steady-state and unsteady dynamics of nonlinear modes in the absence of modal interactions. They used a multi-harmonic analysis to numerically compute the amplitude-dependent characteristics of the nonlinear mode of interest, applying the method of averaging to compute the slow dynamics of the system. The present paper proposes a quasi-linear approach in which the response is assumed to be monoharmonic, and the amplitude-dependent damping and natural frequency are calculated using analytical expressions specifically applicable to Iwan elements.

The following section of the paper gives an overview of the four-parameter Iwan model, highlights the drawbacks of the Newmark-β method [44] and explains the theory behind the alternative integration algorithm proposed. This is followed by examining it's applicability to an SDOF system with three types of input force - an impulse, a sine beat and a bandlimited random input. Next, to test the algorithm on a more realistic structure, a test case of a finite element model of two beams bolted together, commonly referred to as the Sumali beam, is presented. The response obtained using the proposed algorithm with a modal Iwan model is compared with that obtained by numerically integrating the finite element model. The algorithm is shown to be fairly accurate and much faster than the Newmark-β method.

2 Theoretical Background

2.1 Overview of the four-parameter Iwan model

The Iwan model [22] consists of a parallel arrangement of springs and sliders connected in series, known as Jenkins elements. The constitutive form of the model is given by Eq. 1,

$$F_{\mathrm{nl}}(t) = \int_0^\infty \rho(\phi)[x(t) - u(t,\phi)]d\phi \tag{1}$$

where $x(t)$ is the imposed displacement, $u(t)$ is the displacement of the Jenkins elements that constitute the Iwan joint, ϕ is the displacement at which $\rho(\phi)$ number of sliders slip. Thus,

$\rho(\phi)$ can be understood as the population density of the sliders. Segalman [35] proposed a power-law population distribution, given by Eq. 2.

$$\rho(\phi) = R\phi^{\chi}[\mathrm{H}(\phi) - \mathrm{H}(\phi - \phi_{\max})] + S\delta(\phi - \phi_{\max}) \tag{2}$$

Segalman's four-parameter model can thus be represented by the parameter set [$\phi_{\max}$, χ, R, S],where $\phi_{\max}$ is the displacement at which all sliders slip (i.e. macroslip occurs), χ is a dimensionless quantity that measures the power-law energy dissipation, and R and S can be understood as the stiffness of the power-law portion of the distribution and the delta function portion of the distribution respectively. Since the parameters R and S have fractional dimension, Segalman proposed using another set of more intuitive parameters, $[F_{\mathrm{S}}, K_{\mathrm{T}}, \chi, \beta]$, with F_{S} being the force required to cause macroslip, K_{T} being the tangential stiffness of the joint at small applied loads, and χ and β being dimensionless parameters that measure the energy dissipation. It must be noted here that the parameter χ is identical in both parameter sets. Further details about the model formulation and conversion from one set of parameters to another can be found in [16].

2.2 Numerical integration using the Newmark-β method

An SDOF system with a single Iwan element has an equation of motion given by Eq. 3,

$$m\ddot{x} + C_{\mathrm{lin}}\dot{x} + K_{\infty}x + F_{\mathrm{nl}}(t) = F_{\mathrm{ext}}(t) \tag{3}$$

where C_{lin} is the linear damping coefficient, K_{∞} is the stiffness of the system when the response amplitude is high enough to cause macroslip in the Iwan element, and $F_{\mathrm{nl}}(t)$ is the nonlinear force due to the Iwan element, given by Eq. 1. As seen in Eq. 1, the distribution of Jenkins elements is theoretically continuous. However, to numerically evaluate the same, the equation is discretized, with 100 sliders typically being a good approximation. The discretization procedure has been explained in [35].

Equation 3 can be integrated using the Newmark-β method derived in [44]. In this method, at every time step, the initial guess for acceleration equals the acceleration corresponding to the previous time step, as shown in Eq. 4. An initial estimate for velocity and displacement can then be obtained using Eqs. 5 and 6,

$$\ddot{x}_{n+1} = \ddot{x}_n \tag{4}$$

$$\dot{x}_{n+1} = \dot{x}_n + \triangle t[\gamma_{\text{nb}}\, \ddot{x}_{n+1} + (1 - \gamma_{\text{nb}})\ddot{x}_n] \tag{5}$$

$$x_{n+1} = x_n + \triangle t\dot{x}_n + \frac{\triangle t^2}{2}[2\beta_{\text{nb}}\, \ddot{x}_{n+1} + (1 - 2\beta_{\text{nb}})\ddot{x}_n] \tag{6}$$

where $(n + 1)$ represents the current time step, n represents the previous time step and $\triangle t$ is the step size. This is an implicit technique, i.e. the state variables, x and $\dot{x}$, depend not only on historical information but also on the current estimate of the variable $\ddot{x}$. Hence, a Newton-Raphson iteration scheme is used to converge on a solution for each time step. The residue function, η_{NR}, for the Newton-Raphson method, given by Eq. 7, is obtained by substituting Eqs. 4-6 in Eq. 3.

$$\eta_{\text{NR}} = m\ddot{x}_{n+1} + C_{\text{lin}}\dot{x}_{n+1} + K_\infty x_{n+1} + F_{\text{nl}}(x_{n+1}, \phi_{n+1}) - F_{\text{ext}}(t_{n+1}) \tag{7}$$

The nonlinear joint force and the corresponding nonlinear tangential stiffness K_{nl}, which depend on the current displacement and state of the sliders, are calculated for every iteration. Since $\dot{x}_{n+1}$ and x_{n+1} in Eq. 7 depend on $\ddot{x}_{n+1}$, the gradient, θ_{NR}, obtained by taking the partial derivative of Eq. 7 with respect to $\ddot{x}_{n+1}$, is given by

$$\theta_{\text{NR}} = m + C_{\text{lin}}\gamma_{\text{nb}}\triangle t + [K_\infty + K_{\text{nl}}]\beta_{\text{nb}}(\triangle t)^2 \tag{8}$$

The variable $\ddot{x}_{n+1}$ is iterated upon until the convergence tolerance ϵ_{NR}, given by Eq. 9, is below a pre-defined value. A very low convergence tolerance of $\epsilon_{\text{NR}} = 10^{-15}$ was chosen for

the presented studies, the reason behind which will be discussed in Section 3.1.1.

$$\epsilon_{\mathrm{NR}} = \frac{\eta_{\mathrm{NR}}^2}{|C_{\mathrm{lin}}\dot{x}_{n+1} + K_\infty x_{n+1}|^2} \tag{9}$$

Once the Newton-Raphson algorithm converges and the corresponding velocity and displacement for a particular time step are calculated using Eqs. 5 and 6, the algorithm marches forward in time.

Either a constant or linear acceleration can be assumed between time steps. The value of β_{nb} and γ_{nb} depend on the acceleration method used. In the constant acceleration method, $\beta_{\mathrm{nb}} = 1/4$ and $\gamma_{\mathrm{nb}} = 1/2$ whereas in the linear acceleration method, $\beta_{\mathrm{nb}} = 1/6$ and $\gamma_{\mathrm{nb}} = 1/2$. Since the constant acceleration method assumes that the acceleration remains constant within an integration step, a small step size is required to obtain an accurate solution [44]. A step size 200 times smaller than the shortest period was required in prior works [19, 20]. Thus, this method can be time consuming and warrants a more efficient approach.

2.3 Proposed alternative: Using closed-form expressions for the nonlinear parameters

Even though the Iwan element is complicated and can be rigorously modeled as given above, in the microslip regime, the weakly nonlinear behavior of the system can be taken advantage of. The damping and stiffness change slowly with response amplitude in a power-law fashion, as observed experimentally [21, 77].

The alternative approach presented here is to modify the equation of motion to be of the form as in Eq. 10, where the natural frequency, ω_{n}, and the damping, ζ, of the system are expressed as functions of the amplitude of the response, referred to as X.

$$\ddot{x} + 2\zeta(X)\omega_{\mathrm{n}}(X)\dot{x} + \omega_{\mathrm{n}}(X)^2 x = \frac{F_{\mathrm{ext}}}{m} \tag{10}$$

To solve this modified equation of motion, closed form expressions derived by Segalman [35] for the dissipation per cycle, $D(X)$, and the joint stiffness, $K_{\mathrm{j}}(X)$, (i.e. Eqs. 11 and 12) that are applicable in the microslip regime, are used,

$$D(X) = \frac{4RX^{\chi+3}}{(\chi+3)(\chi+2)} \tag{11}$$

$$K_{\mathrm{j}}(X) = K_{\mathrm{T}}\left[1 - \frac{r^{\chi+1}}{(\chi+2)(\beta+1)}\right] \tag{12}$$

where $r = X/\phi_{\max}$. The damping and natural frequency can then be calculated using Eqs. 13 and 14,

$$\zeta(X) = \zeta_{\mathrm{lin}} + \frac{D(X)}{2\pi m[\omega_{\mathrm{n}}(X)]^2 X^2} \tag{13}$$

$$\omega_{\mathrm{n}}(X) = \sqrt{\frac{K_{\mathrm{j}}(X) + K_{\infty}}{m}} \tag{14}$$

where ζ_{lin} is the linear damping ratio and K_{∞} is the linear, macroslip stiffness.

What remains is a nonlinear, second-order ordinary differential equation (ODE) with inhomogeneity due to the forcing function, which can be integrated using the fourth-order adaptive Runge-Kutta (RK) method. This requires that the ODE be defined in the form $\dot{x} = f(x,t)$ with the initial conditions provided as input. It is important to note that the traditional Iwan element cannot be integrated using Runge-Kutta, because it is hysteretic by definition and hence cannot be written in the form given by Eq. 10 (without some kind of approximation). For that reason, the Newmark-β algorithm with a fixed time step has been used in most cases in the literature. The following subsections discuss two ways to perform this integration, the difference between them being the method used to obtain the response amplitude.

2.3.1 Integrating the inhomogeneous ODE

The inhomogeneous ODE can be integrated with displacement, $x(t)$, and velocity, $\dot{x}(t)$, as state variables if the amplitude X can be expressed as a function of $x(t)$ and $\dot{x}(t)$. Assuming

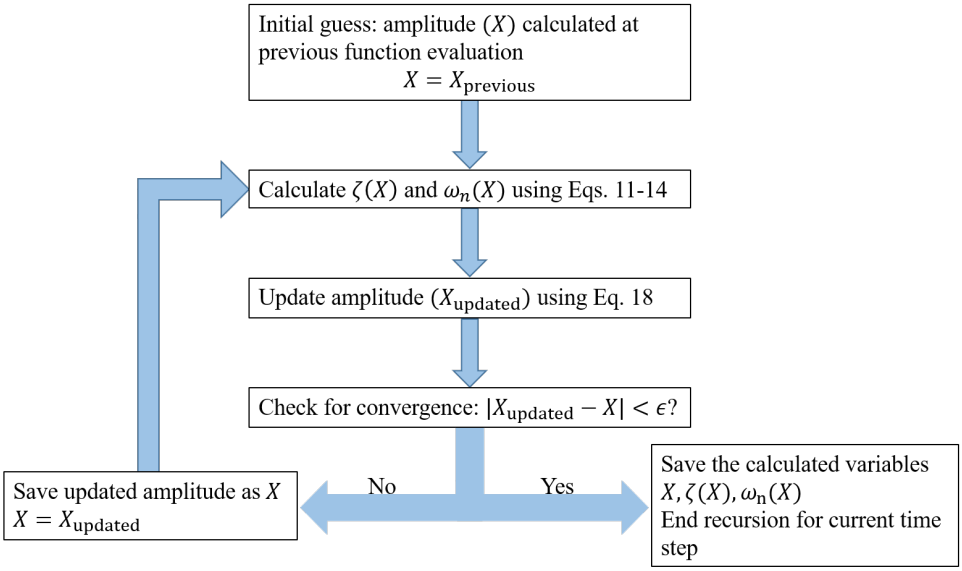

Figure 1: Depiction of the recursive scheme implemented to estimate the response amplitude within the inhomogeneous ODE function definition

the response to be harmonic at each time instant, the displacement can be given by Eq. 15. It must be noted here that the assumption of a single harmonic response may not be applicable for every type of excitation, but is reasonable for weakly nonlinear vibratory systems.

$$x(t) = X \sin(\omega_{\mathrm{d}}(X)t + \phi_0) \tag{15}$$

Differentiating Eq. 15 with respect to time gives,

$$\dot{x}(t) = \left[\omega_{\mathrm{d}}(X) + t\frac{d\omega_{\mathrm{d}}(X)}{dX}\dot{X}\right] X \cos[\omega_{\mathrm{d}}(X)t + \phi_0] + \dot{X} \sin[\omega_{\mathrm{d}}(X)t + \phi_0] \tag{16}$$

If the change in amplitude with time is small, $\dot{X}$ is negligible and Eq. 16 can be simplified to

$$\dot{x}(t) \approx X\omega_{\mathrm{d}}(X) \cos(\omega_{\mathrm{d}}(X)t + \phi_0) \tag{17}$$

The amplitude, X, can then be estimated as,

$$X \approx \sqrt{x(t)^2 + \left[\frac{\dot{x}(t)}{\omega_{\mathrm{d}}(X)}\right]^2} \tag{18}$$

where $\omega_{\mathrm{d}}(X) = \omega_{\mathrm{n}}(X)\sqrt{1-\zeta(X)^2}$. It can be seen that the amplitude, natural frequency and damping are interdependent variables. Hence, an iterative scheme, shown in Fig. 1, needs to be implemented within the RK integrator function definition. The amplitude and corresponding ω_{n} and ζ are calculated iteratively until the absolute difference between the amplitude calculated in successive iterations falls within a pre-defined tolerance ϵ, given by Eq. 19,

$$\epsilon = |X_{j+1} - X_j| \tag{19}$$

where X_j corresponds to the amplitude calculated in the previous loop and X_{j+1} is the amplitude calculated in the current loop. A convergence tolerance of 10^{-13} was found to be sufficient for the cases presented here.

In this way, all the terms required to perform the integration of the inhomogeneous ODE can be obtained.

2.3.2 Integrating the homogeneous ODE

In many cases, the external force lasts only for a short period and one is concerned with the free response of the system, which is governed by Eq. 20.

$$\ddot{x} + 2\zeta(X)\omega_{\mathrm{n}}(X)\dot{x} + \omega_{\mathrm{n}}(X)^2 x = 0 \tag{20}$$

While the previous method could be used to integrate the homogeneous ODE as well, a quicker solution can be obtained by changing the state variables. Figure 2 shows an example of the transient response of an SDOF system. It can be seen that although the response itself changes quickly with time, the amplitude and phase of the response change relatively slowly

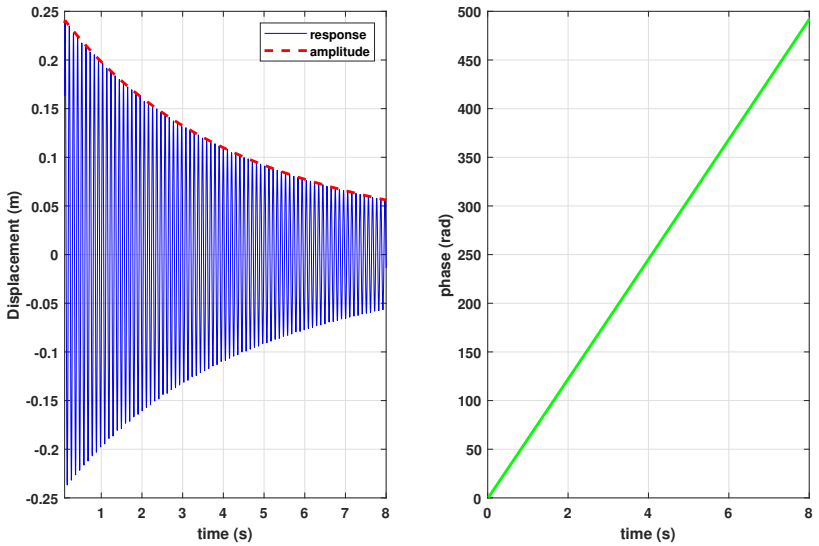

Figure 2: Transient response showing the amplitude and phase changing slowly with time

with time. Hence, changing the state variables from displacement and velocity to amplitude and phase allows a larger time step to be used, thus speeding up the integration further.

The equations for change in amplitude, $\dot{X}$, and phase, $\dot{\gamma}$, can by found by applying the averaging method [74]. This was done, for example, in [78]. The displacement and velocity are written considering amplitude and phase to be time-dependent rather than constant, as shown in Eqs. 21 and 22.

$$x = X(t)e^{i\gamma(t)} \tag{21}$$

$$\dot{x} = \dot{X}(t)e^{i\gamma(t)} + X(t)\dot{\gamma}(t)ie^{i\gamma(t)} \tag{22}$$

The acceleration can be obtained by differentiating Eq. 22 with respect to time. Since bolted joints exhibit weak nonlinearity in the microslip regime, the frequency (and hence change in phase) varies slowly with time. Therefore, $\ddot{\gamma}(t)$ can be neglected and the acceleration equation can be given as

$$\ddot{x} = [\ddot{X}(t) + 2\dot{X}(t)\dot{\gamma}(t)i - X\dot{\gamma}(t)^2]e^{i\gamma(t)} \tag{23}$$

The equations for $x(t), \dot{x}(t)$ and $\ddot{x}(t)$ are then substituted in the equation of motion, i.e. Eq. 20. The real and imaginary parts are equated, resulting in Eqs. 24 and 25.

$$\dot{X}(t) = -X(t)\omega_{\mathrm{n}}(X)\zeta(X) \tag{24}$$

$$\dot{\gamma}(t)^2 - \frac{\ddot{X}(t)}{X(t)} = \omega_{\mathrm{n}}(X)^2(1 - 2\zeta(X)^2) \tag{25}$$

Equation 24 is a first order ODE for the instantaneous amplitude. Exploiting the weakly nonlinear behavior of bolted joints, $\omega_{\mathrm{n}}(X)$ and $\zeta(X)$ in Eq. 24 can be considered constant locally. Thus, differentiating Eq. 24 with respect to time results in the equation,

$$\ddot{X}(t) = -\dot{X}(t)\omega_{\mathrm{n}}(X)\zeta(X) \tag{26}$$

Substituting Eq. 24 for $\dot{X}(t)$ in Eq. 26 gives,

$$\ddot{X}(t) = -X(t)\omega_{\mathrm{n}}(X)^2\zeta(X)^2 \tag{27}$$

which can then be substituted in Eq. 25 to obtain an ODE for the instantaneous phase, as given by Eq. 28. It must be noted here that ω_{n} and ζ are locally constant but still need to be calculated for different amplitude values using Eqs. 11–14.

$$\dot{\gamma}(t) = \omega_{\mathrm{n}}(X)\sqrt{1 - \zeta(X)^2} \tag{28}$$

In this way, the state variables can be changed from displacement and velocity to amplitude and phase. The ODEs for amplitude and phase (Eqs. 24 and 28) can then be integrated using the Runge-Kutta integration scheme, and the response displacement and velocity can be retrieved using Eqs. 21 and 22.

The two integration methods explained in the above subsections can be combined to obtain the ring-down response of an SDOF system with an Iwan element. The forced response (inhomogeneous ODE) is obtained using the technique described in section 2.3.1. The amplitude and phase at the end of this integration are calculated and provided as initial conditions to the next integration method, where the free response (homogeneous ODE) is obtained using the method of averaging described in section 2.3.2. Moving forward, the algorithm obtained by combining these two techniques has been referred to as the Averaging algorithm. It must be noted, however, that the method of averaging is only applied in the homogeneous ODE integration and not throughout the numerical simulation.

3 Test case 1: SDOF system

The above described algorithm was tested against the Newmark-β method for speed and accuracy. First, an impulsive force of varying amplitude was applied (section 3.1). To further verify the results, it was also tested with a sine beat input of varying bandwidth (section 3.2), and a multi-amplitude, bandlimited random input (Section 3.3). The linear and nonlinear system parameters are given in Table 1. These parameters result in a frequency at macroslip, $f_{\mathrm{n},\infty}$ of 30 Hz and a stuck natural frequency (frequency at low vibration amplitude), $f_{\mathrm{n},0}$ of 50 Hz, and are representative of the nonlinear response of a typical mode of a structure with bolted joints.

Table 1: Properties of the nonlinear SDOF system used in Test case 1

Parameter	Value
Mass (m)	1 kg
Macroslip stiffness (K_∞)	3.55×10^4 N/m
Material damping (ζ_{lin})	1×10^{-4}
Iwan joint $[F_{\mathrm{s}}, K_{\mathrm{T}}, \chi, \beta]$	[100 N,6.32×10^4 N/m,-0.75,5]

3.1 Input: Impulse

For the first input case, the force applied to the SDOF system was one half cycle of a sinusoid with width of 0.02 s. This was applied at various amplitudes, gradually increasing the amplitude such that the Iwan element progressed from microslip to macroslip, which was verified by checking the displacement of the sliders in the Iwan joint. The time responses for a simulation period of 35s were obtained by each method. These were then processed using the Hilbert transform, as described in [75], to estimate the instantaneous damping and natural frequency.

The system response can be divided into two parts - the initial period (when the external force is present) and the ring-down period (when the external force is zero). The accuracy in capturing the ring-down behavior can be measured in terms of the amplitude-dependent damping and natural frequency obtained using the Hilbert transform, as shown in section 3.1.1, while the initial response accuracy can be measured in terms of the displacement amplitude just after the impulse ends (i.e. the response amplitude at $t = T_{\text{pulse}}$), as shown in section 3.1.2.

3.1.1 Accuracy: Transient behaviour

To test how accurately the Averaging algorithm predicts the transient behavior, the response of the SDOF system was simulated for an impulse of amplitude 50 N using both integration schemes. This force amplitude is low enough for the Iwan element to remain in the microslip regime. The Hilbert transform of the simulated time response was computed and trimmed to mitigate the end effects. To maintain consistency, the same trim points were used for both simulation methods. A piece-wise linear function was fit to the Hilbert transform to minimize noise when computing its derivative. The instantaneous damping and natural frequency obtained from the Hilbert transform were then plotted against the response velocity amplitude, resulting in the plots shown in Fig. 4. To generalize the results, the non-dimensional velocity was defined as the ratio of the velocity to the product $(\omega_{\text{n},0}\phi_{\max})$, where $\omega_{\text{n},0}$ is the

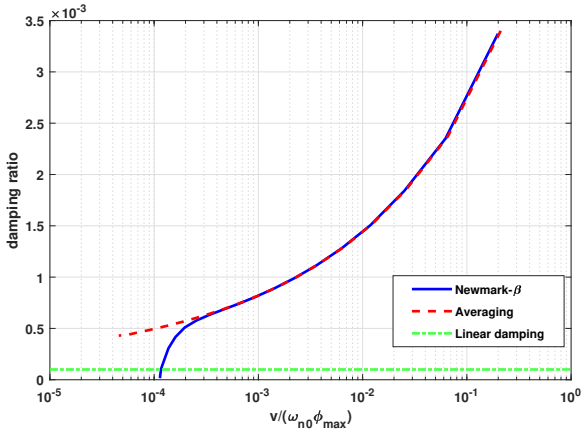

Figure 3: Comparison of amplitude-dependent damping obtained from the Newmark-β and Averaging algorithms. The Newmark-β algorithm has a Newton-Raphson iteration tolerance of $\epsilon_{\mathrm{NR}} = 10^{-10}$

stuck natural frequency and $\phi_{\max}$, the displacement of the joint at macroslip. The error in damping ratio and natural frequency was then calculated as a percentage of the Newmark-β solution, which was considered to be the true solution.

It was initially observed that the damping ratio (and natural frequency) estimated by the Newmark-β solution deviated from the Averaging algorithm at low response amplitudes, as shown in Fig. 3. The Newmark-β solution predicted a damping lower than the linear damping of the system, which is unrealistic. It was then found that the solution predicted by Newmark-β algorithm was sensitive to the convergence tolerance of the Newton-Raphson iteration loop, ϵ_{NR}. This was surprising, because the tolerance of 10^{-10} had been used in many previous studies [19, 20, 57] without difficulty. The tolerance was reduced gradually until further reduction did not have a significant effect on the output. Finally, a tolerance of 10^{-15} was found suitable for the range of forces analyzed in this work. The arbitrary nature of this selection highlights a possible drawback of the existing integration method and further warrants development of a more robust technique.

Figures 4a and 4b show that the transient behavior predicted by the Averaging algorithm agrees well with the Newmark-β algorithm after reducing the convergence tolerance for the Newton-Raphson iteration loop. It must be noted here that these graphs progress from

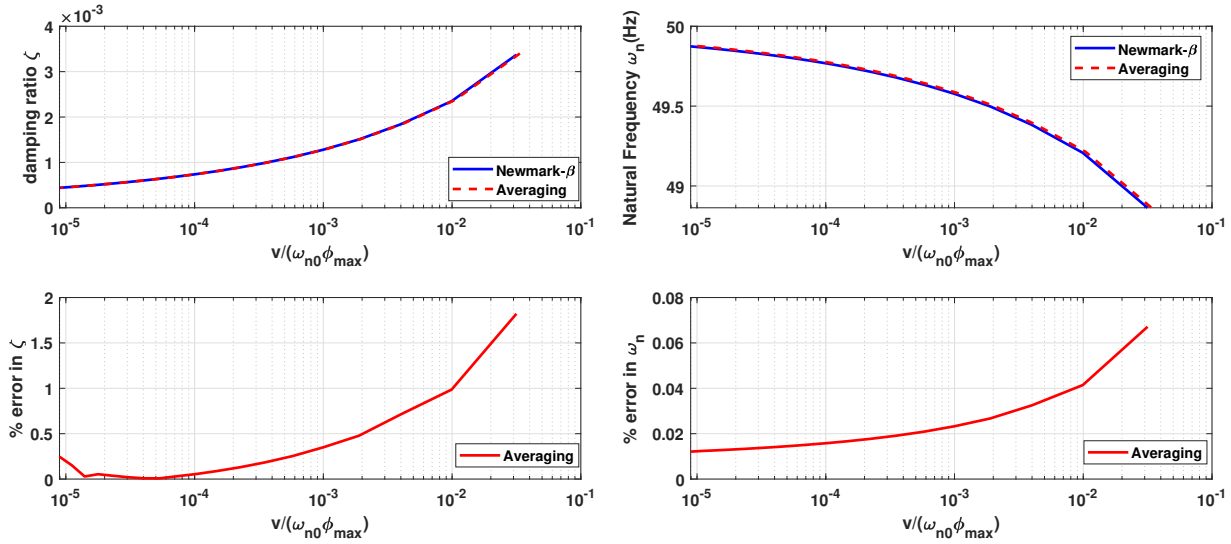

(a) Damping (top) and % error in damping (bottom)

(b) Natural frequency (top) and % error in frequency (bottom)

Figure 4: Comparison of (a) damping and (b) frequency obtained from the Newmark-β (with Newton-Raphson tolerance of $\epsilon_{\mathrm{NR}} = 10^{-15}$) and the Averaging algorithms. The % error is calculated treating Newmark-β as the true solution.

right to left (i.e. from higher velocity amplitudes to lower velocity amplitudes) since the response velocity decreases with time. A maximum error of 1.86% in the damping estimate and 0.07% in the natural frequency estimate is observed. The estimations improve as the velocity amplitude reduces with the percentage error being nearly zero at low velocities.

The Averaging algorithm also estimates the amplitude-dependent natural frequency and damping ratio for the free decay using the closed-form expressions, given by Eqs. 11-14, without requiring any Hilbert processing. The states used by the Newmark-β method, on the other hand, are the displacement, x and velocity, $\dot{x}$, and so the Hilbert transform is required to estimate the response amplitude, X, and the instantaneous natural frequency and damping. Figure 5 shows that the amplitude-dependent damping curve obtained from the closed-form expressions agrees well with the one obtained using the Hilbert transform applied to the Newmark-β method. The same result could also be drawn from the amplitude-dependent frequency curve, which has not been shown here for brevity. Thus, the Averaging algorithm requires only algebraic processing in the form of evaluating Eqs. 11-12 to obtain

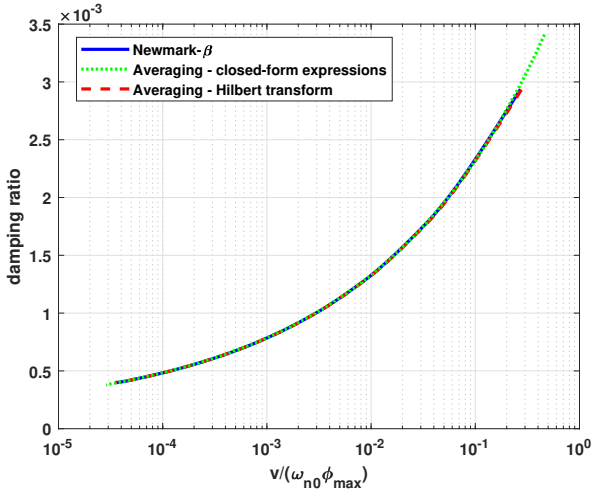

Figure 5: Comparison of the damping obtained using Eqs. 11-14 in the Averaging algorithm with the damping obtained using the Hilbert transform method

the amplitude-dependent frequency and damping as opposed to Hilbert processing required in the conventional Newmark-β algorithm, which is discussed in [75].

3.1.2 Accuracy: Initial response

Figure 6 shows the time response from both integration schemes for low amplitude impulsive forces. Both the amplitude and the phase of the response predicted by the Averaging algorithm are in good agreement with the Newmark-β method. However, at higher force amplitudes, when the system is well into macroslip, the Averaging solution starts to deviate from the true response, as can be seen in Fig. 7. This is likely due to the fact that Eqs. 11-14 are applicable solely in the microslip regime. Another source of error is the approximate amplitude equation (i.e. Eq. 18) that assumes small changes in amplitude with time. This approximation could fail at high impulsive forces. These inaccuracies, however, only affect the forced part of the response. If the correct amplitude and phase are given to the homogeneous ODE solver in section 2.3.2 and the response is well approximated as harmonic, it will give the correct response from that point forward.

To further quantify this, the response was simulated for multiple force amplitudes of increasing magnitude using both integration methods. To generalize the results, the non-

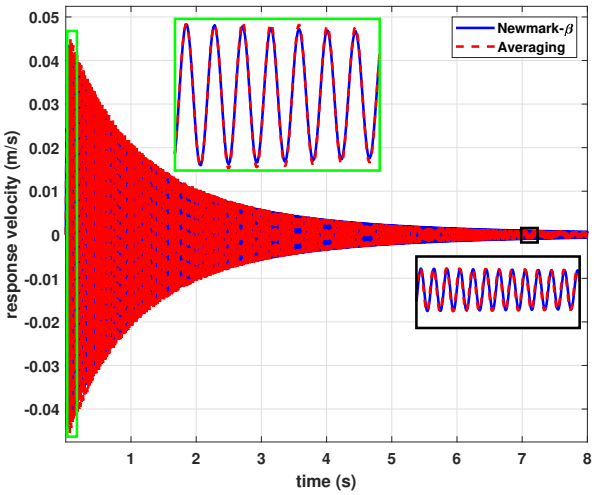

Figure 6: Response velocity simulated by the Newmark-β and the Averaging algorithms in the microslip regime ($E_{\mathrm{r}} = 0.05$)

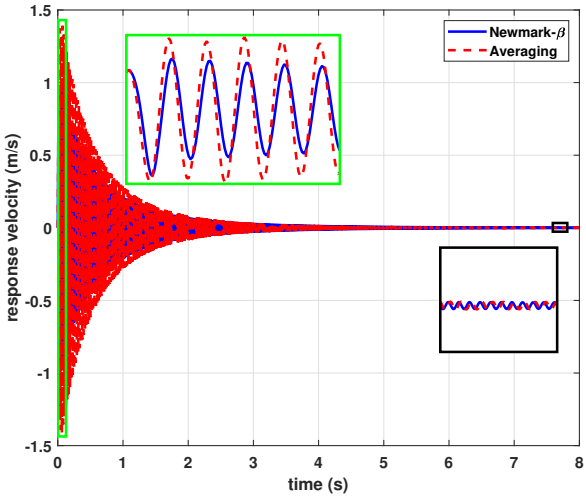

Figure 7: Response velocity simulated by the Newmark-β and the Averaging algorithms in the macroslip regime ($E_{\mathrm{r}} = 11.07$)

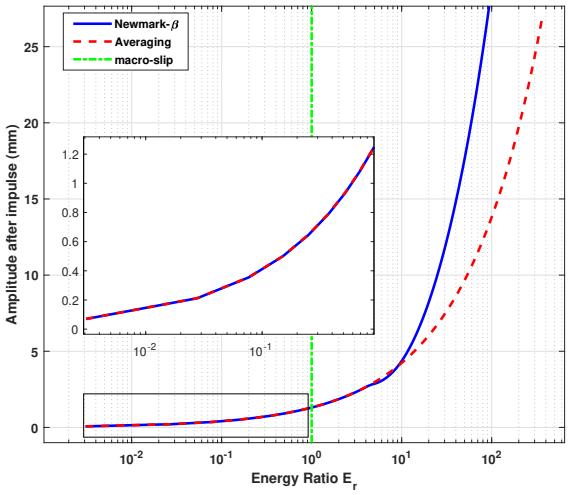

Figure 8: Response amplitude after the impulse has ended plotted against energy ratio E_r, where $E_\mathrm{r} < 1$ indicates microslip and $E_\mathrm{r} \geq 1$ indicates macroslip

dimensional force amplitude was expressed as an energy ratio $E_\mathrm{r} = E_\mathrm{impulse}/PE_\mathrm{max}$, where the numerator is the energy imparted by the impulse (Eq. 29) and the denominator is the approximate potential energy for which the joint fully slips (Eq. 30). Macroslip occurs when $E_\mathrm{impulse} \approx PE_\mathrm{max}$, i.e. when $E_\mathrm{r} \approx 1$.

$$E_\mathrm{impulse} = \frac{1}{2m}\Big(\int_0^{T_\mathrm{pulse}} f(t)dt\Big)^2 \tag{29}$$

$$PE_\mathrm{max} \approx \frac{1}{2}(K_\mathrm{T} + K_\infty)\phi_\mathrm{max}^2 \tag{30}$$

The response amplitude just after the impulse has ended was then plotted against this energy ratio E_r. Figure 8 shows that for $E_\mathrm{r} < 1$, there is negligible difference in the velocity amplitude predicted by the two integration schemes. As E_r increases to values above 9.3, significant deviations in the amplitude predicted by the two methods are observed. We would expect the Averaging algorithm to lose accuracy in the macroslip regime ($E_\mathrm{r} > 1$) since the closed-form expressions used in this algorithm are applicable only in the microslip regime. Surprisingly, however, the Averaging algorithm doesn't significantly deviate from the truth solution until E_r reaches values nearly ten times greater than the macroslip value. It must

be noted here that one could limit the applicability of the algorithm to the microslip regime to avoid the possibility of inaccurate response estimation at very high force values. This can be done by enforcing $E_r < 1$, or equivalently, $X/\phi_{max} < 1$. However, in the case studies shown here the algorithm was actually quite accurate up until $E_r = 10$.

3.1.3 Speed

Table 2 provides the simulation time, in seconds, for each of the two methods when computed on an Intel® Core™ i7-950 (3.07 GHz) processor for the case where an impulsive force having an amplitude of 50 N is applied on the SDOF system under consideration.

Table 2: Simulation time of the Newmark-β and the Averaging methods when a 50 N impulsive force is applied on the SDOF system

Method	No. of time steps	Simulation time (s)
Newmark-β	35001	72.96
Averaging	$1092 + 241 = 1333$	0.1193

It can be seen that the Averaging algorithm significantly speeds up the integration process. This was anticipated as applying the concept of averaging allows for a larger time step, thus lowering the number of integration steps. 35001 time steps were required for the Newmark-β approach (200 samples per period) whereas for the same duration of interest, with the method of averaging, the RK integrator used 1092 time steps to solve the inhomogeneous ODE and another 241 time steps to solve the homogeneous part, resulting in a total of 1333 time steps. The homogeneous ODE requires a much smaller number of time steps than the inhomogeneous section, due to the use of the averaging method. It must also be noted that the time taken by Newmark-β scheme depends on the number of sliders used in the integration. The Averaging algorithm has no such issue since it uses closed-form expressions instead of calculating the slider positions.

Table 3 shows the time taken to evaluate the nonlinear force (discretized form of Eq. 1) in the Newmark-β algorithm for 30 versus 100 sliders. The times listed are that for a

Table 3: Time taken to evaluate the discretized, nonlinear force in the Newmark-β algorithm compared against its Averaging counterpart, the time taken to evaluate the closed-form damping and frequency expressions

Method	No. of sliders	Function evaluation time (s)
Newmark-β	30	7.04×10^{-5}
Newmark-β	100	1.04×10^{-4}
Averaging	-	5.98×10^{-7}

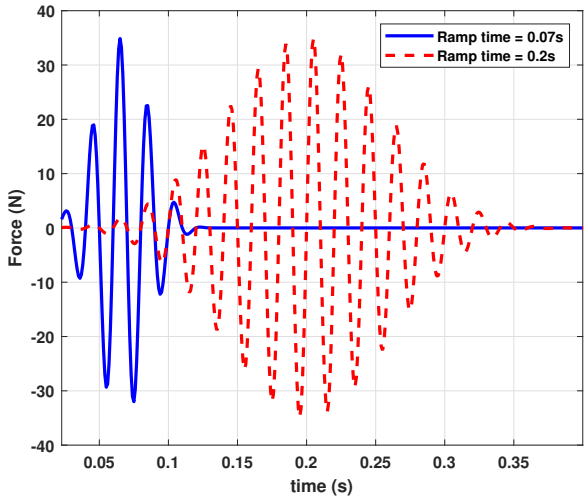

Figure 9: Force vs time plot for two different ramp times, showing that a larger ramp time implies a longer duration of force

single evaluation, obtained by performing an average over $500,000$ calculations to reduce the effect of variability in computation time. A larger number of sliders are required for higher accuracy but also significantly increase the computational burden. On the other hand, the time taken to evaluate the closed-form expressions for amplitude-dependant damping and frequency (Eqs.11–14) used in the Averaging algorithm is orders of magnitude lower.

3.2 Input: Sine beat

For a sine beat, the force input is created by applying a Blackman-Harris window to a monoharmonic sine wave, resulting in a signal that starts with zero amplitude, increases in amplitude to a peak value, dwells at this peak value and then decreases in amplitude back to

zero. The frequency, f_{n}, and peak amplitude, F, of the sine wave, ramp time (or frequency band, dF) and dwell time, t_{d}, can be varied. A wider frequency band (or higher value of dF) results in a shorter force signal and can be interpreted as getting "closer" to an impulse. For the purpose of this analysis, dF was varied to excite gradually narrowing frequency bands, keeping all other parameters constant. A narrower frequency band (or larger ramp time) means the force is applied over a longer duration, as seen in Fig. 9. Ideally the sine beat would focus on just the resonant frequency. However, for the nonlinear SDOF system being studied here, the effective natural frequency decreases as amplitude increases, requiring a bandwidth wide enough to account for this variation. The parameters of the input force are provided in Table 4.

Table 4: Parameters of the sine beat applied to the nonlinear SDOF system

Parameter	Value
Frequency (f_{n})	50 Hz
Peak amplitude (F)	35 N
dwell time (t_{d})	0 s
Bandwidth (dF)	varies

The response was simulated using the two integration schemes for different ramp times and the amplitude of the response at time greater than T_{ramp} was tracked. Figure 10 plots the response amplitude for different ramp times on the left Y-axis, and the corresponding maximum slider displacement of the last slider, obtained from the Newmark-β method, on the right Y-axis. If this slider's displacement is greater than zero, the system has gone into macroslip. It can be observed that within the microslip regime, the Averaging algorithm accurately predicts the response irrespective of the ramp time (or how long the external force lasts). It is only when the system is well into macroslip that significant deviations are observed. This shows that the algorithm can be used for more persistent forces than an impulse, provided the system remains in microslip.

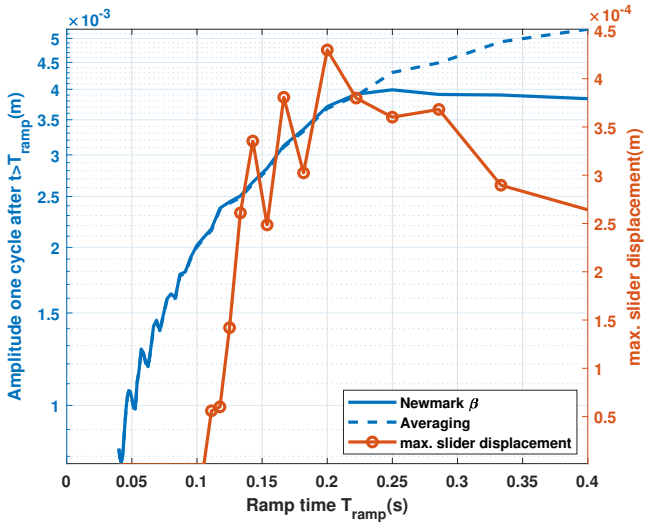

Figure 10: Response amplitude when $t > T_{\text{ramp}}$ plotted against varying ramp time. The maximum slider displacement of the last slider to slip is tracked on the right axis, with non-zero values corresponding to macroslip.

3.3 Input: Bandlimited random force

To test the algorithm's efficiency in simulating the response of randomly excited systems, a third input type was considered. A uniformly-distributed random force was generated, which was then filtered to focus on the frequency range of interest. This was done using a low-pass Butterworth filter with a cutoff frequency equal to 1.25 times the stuck frequency ($f_{\text{n},0}$). Three different peak forcing amplitudes were considered, resulting in increasing levels of nonlinearity of the system. The response for each forcing level was computed over a time interval of 3200 s using the Newmark-β and the Averaging algorithms respectively, and the power spectral density (PSD) of the response was calculated.

Figure 11a compares the PSDs obtained for the three different force levels using the two algorithms. The response is nonlinear at the higher force levels, with a frequency shift of nearly 1.5 Hz for the force level of $\pm$150 N. The closely matching PSDs obtained from the two integration approaches indicate that the Averaging algorithm is able to accurately simulate the response of a nonlinear system to a random input. The time-domain displacement, plotted in Fig. 11b, shows that the response is sinusoidal in nature at each time instant,

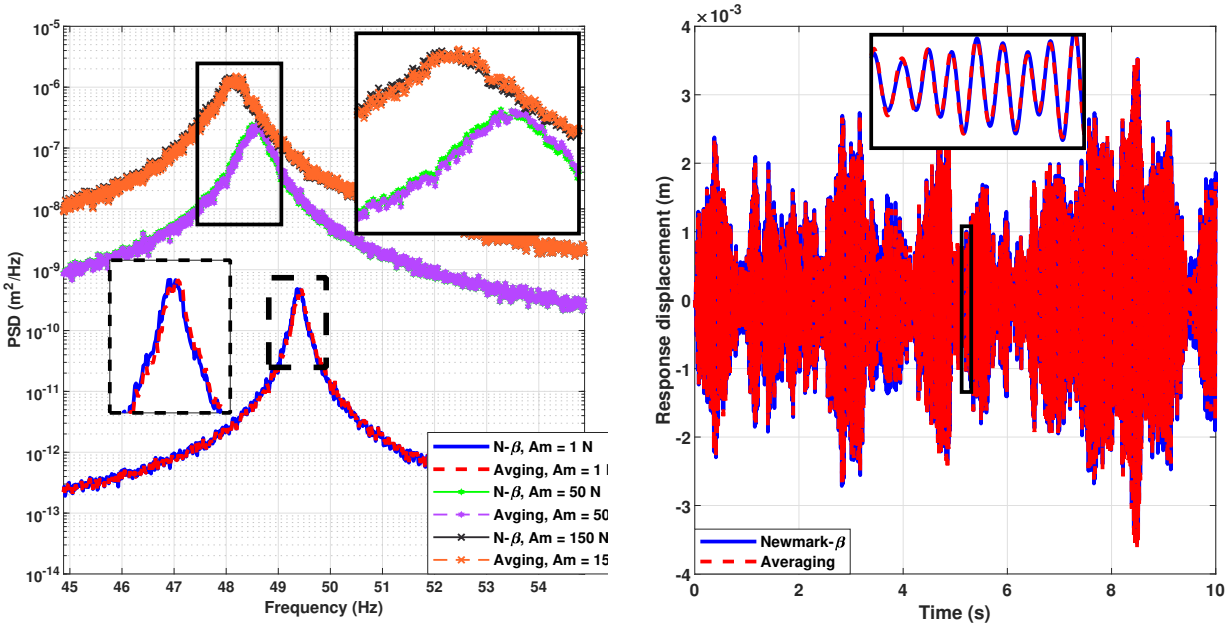

(a) (b)

Figure 11: a) PSDs for bandlimited random input with three different peak force amplitudes (Am) and b) Time-domain response to random input with force level ± 150 N, obtained by the Nemark-β and Averaging algorithms

even though the applied input is random. This explains why the Averaging algorithm is still able to predict the response fairly accurately. Table 5 lists the time taken by the Newmark-β and the Averaging algorithms to compute the response for the three different force amplitudes considered. It must be noted that since the external force is always active, the ODE to be integrated is inhomogeneous throughout the time interval and hence, only the part of the Averaging algorithm derived in Section 2.3.1 is being implemented. The evaluation times show that the computation time can be reduced by more than an order of magnitude by implementing the amplitude approximation equation (Eq. 18) along with the recursive scheme described in Section 2.3.1, even without the method of averaging being used.

Table 5: Computation time for the two integration algorithms for a bandlimited random input when the peak force amplitude is a) 1 N, b) 50 N, and c) 150 N

	Peak Force	Newmark-β evaluation time	Averaging evaluation time
a)	$\pm$1 N	8908 s	386 s
b)	$\pm$50 N	7221 s	380 s
c)	$\pm$150 N	7223 s	385 s

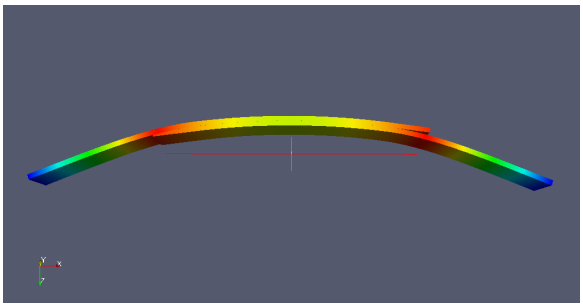

(a) First bending mode (mode 7)

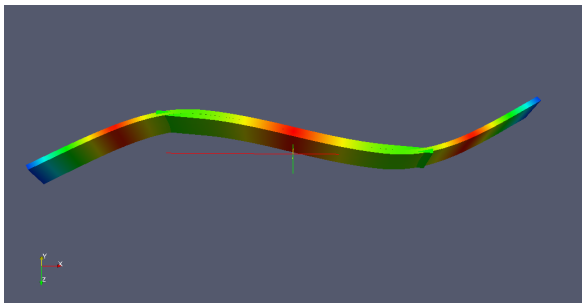

(b) Second bending mode (mode 8)

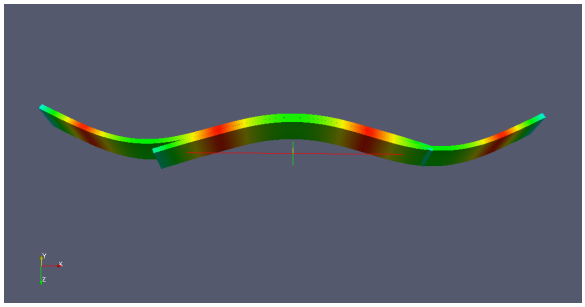

(c) Third bending mode (mode 9)

Figure 12: Linear mode shapes of modes 7, 8 and 9, the nonlinear modes of the Sumali beam

4 Test case 2: Sumali beam finite element model

To test the algorithm's accuracy on a more realistic structure, an assembly of two beams commonly referred to as the Sumali beam, was considered. The Sumali beam structure consists of two thin, identical, stainless steel beams of length 508.00 mm, width 50.80 mm, and thickness 6.35 mm, that overlap and are connected using four bolts. The area of overlap extends 355.60 mm along the length of each beam.

Lacayo et al. [57] performed model correlation and updating on a finite element (FE) model of this beam. The Hurty/Craig-Bampton reduction technique [79, 80] was used to

obtain a reduced FE model, consisting of 49 degrees of freedom (DOF). Each of the four bolts were modeled using the whole-joint approach [16], i.e. they were represented by a single Iwan element in the x-translation direction (axial to the beam). All the Iwan elements were assumed to have the same parameters which were iterated upon to match the experimental results obtained by Deaner et al. [19]. The structure was modeled to have free-free boundary conditions. Hence, the first six modes are rigid body modes. Modes 7, 8 and 9 are the first three elastic bending modes, as shown in Fig. 12. These modes exhibit nonlinearity. Further information on the FE model and the updating routine used can be found in [57]. Apart from this, [57] also implements the modal Iwan modeling approach [25], representing each of the nonlinear modes of the Sumali beam as a SDOF system containing an Iwan element. To do so, first an impulsive force was applied on the FE model to excite only the mode of interest. The response of the 49 DOFs to this force was simulated using the Newmark-β integration method. The simulated response was then modally filtered and Hilbert analysis was performed on the velocity of the nonlinear mode of interest (r) to obtain its amplitude-dependent natural frequency, $\omega_{\mathrm{r,meas}}$), and damping ratio, $\zeta_{\mathrm{r,meas}}$. The closed-form expressions for damping and frequency (Eqs. 11-14) were then used, treating the Iwan parameters as variables that were optimized to match $\omega_{\mathrm{r,meas}}$ and $\zeta_{\mathrm{r,meas}}$. Table 6 lists the Iwan parameters calculated in [57] for the three nonlinear modes of the Sumali beam.

Table 6: Modal Iwan parameters for the Sumali beam reduced-order model, obtained from [57]

Parameter	Mode 7	Mode 8	Mode 9
K_∞ [s^{-2}]	4.235×10^5	1.673×10^6	7.321×10^6
ζ_{lin}	1×10^{-4}	1×10^{-4}	1×10^{-4}
F_s [$\mathrm{kg}^{1/2}\mathrm{ms}^{-2}$]	1.802	1.518	6.934
K_T [s^{-2}]	1.537×10^5	1.340×10^5	2.822×10^6
χ	-0.1369	-0.1620	-0.1008
β	2.561	2.000	1.529

The above described modal model has been used here to test the applicability of the Averaging algorithm to a realistic structure. An impulsive force of 0.5 N was applied along the positive Z axis at the end of the beam. This force level was chosen to ensure that all the Iwan elements are within the microslip region and the nonlinearity is weak enough for the modal Iwan modeling approach to hold. The equation of motion for the FE model is given by Eq. 31.

$$\mathbf{M}\ddot{\mathbf{x}} + \mathbf{C}_{\text{lin}}\dot{\mathbf{x}} + \mathbf{K}_{\text{lin}}\mathbf{x} + \mathbf{F}_{\text{joint}}(\mathbf{x}) = \mathbf{F}_{\text{ext}} \tag{31}$$

Time integration of the reduced FE model, henceforth referred to as the whole-joint model, was performed using the Newmark-β method and the response obtained in the physical domain was modally filtered to get the displacement and velocity of the nonlinear modes of the system. This was then compared with the response obtained using the modal Iwan model of the beam, integrated using the Averaging algorithm. The equation of motion for an MDOF system can be converted from physical to modal co-ordinates by pre-multiplying the equation by the transpose of the linear, mass-normalized mode shape matrix Φ, assuming the mode shapes remain constant and equal to the linear modes of the system. This is a reasonable assumption for the weak nonlinearity exhibited by bolted joints in the microslip regime, with the results obtained in [19, 20] proving the same. The equation of motion for any of the modes of the system can then be written in the form that is compatible with the Averaging algorithm, as shown in Eq. 32.

$$\ddot{q}_r + 2\zeta_r\omega_r\dot{q}_r + \omega_r^2 q_r = \Phi_{0r}^T F_{\text{ext}} \tag{32}$$

where ζ_r and ω_r correspond to the linear damping ratio and natural frequency respectively for linear modes and to the amplitude-dependent damping and natural frequency for nonlinear modes.

Each of the three nonlinear modes can then be treated as an SDOF system which can be integrated in time using the Averaging algorithm. The remaining 46 modes can be

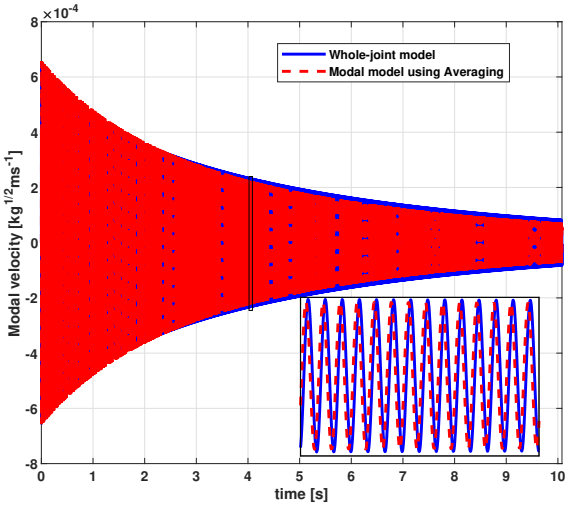

Figure 13: Modal response of the nonlinear mode 8, with the modal model, integrated using the Averaging algorithm, being compared against the modally-filtered response from the whole-joint model

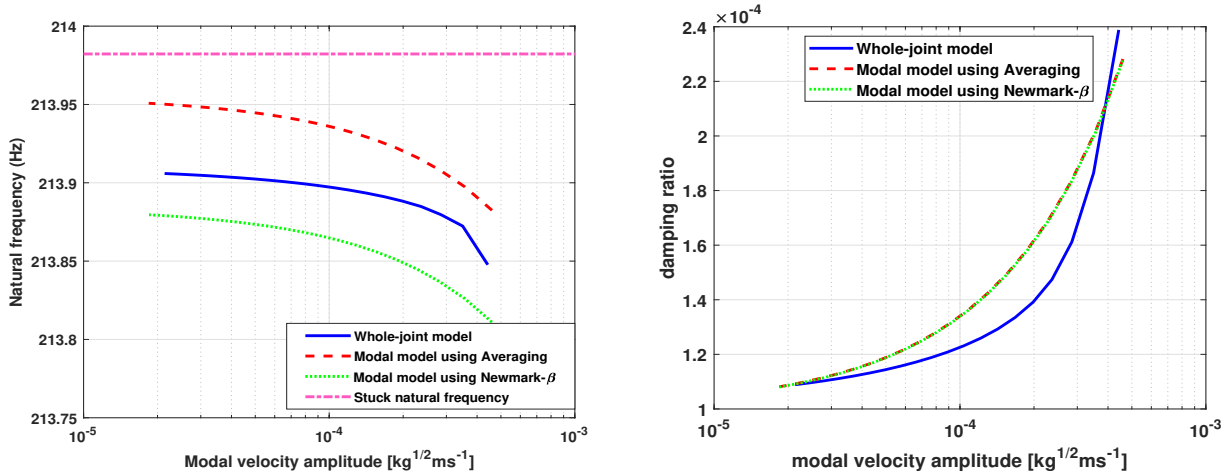

(a) Frequency vs velocity amplitude

(b) Damping vs velocity amplitude

Figure 14: Comparison of the amplitude-dependent (a) frequency and (b) damping obtained from three integration approaches: integrating the whole-joint model using the Newmark-β method, integrating the modal model using the Averaging algorithm, and integrating the modal model using the Newmark-β method

approximated as linear and integrated directly using any numerical integration method. In fact, for the linear modes, once the external force goes to zero, the classical expressions for displacement and velocity for free vibration of an under-damped SDOF system, given by Eqs. 33 and 34 respectively and derived in [81], can be used,

$$q_r = e^{-\zeta_r \omega_r t}\left[q_0 \cos(\omega_d t) + \frac{\dot{q}_0 + \zeta_r \omega_r q_0}{\omega_\mathrm{d}} \sin(\omega_\mathrm{d} t)\right] \tag{33}$$

$$\dot{q}_r = e^{-\zeta_r \omega_r t}\left[\dot{q}_0 \cos(\omega_\mathrm{d} t) - \frac{\omega_r}{\omega_\mathrm{d}}(\zeta_r \dot{q}_0 + \omega_r q_0) \sin(\omega_\mathrm{d} t)\right] \tag{34}$$

where ω_d is the damped natural frequency, q_0 is the initial displacement and $\dot{q}_0$ is the initial velocity. The initial conditions are equal to the displacement and velocity at the last time step of the numerical integration solution.

Figure 13 shows the response velocity for mode 8 of the Sumali beam obtained by the two methods - integrating the whole-joint model, and using the Averaging algorithm. The two time histories are in fairly good agreement. The responses can be further processed by performing the Hilbert transform described in section 3.1.1 to obtain the amplitude-dependent natural frequency and damping, shown in Fig. 14. The modal Iwan model can also be integrated using the Newmark-β method, the results of which have also been shown in Fig. 14. The natural frequency predicted by the Averaging algorithm is in close agreement with the whole-joint model, with the maximum percentage error being 0.021%. The damping predicted by the Averaging algorithm shows some deviation, with the maximum percentage error being 15.58%, treating the whole-joint model as the truth solution. However, it can be seen in Fig. 14b that the damping curves obtained by integrating the modal Iwan model using the Newmark-β method and the Averaging algorithm (i.e. the green and red curves in Fig. 14b) overlay. Hence, the difference in damping observed between the whole-joint model and the Averaging algorithm is a consequence of the modal Iwan approach and not an integration error caused by the method of averaging.

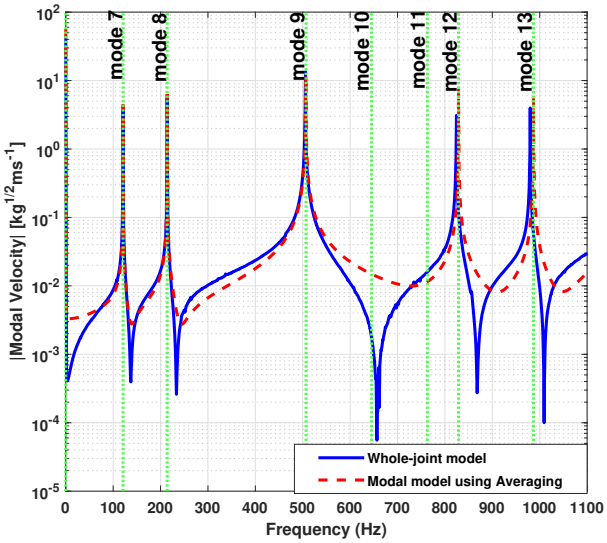

Figure 15: FFT of the response velocity at the end of the beam

Figure 15 shows the Fast Fourier Transform (FFT) of the response velocity at the end of the beam. Since modes up to 1050 Hz were used to update the FE model, only the modes in that frequency range were compared. It can be seen that there is good agreement between the two integration methods for modes 7, 8 and 9. At higher frequencies, the whole-joint model deviates from the natural frequency of the mode, possibly due to integration errors introduced by the Newmark-β method. The modal approach using the Averaging algorithm, on the other hand, aligns well with the system natural frequencies.

Table 7: Computation time for the three integration approaches: using the Newmark-β method for a) the whole-joint model, b) the nonlinear modes in the modal model and c) using the Averaging algorithm for the modal model

	Method	Nonlinear modes	Linear modes	Total time
a)	Newmark-β whole-joint model	-	-	997.97 s
b)	Newmark-β modal model	257.19 s	2.91 s	260.10 s
c)	Averaging modal model	0.36 s	2.91 s	3.27 s

Table 7 lists the computation time for the three approaches: integrating the whole-joint model using the Newmark-β method, integrating the modal model using the Newmark-β method, and integrating the modal model using the Averaging algorithm. In the modal ap-

proach, the response of the linear modes is obtained by direct numerical integration coupled with evaluation of analytical expressions (i.e. Eqs. 33 and 34). The table highlights the significant improvement in speed the Averaging algorithm offers; it is nearly 300 times faster than integrating the whole-joint model and over 80 times faster than using the Newmark-β method for the modal model.

This shows that applying the proposed Averaging algorithm to realistic structures can be computationally more efficient than integrating the whole FE model, without significant loss of accuracy.

5 Conclusions

This paper presents an algorithm that can be effectively used to integrate a single degree of freedom system with an Iwan element in order to simulate a ring-down response. The method of averaging can be used when the external force goes to zero to speed up the integration. The proposed algorithm is much more computationally efficient than the prevalent implicit integration approaches with minimal loss in accuracy, even for impulsive forces large enough to cause the joints to go into macroslip. For example, in the SDOF system considered, accurate response is estimated for energy ratios as high as $E_{\mathrm{r}} = 9.3$. The sine beat and random input case studies show that the method of averaging gives accurate results irrespective of how long the input force lasts, as long as the system is in or near microslip. In the microslip regime, the amplitude-dependent natural frequency and damping ratio were found to be comparable to the Newmark-β algorithm. In fact, the Newmark-β algorithm required adjusting the ad-hoc convergence tolerance in the Newton-Raphson iteration loop to accurately capture the damping and frequency at low vibration amplitudes, making the Averaging solution more reliable in the cases considered. The Averaging algorithm is also preferable if the final goal is to estimate damping and frequency versus time, because no further processing (i.e. with the Hilbert transform) is required to obtain these. A drawback

of the integration technique is that the closed-form expressions used are fundamentally limited to microslip only, even though results show that the approach is fairly accurate even for forces larger than macroslip. Another limitation is that this algorithm is applicable to SDOF systems or modal Iwan models; the latter are only valid for MDOF systems if the modes are uncoupled and the nonlinearity is weak. The Sumali beam test case shows that if the modal Iwan approach holds, the Averaging algorithm offers great computational efficiency without much loss of accuracy.

Paper II: A Parametric Study of the Bouc-Wen Model for Bolted Joint Dynamics

Built-up structures exhibit nonlinear dynamics due to friction at the surfaces that are held together using mechanical fasteners. This nonlinearity is hysteretic, or history dependent. Additionally, slip between the surfaces results in small changes in frequencies and significant changes in damping, both of which are a function of the amplitude of vibration. At low tangential loads, before gross slip of the contact surfaces occurs, the dissipation varies as a power of the load amplitude. The four-parameter Iwan model is most commonly used in bolted joints simulation, since it captures both the hysteretic and power-law dissipation behavior that is characteristic of bolted joints. However, dynamic simulation of the four-parameter model is computationally intensive since implicit integration schemes with small time steps must be used. The Bouc-Wen model is an alternative hysteretic model with a formulation such that explicit integration schemes can be used, resulting in faster dynamic simulations. Existing literature predominantly focuses on studying the hysteretic behavior of this model. This paper tests the effectiveness of the Bouc-Wen model in capturing the power-law dissipation that is characteristic of bolted joint dynamics by comparing it against an equivalent four-parameter Iwan model.

1 Introduction

Mechanical fasteners are commonly used to assemble various parts together in built-up structures, making manufacturing and maintenance of these structures convenient. These fasteners have a nonlinear effect on the overall stiffness and damping of the structure due to frictional energy losses at the interface [4, 5]. The contact pressure at the interface due to bolt preload is non-uniform, with the pressure being high near the bolt hole and gradually decreasing further away [15]. As a result, at low tangential loads, the area near the bolt hole remains stuck whereas the edges of the contact interface start to slip. This phenomenon is termed as microslip. The area that remains stuck can be understood to behave like a linear spring, whereas the area that slips results in frictional energy dissipation and a loss of stiffness [17]. As a result, the stiffness of the joint decreases slightly while the damping increases by orders of magnitude. This behavior has been corroborated by several experimental studies [18–20]. The nonlinear frequency and dissipation can be quantified as a function of the amplitude. In case of bolted joints, the dissipation is found to vary as a power of the load amplitude [16, 82]. This is referred to as the power-law behavior of dissipation. As the force amplitude increases, the area of contact reduces, ultimately resulting in relative motion between the surfaces, also known as macroslip. In macroslip, the joint stiffness decreases significantly and the dissipation does not exhibit power-law behavior. Additionally, due to the interfacial slip behavior, the stress-strain, or force-displacement relationship is hysteretic in nature, i.e. the restoring force depends not only on the displacement but also on the past state of the system.

One approach to simulate the dynamics of jointed structures could be to create a high-fidelity finite element (FE) model of the bolts that is able to capture the dissipation due to friction in the microslip and macroslip regime [8, 9]. However, due to the orders-of-magnitude difference in the length scales associated with microslip and that of the whole model, this approach is highly computationally expensive [14]. Jewell et al. [9] observed that a very fine mesh is needed around the contact region to effectively capture microslip

nonlinearity. An alternative is to replace the contact interface with a constitutive model capable of simulating the hysteretic and amplitude-dependent nonlinear behavior that has been observed experimentally. The constitutive model could then be incorporated into the FE model using the whole-joint modeling approach [16]. In this approach, the nodes on a contact surface are constrained to a single, virtual node. The appropriate hysteretic model is then applied between the virtual nodes of the surfaces in contact. While this approach is computationally more efficient than creating a high-fidelity FE model, it is difficult to isolate the effect of each joint on the overall system dynamics. Therefore, computationally intensive optimization schemes are required to calibrate the constitutive models [53]. Alternatively, a modal modeling approach can be used [25], in which each mode is represented by a single degree-of-freedom (SDOF) system with a parallel arrangement of a linear spring, linear damper and the hysteretic model.

In either of the modeling approaches, a suitable constitutive model is required to capture the nonlinear dynamics of the bolted joint(s). Gaul and Nitsche [29] reviewed different models that can be used to estimate the dynamics due to bolted joints. More recently, Mathis et al. [30] presented an overview of various rate-dependent and rate-independent hysteretic models. One such model prevalent in bolted joint dynamic analysis is the Iwan model [22]. It consists of a parallel arrangement of spring-slider units, known as Jenkins elements, with all elements having the same spring stiffness but different slider strengths. A distribution function is defined to specify the strength of the sliders. Several forms of the Iwan model have been developed for bolted joints applications [34, 35, 37]. Among them, Segalman's four-parameter Iwan model [35] is most popular since it can capture the microslip power-law dissipation behavior that has been experimentally observed. However, an implicit integration scheme is required to simulate the dynamic behavior of this model, with the state of the sliders being evaluated at each time step. Brake [36] presented a reduced formulation of the four-parameter model that makes it possible to derive an analytical expression for the nonlinear force, thus circumventing the slider state calculations. Alternatively, Shetty

and Allen [83] used closed-form expressions for stiffness and dissipation to reformulate the differential equations of the four-parameter model such that explicit ODE solvers can be used. However, the closed-form expressions used are applicable only in the microslip regime.

The Bouc-Wen model [23, 24] is another semi-physical, rate-independent model that can capture hysteretic behavior. It consists of a nonlinear, first-order ordinary differential equation (ODE) that relates the input displacement to the output restoring force in a hysteretic way. This differential equation can be easily integrated using explicit ODE solvers to obtain the nonlinear restoring force. Therefore, dynamic simulation of the Bouc-Wen model is more computationally efficient than the four-parameter Iwan model. The Bouc-Wen model is regarded as semi-physical since its formulation is based on some physical understanding of hysteresis but its parameters are non-physical. Ismail et al. [84] provide an extensive survey of the Bouc-Wen model. A vast majority of the existing literature focuses on applying this model to capture steady-state hysteretic behavior of various nonlinear systems [46–48]. There has been some effort to simulate the hysteretic behavior due to friction using the Bouc-Wen model [11, 85]. However, the nonlinearity in bolted joints is also characterized by the amplitude-dependent frequency and damping behavior, specifically the power-law dissipation in the microslip regime. This paper analyzes the effectiveness of the Bouc-Wen model in capturing the power-law behavior by comparing it against the four-parameter Iwan model, derived specifically to simulate bolted joint dynamics.

The following section provides background on the four-parameter Iwan model, the Bouc-Wen model, and the modal modeling approach. A method to identify the Bouc-Wen model parameters is also included. Section 3 compares the dynamic response of the two hysteretic models to an impulsive force, analyzing the Bouc-Wen model's effectiveness in simulating power-law dissipation behavior. Section 4 provides an analysis of the effect of each Bouc-Wen parameter on the overall damping of the system. Finally, the conclusions are presented in Sec. 5.

2 Background

2.1 The Four-Parameter Iwan Model

The Iwan model [22] is a lumped, hysteretic model that was originally developed to characterize metal elastoplasticity. It consists of a parallel arrangement of spring-slider units, also known as Jenkins elements. The nonlinear restoring force due to the Iwan model is given by Eq. 1,

$$f_{\text{nl,Iwan}}(x,t,\phi) = \int_0^\infty \rho(\phi)[x(t) - u(t,\phi)]d\phi \tag{1}$$

where $x(t)$ is the imposed displacement, $u(t)$ is the displacement of the Jenkins elements that constitute the Iwan model, and ϕ is the displacement at which $\rho(\phi)$ number of sliders slip. Thus, $\rho(\phi)$, also referred to as the distribution function, can be understood as the population density of the sliders, and its formulation defines the slip behavior of the Iwan model. Note that, for an SDOF system, $x(t)$ is the directly the displacement whereas for an MDOF system, it is the difference between the displacements of the DOFs that comprise the Iwan element. The dissipation due to bolted joints in the microslip regime exhibits power-law behavior [16, 82], i.e. the dissipation is a power of the amplitude of the applied load. Segalman [35] defined a distribution function for the Iwan model that is able to capture this power-law behavior. The resulting model is referred to as the four-parameter Iwan model, and its distribution function can be written as

$$\rho(\phi) = R\phi^{\chi}[\mathrm{H}(\phi) - \mathrm{H}(\phi - \phi_{\max})] + S\delta(\phi - \phi_{\max}), \tag{2}$$

where $H(.)$ and $\delta(.)$ are Heaviside and Dirac-delta functions respectively. This model form can thus be represented by the parameter set $[\phi_{\max}, \chi, R, S]$,where $\phi_{\max}$ is the displacement at which all sliders slip (i.e. macroslip occurs), χ is a dimensionless quantity that measures the power-law energy dissipation, and R and S can be understood as the stiffness of the power-law portion of the distribution and the delta function portion of the distribution respectively.

Since the parameters R and S have fractional dimension, Segalman proposed using another set of more intuitive parameters, $[F_{\mathrm{S}}, K_{\mathrm{T}}, \chi, \beta]$, with F_{S} being the force required to cause macroslip, K_{T} being the tangential stiffness of the joint at small applied loads, and χ and β being dimensionless parameters that measure the energy dissipation. Further details about the model formulation and conversion from one set of parameters to another can be found in [16].

The four-parameter Iwan model has been found effective in capturing the nonlinear hysteretic behavior due to bolted joints, in numerical case studies [19] as well as industrial structures [20]. However, simulating the dynamic response of the model can be computationally expensive since an implicit integration scheme with a small time step is required to accurately calculate the nonlinear force, and the state of all the sliders needs to be evaluated at each time step.

2.2 The Bouc-Wen Model

Another model that can capture hysteretic behavior is the Bouc-Wen model [23, 24]. This formulation is intended for any form of hysteresis and was originally applied to force – deflection and flux– current diagrams of mechanical and ferromagnetic hysteresis. In case of the Bouc-Wen model, the nonlinear restoring force is given as

$$f_{\mathrm{nl,BW}}(x, z) = (1 - \alpha) K_0 z \tag{3}$$

where K_0 is the initial low-amplitude stiffness and α is defined as the ratio of macroslip stiffness to initial stiffness. The hysteretic state variable, $z(t)$ is defined by the following ODE,

$$\dot{z} = A\dot{x} - \beta|\dot{x}||z|^{n-1}z - \gamma\dot{x}|z|^n \tag{4}$$

where A, β, γ and n are the Bouc-Wen parameters that can be tuned to fit force-displacement data obtained either experimentally or using FE simulations. This formulation provides a

computational advantage over the four-parameter Iwan model since the state variable is given by a nonlinear, first-order ODE that can easily and quickly be integrated using explicit ODE solvers. For $n = [1, 2]$, closed-form solutions for z can be obtained [45]. For other values of n, however, no further simplifications to the ODE can be made. It is preferable to allow non-integer values of n so there is more flexibility when calibrating the model. In the context of structural dynamics, the Bouc-Wen model is considered semi-physical in nature since unlike the spring-slider units in Iwan models, the state variable $z(t)$ does not have any known physical interpretation. Guo et al. [49] proposed an equivalent normalized Bouc-Wen model with parameters that can be qualitatively linked to the shape of the hysteresis curve.

The existing literature predominantly focuses on applying the Bouc-Wen model to capture the steady-state hysteretic behavior of various nonlinear systems. There has been some effort to model the hysteretic behavior of joints using the Bouc-Wen model [11,85]. Allen et al. [86] observed good agreement between a reduced-order model with nonlinearity represented using the Bouc-Wen formulation and the corresponding full FE model of a complex, large-scale aerospace structure. In bolted joints, however, the nonlinearity is also characterized by power-law dissipation behavior. This work analyses the effectiveness of the Bouc-Wen model in capturing this power-law behavior by comparing it against the four-parameter Iwan model. To do so, the Bouc-Wen parameters that best fit the force-displacement relationship of the Iwan model need to be identified.

2.3 Identifying the Parameters of the Bouc-Wen Model

An adaptation of the parametric identification method presented in [52] has been used to identify the Bouc-Wen parameters for a given load-displacement hysteretic loop. Consider an SDOF system with hysteretic nonlinearity that must be fit using the Bouc-Wen model. Let $\mathbf{x}$ be the vector of discrete displacement values and $\mathbf{f}_{\text{nl}}$ be the corresponding nonlinear restoring force, together resulting in the hysteresis loop due to steady-state oscillation. The equations for the Bouc-Wen formulation are given by Eq. 3,4. Firstly, the initial stiffness

K_0 and the parameter α can be obtained from the low-amplitude linear frequency, ω_0, and the high-amplitude slip frequency, ω_∞, of the system using the relation

$$\alpha = \left(\frac{K_\infty}{K_0}\right) = \left(\frac{\omega_\infty}{\omega_0}\right)^2. \tag{5}$$

Since the parameter A is the coefficient of the linear term in Eq. 4, it can be set to unity if the estimate of stiffness using the low-amplitude linear frequency is expected to be accurate. Next, eliminating the time dependence in Eq. 4 and switching from differential of the variables x, z to difference gives

$$\triangle z = \triangle x - \beta|\triangle x||z|^{n-1}z - \gamma\triangle x|z|^n. \tag{6}$$

The hysteretic variable z can be calculated from the nonlinear force and displacement vectors, i.e. $\mathbf{f}_{\text{nl}}$ and $\mathbf{x}$ respectively, using Eq. 7, obtained by re-arranging Eq. 3.

$$\mathbf{z} = \frac{1}{(1-\alpha)K_0}\mathbf{f}_{\text{nl}} \tag{7}$$

Note that $\mathbf{z}$ in Eq. 7 is a vector, giving the value of the hysteretic variable for every value of $\mathbf{f}_{\text{nl}}$. Therefore, from Eq. 7,

$$\triangle\mathbf{z} = \frac{1}{(1-\alpha)K_0}\triangle\mathbf{f}_{\text{nl}} \tag{8}$$

where $\triangle\mathbf{f}_{\text{nl}}$ is the difference between consecutive values of the vector $\triangle\mathbf{f}_{\text{nl}}$. Substituting Eq. 8 in Eq. 6 gives

$$\frac{\triangle\mathbf{f}_{\text{nl}}}{(1-\alpha)K_0} - \triangle\mathbf{x} = \begin{bmatrix} -\triangle\mathbf{x}|\mathbf{z}|^{n-1}\mathbf{z} & -\triangle\mathbf{x}|\mathbf{z}|^n \end{bmatrix} \begin{bmatrix} \beta \\ \gamma \end{bmatrix}. \tag{9}$$

Equation 9 is of the form $\mathbf{Y} = \Phi\Theta$ which can be solved for Θ by taking the pseudo-inverse of Φ and keeping n constant. In this way, the parameters β and γ can be calculated using

the method of least squares. To ensure that the matrix Φ is well-conditioned, each column of Φ is normalized to its corresponding maximum value. The least-squares problem is solved iteratively for different values of n, and the parameter set that results in the lowest error is used. Although the method presented in [52] considered n to be constant, variable n has been considered here since it impacts the amplitude-dependent dynamic behavior of the Bouc-Wen model, as will be discussed in Sec. 3.2. Note that this method can also be used to fit a modal Bouc-Wen model.

2.4 Modal Modeling Approach

Consider the FE model of a jointed structure with each bolted joint represented by a constitutive model. The resulting equation of motion (EoM) is given by Eq. 10,

$$\mathbf{M}\ddot{\mathbf{x}} + \mathbf{C}\dot{\mathbf{x}} + \mathbf{K}_\infty \mathbf{x} + \mathbf{f}_{\text{nl}}(x, t, h) = \mathbf{f}_{\text{ext}}(t) \tag{10}$$

where $\mathbf{M}$ is the mass matrix, $\mathbf{C}$ is the linear damping matrix, $\mathbf{K}_\infty$ is the linear stiffness matrix if all the joints were disconnected, and $\mathbf{f}_{\text{nl}}(x, t, h)$ is the vector of nonlinear joint forces given by a hysteretic model, that depend on the nodal displacement x, time t and previous state of the system h. The definition of h varies for different hysteretic models. For example, it corresponds to the slider state ϕ for the Iwan model and the hysteretic variable z for the Bouc-Wen model. As discussed earlier, it is difficult to isolate the effect of each joint on the overall system dynamics, and therefore, the calibration of the hysteretic model parameters is non-trivial.

As an alternative, Segalman [25] proposed a modal modeling approach, where each nonlinear mode of the structure is represented by a single degree-of-freedom (SDOF) system with a parallel arrangement of a linear spring, linear damper and a nonlinear hysteretic element. This approach makes two important assumptions. Firstly, it assumes that there is no coupling, or energy transfer, between the modes. This assumption holds true if the

external force results in excitation of a single, dominant mode. Eriten et al. [54] showed that in a weakly nonlinear structure, the interaction between modes is not significant if their natural frequencies, or harmonics of the frequencies, are sufficiently spaced. On the other hand, Moldenhauer et al. [55] and Wall et al. [56] showed the presence of modal coupling in two different jointed structures. Therefore, ther are limitations to the applicability of this method. In this paper, however, the modal modeling approach has been applied to a case that does not exhibit modal coupling. The second assumption is that the low-amplitude, linear mode shapes of the system are preserved and hence applicable in the amplitude range being analyzed. For weakly nonlinear structures like the ones under consideration, this is a reasonable assumption to make.

Under these assumptions, Eq. 10 is transformed to the modal domain using $\mathbf{x} = \mathbf{\Phi}_0\mathbf{q}$, where $\mathbf{\Phi}_0$ is the low-amplitude, linear mode shape matrix and $\mathbf{q}$ is the vector of modal displacements. If there is no modal coupling, the modal transformation results in the nonlinear joint force $\mathbf{f}_{\text{nl}}$ being projected onto each mode and being a function of the corresponding modal displacement, i.e. $\mathbf{\Phi}_{0r}^T\mathbf{f}_{\text{nl}}(x,h) = \hat{f}_{\text{nl}}(q_r,\hat{h})$. As a result, Eq. 10 reduces to

$$\ddot{q}_r + 2\zeta_{0r}\omega_{0r}\dot{q} + \omega_{\infty r}^2 q + \hat{f}_{\text{nl}}(q_r,\hat{h}) = \mathbf{\Phi}_{0r}^T\mathbf{f}_{\text{ext}} \tag{11}$$

for the r^{th} mode. Here, ω_{0r} is the linear frequency of the r^{th} mode at low amplitudes, when there is no slip occurring, whereas $\omega_{\infty r}$ is the frequency at macroslip. It is also assumed that the modal transformation results in a diagonal linear damping matrix, with ζ_{0r} being the low-amplitude damping ratio of the r^{th} mode. Each nonlinear mode can be independently analyzed using a suitable hysteretic model to represent the modal joint force, $\hat{f}_{\text{nl}}(q_r,h)$. Figure 1 provides a schematic of the modal model.

Modal models significantly reduce the computation cost of dynamic simulations. Deaner et al. [19] and Roettgen and Allen [20] showed that the modal Iwan model is capable of describing the nonlinearity in various bolted structures. Further, Lacayo et al. [57] found that

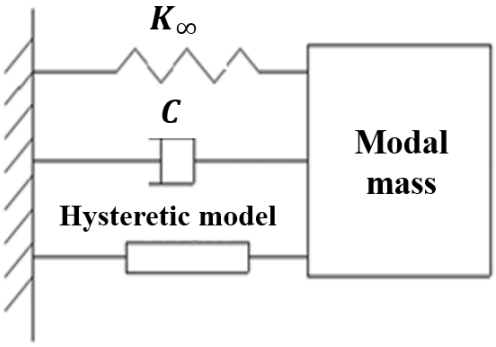

Figure 1: Modal model: SDOF system with a linear spring, damper and nonlinear element in parallel

this approach can accurately capture the nonlinear response to an impulse-type excitation (that excites different modes of the structure to varying extents) if it consists of one dominant mode, and may still be fairly acceptable in cases of more than one dominant mode, provided the mode being studied is a dominant one. This paper uses the modal modeling approach with the four-parameter Iwan model and an equivalent Bouc-Wen model fit to the nonlinear mode of a jointed structure.

3 Comparing the Bouc-Wen and Iwan models

An assembly of two beams bolted together, commonly referred to as the Sumali beam was used to compare the dynamic behavior of the Bouc-Wen and four-parameter Iwan models. The structure, as seen in Fig. 2a), consists of two thin, identical, stainless steel beams of length 508 mm, width 50.8 mm, and thickness 6.35 mm, that overlap and are joined with four bolts. Deaner et al. [19] experimentally analyzed the first three elastic modes of this structure and fit suitable modal Iwan models to capture the observed amplitude-dependent behavior. Further, Lacayo et al. [57] created an FE model of the Sumali beam and tuned the modal Iwan models such that their FE simulations closely matched the dynamic response measured by Deaner et al. In this work, the modal Iwan model identified in [57] for the second bending mode of the Sumali beam (shown in Fig. 2b) has been used. It must be noted that

the Sumali beam tends to have lower damping than other jointed structures [87]. Regardless, this structure has been considered here since its modal behavior has been thoroughly studied. Table 8 lists the parameters of the modal Iwan model that best fits the second bending mode of the Sumali beam. These parameters result in a low-amplitude linear frequency of 213.94 Hz, and a macroslip frequency of 205.86 Hz.

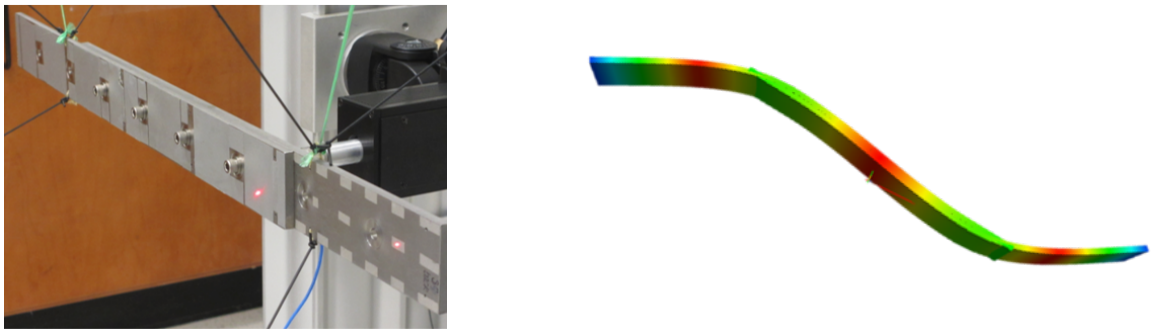

(a) **(b)**

Figure 2: (a) Sumali beam structure and (b) Mode 8, i.e. second bending mode of the Sumali beam

Table 8: Parameters of the four-parameter modal Iwan model that fits mode 8 of the Sumali beam

Parameter	Value
(K_∞) $[\mathrm{s}^{-2}]$	1.67×10^6
low-amplitude damping (ξ_0)	1×10^{-4}
F_s $[\mathrm{N\ kg}^{-1/2}]$	1.518
(K_T) $[\mathrm{s}^{-2}]$	1.34×10^5
χ	-0.162
β	2.000

3.1 Procedure for Comparison Between the Hysteretic Models

First, an equivalent Bouc-Wen model must be identified using the method of least squares, outlined in Sec. 2.3. To do so, the force-displacement relationship of the modal Iwan model was estimated by performing a quasi-static analysis. The equation for the Iwan model under static loading reduces to

$$K_\infty q + F_{\text{nl,Iwan}}(q, \phi) - F_{\text{static}} = 0, \tag{12}$$

where q is the displacement of the mode under consideration, i.e. the second bending mode of the Sumali beam in the case presented. The above equation is nonlinear in nature and of the form $f(q) = 0$. Therefore, the displacement of the modal Iwan model, q, at a particular static force can be obtained by using the Newton-Raphson method to solve Eq. 12. This was done over a range of monotonically increasing static force amplitudes, up to a maximum value of $F_{\max}$, to generate the force-displacement backbone curve. Since the Iwan model is a Masing model, Masing's rules could be applied to estimate the complete hysteresis loop at the maximum force amplitude [88]. Note that, alternatively, one could use the Newton-Raphson method to estimate the complete hysteresis loop by applying static loads that result in loading, unloading and then reloading of the system. However, application of Masing's rules gives a quicker and equally accurate result. Once the complete force-displacement hysteresis loop was calculated, the method described in Sec. 2.3 was used to estimate the equivalent Bouc-Wen model parameters.

The resultant Bouc-Wen model was first statically excited to verify the least squares solution. The Bouc-Wen static formulation can be written as

$$K_\infty q + (1 - \alpha) K_0 z - F_{\text{static}} = 0 \tag{13}$$

where the hysteretic variable, z, is calculated by solving Eq. 4. To solve Eq. 13 using the Newton-Raphson method, the modal displacement q was defined as a function of z. To do

so, first, Eq. 4 can be rearranged as

$$\dot{z} = \dot{q}(1 - |z|^n(\text{sgn}(\dot{q}z)\beta + \gamma)). \tag{14}$$

The time dependence in Eq. 14 can be eliminated, resulting in Eq. 15.

$$dq = \frac{dz}{(1 - |z|^n(\text{sgn}(\dot{q}z)\beta + \gamma))} \tag{15}$$

The integral of the above equation is given by Gauss' hypergeometric function, ${}_2F_1(a, b; c; z)$, as shown in [45]. Therefore,

$$q = q_0 + z\,{}_2F_1\left(1, \frac{1}{n}; 1 + \frac{1}{n}; (\text{sgn}(\dot{q}z)\beta + \gamma)|z|^n\right)\Bigg|_{z_0}^{z} \tag{16}$$

Substituting Eq. 16 in Eq. 13 results in a nonlinear equation of the form $f(z) = 0$, which can be solved for z using the Newton-Raphson iteration method. Equation 16 can then be used to calculate the modal displacement at the force amplitude under consideration. The Bouc-Wen system was excited up to $F_{\max}$, the same maximum force amplitude as the Iwan model, followed by a decrease in the force to cause unloading up to $-F_{\max}$, and then an increase again to cause reloading up to $F_{\max}$. Thus, the complete hysteresis loop for the Bouc-Wen model was identified. Unlike the Iwan model, the Bouc-Wen model does not obey Masing's rules. Therefore, the complete cycle needs to be numerically simulated. Note that, alternatively, the Bouc-Wen response can also be numerically estimated by applying a harmonic force of low enough frequency such that the system can be approximated as being quasi-statically excited. The nonlinear EoM can then be solved using the Runge Kutta method.

Once the equivalent Bouc-Wen model that can capture the steady-state hysteretic behavior was obtained, its ability to capture the amplitude-dependent system dynamics was tested. The response of the Bouc-Wen model to an impulsive force was simulated using the

Runge-Kutta explicit ODE solver. On the other hand, the Newmark-β method was used to simulate the response of the Iwan model. In both cases, the impulsive force was modeled as one half of a sinusoid with a width of 0.005 s and 10 s of the dynamic response was simulated. Note that one dynamic analysis of the Iwan model using the Newmark-β method took 93.22 s, whereas the Runge-Kutta method for the Bouc-Wen model took 3.86 s. Both models were being simulated on an Intel(R) Core(TM) i7 CPU 950 @ 3.07GHz. This highlights the computational advantage offered by the Bouc-Wen model. The resulting time history in both cases was then post-processed using the Hilbert transform [75, 89] to compute the amplitude-dependent frequency and damping for comparison.

This analysis method was applied to three different cases comparing the Bouc-Wen model to the Iwan model. A description of the three cases and the results are discussed below.

3.2 Effect of the Parameter n on Dynamic Behavior

The parameter n in the Bouc-Wen model is known to determine the smoothness of the transition from microslip to macroslip [84]. When the parameter n tends to infinity, a bilinear model is obtained. According to existing literature, the Bouc-Wen model is not sensitive to n [52] and in some applications, varying n does not significantly impact the results [11, 86]. The validity of this claim in case of bolted joints dynamics has been tested here.

Figure 3 shows the hysteresis loops calculated using the quasi-static analysis described in Sec. 3.1. The solid line is the estimate using the Iwan model, the dashed line is from the Bouc-Wen model with $n = 1$, and the dashed-dotted line is from the Bouc-Wen model with $n = 2$. It can be observed that the two values of n result in very similar steady-state behavior. The area inside the hysteresis loop for $n = 1$ equals 3.303×10^{-6} kgNm while that inside the hysteresis loop for $n = 2$ equals 3.725×10^{-6} kgNm, giving a difference of $\approx 12\%$. However, the amplitude-dependent frequency and damping are of primary interest when characterizing bolted joint dynamics. Therefore, the effect of change in 'n' on the

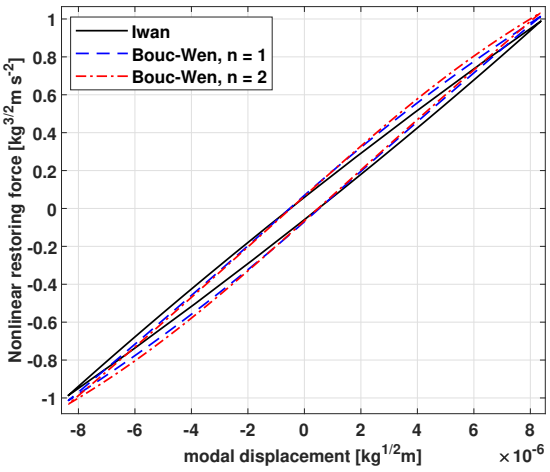

Figure 3: Hysteresis curve when $n = 1$ (dashed line) and when $n = 2$ (dashed-dotted line) compared against the Iwan model (solid line)

amplitude-dependent behavior was studied by applying an impulsive force, as described in Sec. 3.1. Figure 4 shows the frequency and the percentage error in the frequency, both plotted against the non-dimensional velocity. Note that due to the non-dimensionalization, the system is in macroslip when the X-coordinate equals 1. In the system presented, $n = 1$ is able to match the frequency estimated by the Iwan model better, with a maximum error of 0.17%. On the other hand, when $n = 2$, the frequency changes abruptly and the maximum error is 0.49%. Figure 4b plots the nonlinear damping as a function of response amplitude. Similar to frequency, the damping estimate when $n = 1$ closely matches the Iwan model, with a maximum error of 17.8% while $n = 2$ shows significant deviation, with a maximum error of 67.4%. Thus, the parameter n appears to influence the amplitude-dependent nonlinear dynamics of the system and must be accounted for when identifying the Bouc-Wen model parameters. In the following cases, the parameter identification process was performed over a range of n values and the parameter set resulting in lowest error in the least squares solution was chosen.

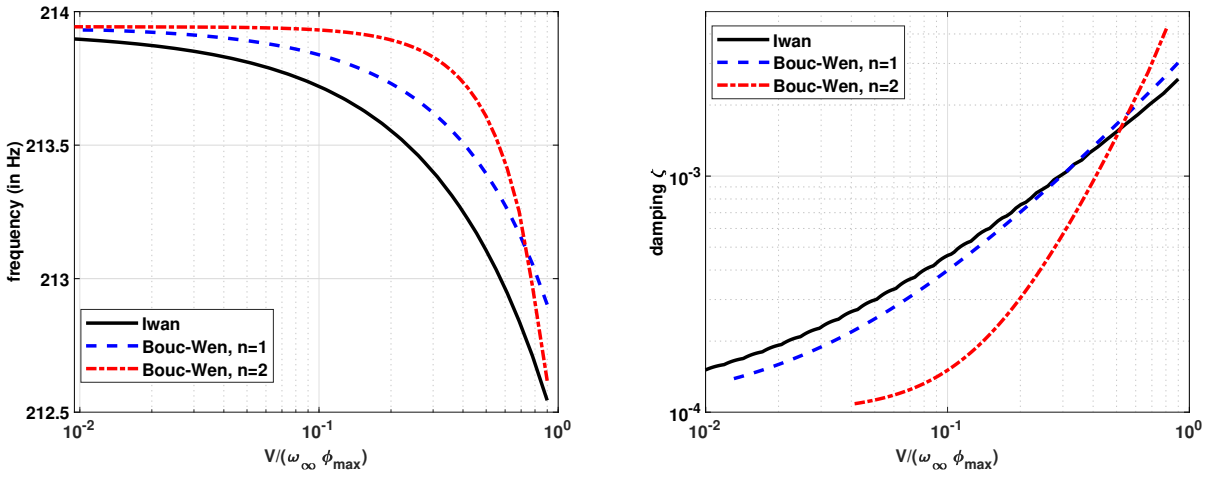

Figure 4: Amplitude-dependent (a) frequency and (b) damping, for two different values of n, compared against the Iwan modal

3.3 Effect of Forcing Amplitude on Parameter Identification

Ideally, for a given system, the resulting Bouc-Wen model obtained should not depend on the excitation level of the quasi-static analysis performed to estimate the model parameters, i.e. $F_{\max}$. This was tested by fitting a Bouc-Wen model to quasi-static hysteresis loops of the Iwan model at varying force amplitudes. To quantify the level of slip at these different force amplitudes, the amplitude ratio, AR, was defined as the ratio of the maximum displacement at the applied load to the displacement at which macroslip occurs (i.e. $\phi_{\max}$). By definition, AR = 1 indicates the amplitude of the quasi-static load applied is sufficient to cause macroslip.

$$\mathrm{AR} = \frac{x_{\max}}{\phi_{\max}} \tag{17}$$

The Bouc-Wen parameters that best fit the hysteresis loop for the different values of AR were calculated. An impulsive force, with amplitude small enough for the system to remain in microslip, was applied to each of these Bouc-Wen models and the Fast Fourier Transform, or FFT, of the dynamic response was calculated. Figure 5 shows that there is a

range of AR, specifically $0.1 < \text{AR} < 1$, for which the resultant Bouc-Wen model gives nearly identical response. If macroslip level data is being fit, i.e. when $\text{AR} > 1$, the Bouc-Wen model obtained is significantly different. This implies that two different Bouc-Wen models are required to simulate the behavior of an Iwan model.

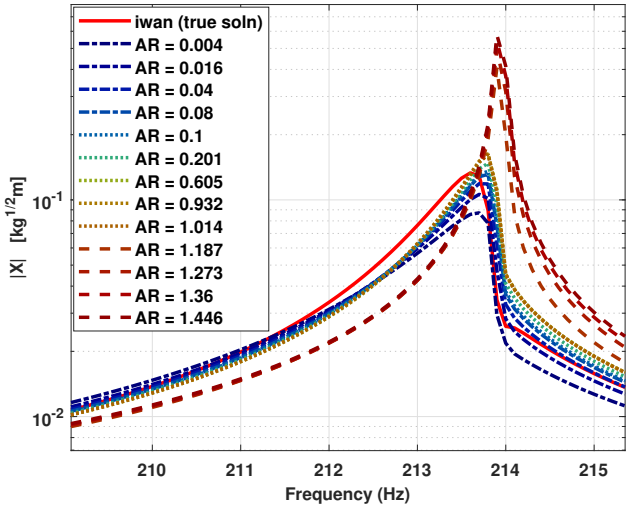

Figure 5: FFT of the response to an impulsive force applied to the Bouc-Wen models obtained using different values of amplitude ratio (AR)

The amplitude-dependent dynamic behavior was analyzed to further verify this claim. Two AR values were considered. For the first value, the model is in microslip ($\text{AR} = 0.4$) while for the second, it is in macroslip ($\text{AR} = 1.23$). An impulsive force large enough to capture both macroslip and microslip behavior was applied to both models and the resultant frequency and damping were calculated. As seen in Fig 6, the Bouc-Wen model obtained using $\text{AR} = 0.4$, shown using dashed lines, is able to estimate the frequency and damping in the microslip regime but is inaccurate in the macroslip regime. Note that a value of 1 on the X-axis corresponds to the onset of macroslip. On the other hand, the nonlinear dynamic behavior obtained using $\text{AR} = 1.23$, shown using dashed-dotted lines, is accurate in the macroslip region but not in microslip. This further proves that the same Bouc-Wen model cannot replicate both microslip as well as macroslip behavior of the Iwan model. Another observation of note here is that the Bouc-Wen model that best fits microslip data has parameter $n = 1$, whereas the model that best fits macroslip data has $n = 5.1$. This also

highlights the need to vary the parameter 'n', as discussed in Sec. 3.2.

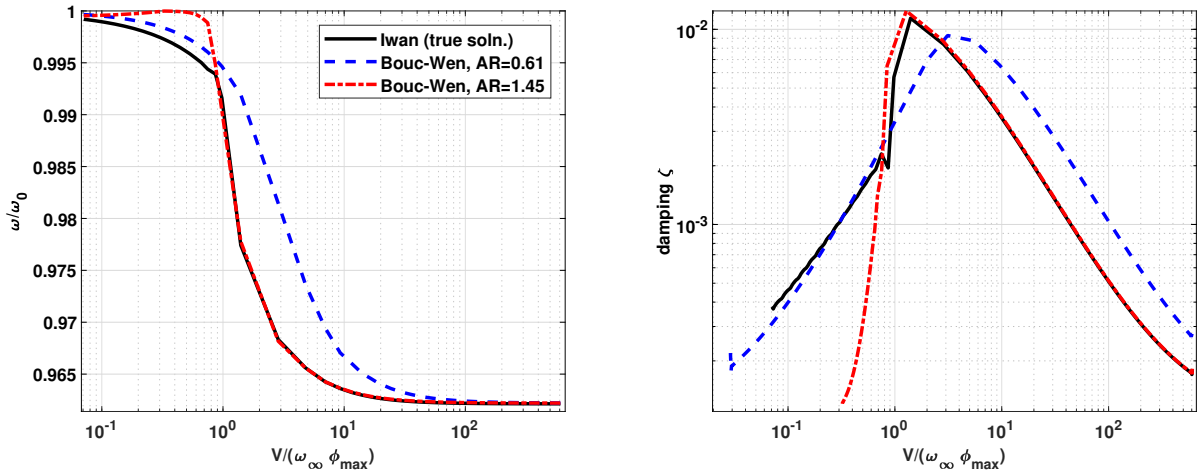

Figure 6: Comparing the nonlinear (a) frequency and, (b) damping when the AR used for fitting the Bouc-Wen model corresponds to microslip (dashed line) vs. macroslip (dashed-dotted line). The solid line is the result from the Iwan model.

3.4 Accuracy of the Bouc-Wen Model at Different Dissipation Levels

The parameter χ in the four-parameter Iwan model directly relates to the power-law behavior of the dissipation per cycle, or the damping [35]. The slope of the damping vs amplitude, when plotted on a logarithmic scale, equals $1+\chi$. This corresponds to the dissipation energy having a slope of $3+\chi$. The value of χ typically varies between -1 and 0, with $\chi = -1$ corresponding to linear damping. To test how well the Bouc-Wen model can simulate the power-law behavior, the parameter χ in the modal Iwan model of the Sumali beam was varied. As seen in Table 8, the Iwan model that best represents mode 8 of the Sumali beam uses $\chi = -0.162$. This corresponds to the damping curve having a slope of 0.838 in the log-log scale. The corresponding Bouc-Wen model was compared against this model using the procedure outlined in Sec. 3.1. Note that a microslip-level Bouc-Wen model was fit,

since the power-law behavior is observed in the microslip region. Therefore, the amplitude of impulsive force applied to compare the two models was also limited to excitation in the microslip regime. The damping curve obtained after post-processing is shown in Fig. 7a. In this case, the Bouc-Wen model exhibits a similar trend to the Iwan model but underestimates the damping, with a maximum error of 18.1%. Next, the value of χ in the model was changed to -0.6, resulting in the damping curve having a slope of 0.4 in the log-log scale. The model identification and dynamic response verification process was repeated. Figure 7b shows the resultant instantaneous damping comparison. Here, the Bouc-Wen model significantly deviates from the Iwan model, with a maximum error of 67.2%. Therefore, it appears that the Bouc-Wen model is less accurate in bolted joint systems where the slope of the damping versus amplitude curve in the logarithmic scale is lower.

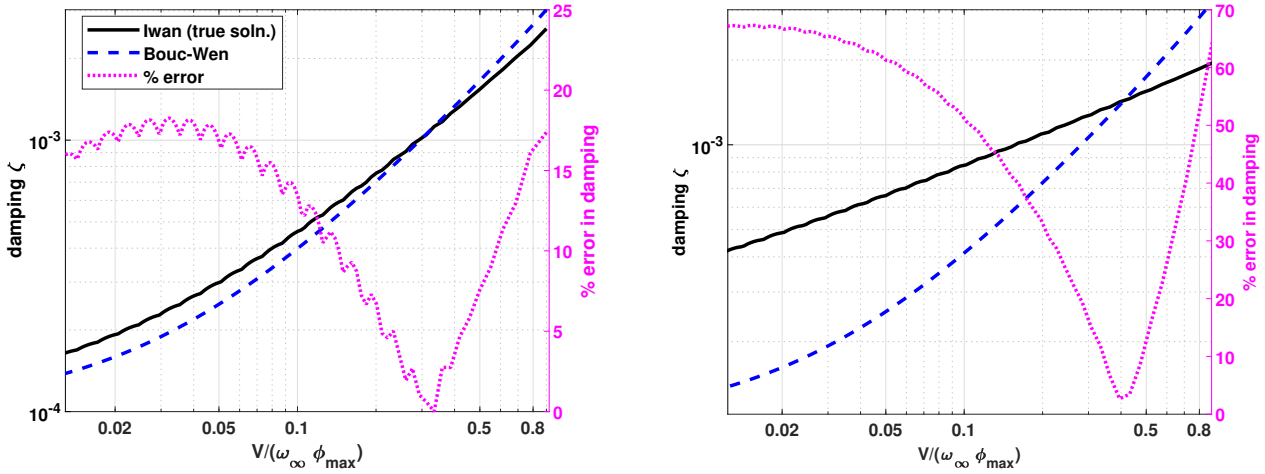

(a) $\chi = -0.162$ **(b)** $\chi = -0.6$

Figure 7: Comparing the damping estimated by the Bouc-Wen model against the Iwan model when (a) $\chi = -0.162$, and when (b)$\chi = -.6$ for the Iwan model

Several different values of the parameter χ were considered to explore the Bouc-Wen model's capability to capture the full range of nonlinear dissipation behavior exhibited by the Iwan model. For every value of χ, the Bouc-Wen model that best fits the quasi-static response of the Iwan model was estimated. Then, the response of both the Bouc-Wen and

Iwan models to an impulsive force was calculated. Figure 8 compares the nonlinear damping as a function of amplitude for five of the χ values considered. The different colors correspond to different values of χ. For each color, the solid line is the damping for the Iwan model, and the dashed-dotted line of the same color is the damping for the best-fit Bouc-Wen model. Both axes have logarithmic scales so that the power-law behavior can be easily observed. As expected, the Iwan model gives straight lines of varying slopes for different χ values, and the slope increases as the value of χ increases (note that χ assumes negative values). The Bouc-Wen model, on the other hand, exhibits little difference in the damping behavior, regardless of the value of χ used to estimate its parameters. While the damping versus amplitude is a straight line, indicating the dissipation is a power of the response amplitude, the slope of the line itself has little variation. For lower values of χ, the equivalent Bouc-Wen model shows significant deviation from the Iwan model damping curve. However, for higher χ values, for example when $\chi = -0.01$, the damping estimated by the Bouc-Wen model closely matches the Iwan model. This indicates that the Bouc-Wen model is more suitable when the power of the damping as a function of response amplitude is closer to 1.

4 Effect of Each Bouc-Wen Parameter on the Damping

In the different case studies considered above, all the parameters of the Bouc-Wen model were allowed to vary such that the resultant set best fit the Iwan model behavior. This section studies the effect of changing a single parameter at a time on the damping behavior of the Bouc-Wen model. To do so, the Bouc-Wen parameters that best fit the Iwan model for mode 8 of the Sumali beam were considered as a starting point. First, the parameter β was varied from 0.8×10^4 to 1.5×10^5, increasing by nearly 20 times over the range. Note that the value of β for the Sumali beam model was 2.38×10^4, thus lying within the range considered here. An impulsive force was applied to the resulting Bouc-Wen model for all values of β, and the time history was post-processed using the Hilbert transform to estimate the amplitude-

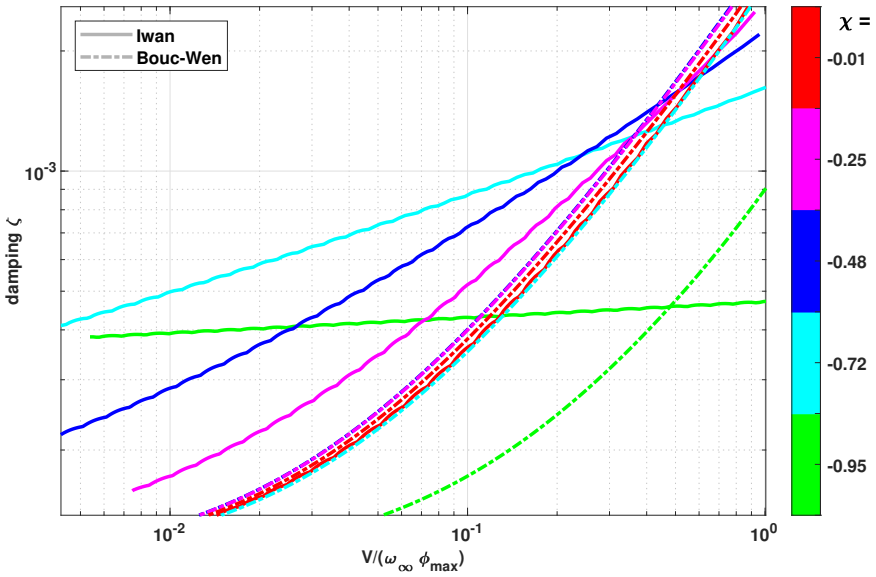

Figure 8: Comparing the damping estimated by the Bouc-Wen model against the Iwan model for different values of the Iwan model parameter χ. This parameter changes the slope of the damping vs. response amplitude curve, when plotted on a logarithmic scale. The solid lines correspond to the Iwan model and the dashed-dotted lines represent the Bouc-Wen model estimate. The different colors correspond to different values of χ between -1 and 0.

dependent damping. Figure 9a shows the damping for the different values of β. It can be seen that increasing β results in the damping curve shifting upwards, along the Y-axis. This means that for the same response amplitude, a higher β results in a higher damping (or dissipation of energy). However, the slope of the curve itself shows negligible change. Next, the Bouc-Wen parameter γ was varied, with all other parameters corresponding to the model that best fit the Sumali beam mode. The original value of γ was 5.18×10^5. Therefore, it was varied from 1×10^4 to 1×10^6, a hundredfold increase over the range. The nonlinear damping for all values of γ was estimated using the response to an impulsive force, with the results plotted in Fig. 9b. At low response amplitudes, the damping curves show negligible difference. However, as the amplitude increases and approaches macroslip, the curves diverge. Note that macroslip is the point at which the damping is the highest. As γ increases, the point at which macroslip occurs shifts to the left along the X-axis, i.e. to a lower response amplitude. Therefore, the parameter γ impacts the damping behavior of the Bouc-Wen

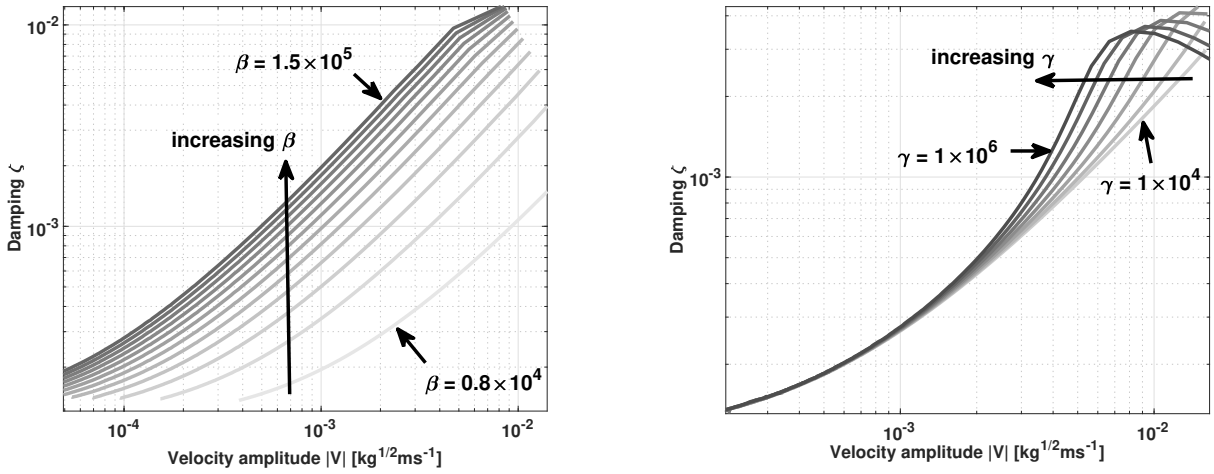

Figure 9: Effect of varying the Bouc-Wen parameters (a) β, and (b) γ on the amplitude-dependent damping

model only near macroslip; the lower-amplitude microslip behavior is largely unaffected. Finally, the parameter n, that appears as an exponent in the differential equation defining the Bouc-Wen model, was varied. Note that in Sec. 3.2, for each value of n considered, all the Bouc-Wen parameters were updated to get the best fit. Here, however, only n was varied, setting all other parameters equal to the modal model for the Sumali beam. Figure 10 shows the resultant amplitude-dependent damping for $1 \leq n \leq 2$. Increasing n results in the damping curve shifting horizontally towards the right. This means that for the same response amplitude, a higher value of n gives lower damping, provided the system is in microslip. The increase in n also results in a delay in macroslip, i.e. a larger amplitude is required to cause the system to go into macroslip. However, the slope of the damping curve in the microslip regime remains largely unaltered. Note that these observations can be extrapolated to higher values of n. A smaller range was chosen here for clear visualization of the trends exhibited.

Through this study, it can be concluded that, unlike the Iwan model, none of the parameters of the Bouc-Wen model can capture the power-law dissipation behavior in the microslip

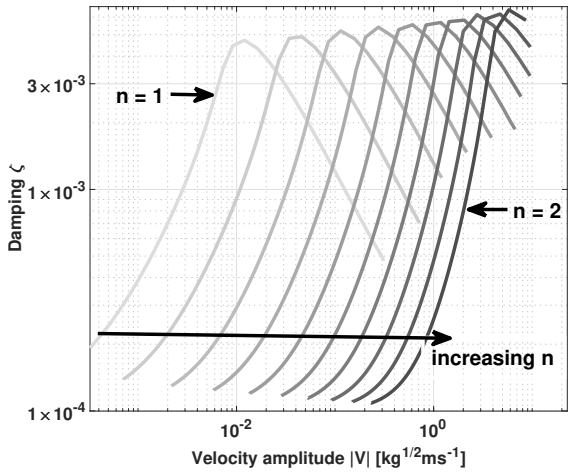

Figure 10: Effect of varying the Bouc-Wen parameter n on the amplitude-dependent damping

regime.

5 Conclusions

This paper compared the nonlinear dynamics simulated by the Bouc-Wen model against the Iwan model. A procedure to estimate the parameters of the Bouc-Wen model from the force-displacement hysteretic loop of an Iwan model was presented. Then, the response of both models to an impulsive force was simulated. The nonlinear frequency and damping were estimated from the dynamic response, and the Bouc-Wen model's ability to capture the amplitude-dependent behavior was studied.

Three important results were obtained by comparing the Bouc-Wen model to the four-parameter Iwan model. First, it was observed that the value of the Bouc-Wen parameter n has a significant effect on the amplitude-dependent frequency and damping estimated by the model. While existing literature shows that the hysteresis loop itself is not sensitive to small changes in n, this paper shows that n needs to be varied to improve the accuracy of transient dynamic response estimated by the Bouc-Wen model. The second observation was that the Bouc-Wen parameters are different for microslip and macroslip level nonlinearity. For low

amplitude ratios, when the system is in microslip, the Bouc-Wen model parameters are repeatable regardless of the amplitude ratio. However, once the system goes into macroslip, a different set of parameters are required to best fit the hysteretic behavior. Thirdly, the effect of changing the parameter χ, that defines the power-law dissipation behavior of the Iwan model, was studied. A lower value of χ corresponds to the dissipation versus amplitude curve having a lower slope, when plotted in the logarithmic scale. It was found that the Bouc-Wen model was better suited to capture the power-law relationship between dissipation and amplitude for values of χ near 1, i.e. when the dissipation is near the third power of the response amplitude.

The effect of each Bouc-Wen parameter on the overall damping was also studied. It was found that increasing the parameter β causes the damping curve to shift vertically upwards, while increasing n results in a horizontal shift. However, the slope of the damping curve in the microslip regime does not change significantly in either case. On the other hand, the parameter γ changes the slope of the curve near macroslip, with the damping at lower-amplitudes remaining largely unaffected. Thus, none of the Bouc-Wen model parameters can capture the microslip-level power-law damping behavior that is known to be characteristic of bolted joints.

Paper III: A Non-Parametric Iwan Model Derived from Quasi-Static Force-Displacement Data

Built-up structures are known to show nonlinear, hysteretic behavior due to the slipping of interfaces that are bolted together. The Iwan model, which is a category of Masing models, is commonly used to simulate this nonlinear behavior. There have been many adaptations of the Iwan model, with the key distinction between them being the definition of the distribution function which determines force-displacement relationship of the joint. These existing models, however, are parametric in nature; the flexibility offered by them is limited to the finite number of parameters that can be tuned and in several cases, this has led to frustration when the model does not fit experimental measurements as well as is expected. This paper presents an alternative, non-parametric approach in which the distribution function itself is derived from the backbone curve of the hysteretic system, thus allowing for greater flexibility. Quasi-static analysis is used to obtain the backbone curve of a system, and a model inversion method is implemented to characterize it using a non-parametric Iwan element, which can then be integrated to simulate the system's dynamic response at a greatly reduced computational cost as compared to integrating the full model. Two numerical case studies are considered to verify the proposed approach. The results show that the proposed model is orders-of-magnitude faster that integrating the whole FE model and provides greater accuracy than the four-parameter Iwan model.

1 Introduction

Built-up structures assembled together using mechanical fasteners exhibit energy dissipation and loss of stiffness due to friction at the contact surfaces [4, 5]. At low tangential loads, the edges of the joint surfaces slip while a majority of the joint remains clamped due to the bolt preload. This is known as microslip. In the microslip regime, the stiffness of the joint decreases only slightly with increase in vibration amplitude, but there is significant energy loss, leading to a large increase in damping [17]. This behavior has been observed in numerous experimental studies [18–20]. As the tangential load amplitude increases, the slip region gradually expands until macroslip occurs. This is characterized by relative motion between the surfaces and significant decrease in joint stiffness. The dynamic response of a structure at resonance, and, as a result, to random excitation, depends on the damping [21]. Thus, it is important to estimate the damping due to friction at the interfaces.

Simulating the dynamic behavior of a built-up structure by creating a high-fidelity Finite Element (FE) model of the bolted interfaces is computationally expensive, since a very fine mesh is required to capture the low-amplitude microslip behavior [9]. An alternative is to replace the contact interface with a lumped, hysteretic model capable of simulating the microslip and macroslip behavior observed. In an FE model, this can be done using the whole-joint modeling approach [16], where the nodes on each contacting surface are tied to a representative node using element spiders. A suitable hysteretic model is then added between the virtual nodes of opposing surfaces. While more efficient in comparison to the high-fidelity FE model, this method requires computationally intensive optimization schemes to identify the underlying hysteretic model(s) [53]. Alternatively, Segalman proposed a modal modeling approach [25] that takes advantage of the weakly nonlinear behavior of jointed structures. In this approach, the nonlinear mode can be represented by a single degree-of-freedom (SDOF) system with a parallel arrangement of a linear spring, linear damper and the hysteretic model, provided there is no coupling between the modes. Lacayo et al. [57] found that the modal modeling approach gives accurate results if the mode of interest is dominant in the

response being studied.

Mathis et al. [30] presented an overview of various rate-dependent and rate-independent hysteretic models that can be used to simulate the nonlinear dynamics due to joints. While several hysteretic models exist [23,27], the Iwan model [22] is commonly used for bolted joint nonlinearity due to its convenient physical interpretation. In the Iwan model, the hysteretic system can be understood as a combination of a large number of ideal elastoplastic elements, also known as Jenkins elements [90], with a distribution function describing the strength of these elements. Segalman [35] derived a four-parameter Iwan model that uses a power law distribution function, which captures energy dissipation that varies exponentially with vibration or load amplitude. The parameters for the hysteretic model can be identified using experimental or numerically simulated data. For example, Deaner et al. [19] fit modal Iwan models to the first three bending modes of a simple two-beam structure using experimental frequency and damping data. Additionally, Roettgen and Allen [20] showed that modal Iwan models could be obtained for a more complex, industrial structure (in this case, two catalytic converters that were joined to a plate using four bolts). On the other hand, quasi-static methods have been developed to numerically simulate the nonlinear force-displacement relationship, which can then be used to identify the hysteretic model parameters that best fit the nonlinearity [26,58,62]. The most commonly used method among them is the method of Quasi-Static Modal Anlaysis, or QSMA [26]. In this method, a quasi-static load of varying amplitude is applied representing the inertial load when the structure vibrates in the shape of the mode of interest. The corresponding deflection is calculated using any finite element package, thus giving the force-displacement backbone curve for initial loading. The Masing hypothesis [88, 91] can then be used to estimate the complete hysteresis loop from the backbone curve Lacayo and Allen further showed how the frequency and damping can be calculated using the secant stiffness and the area inside the hysteresis loop. While Lacayo and Allen used QSMA to update FE model parameters to match experimental data, other studies have applied QSMA to predict the damping and frequency of nonlinear modes of a

jointed structure using its FE model [59, 60].

The constitutive relationship of the Iwan model is described by the definition of the distribution function. There are numerous adaptations of the Iwan model [36, 37, 39], other than Segalman's four-parameter model. However, all of these models rely on a fixed number of parameters that define the distribution function. Therefore, they are limited in their ability to capture the hysteretic behavior of a joint. There are some cases where the nonlinearity due to bolted joints cannot be well-represented by the parametric Iwan model [86], thus motivating the development of a more flexible Iwan model. This paper proposes a novel, non-parametric form of the Iwan model, using the backbone curve due to initial loading to directly obtain the distribution function. Segalman and Starr [92] presented a relationship between the backbone curve and the distribution function for a Masing model. They applied this relationship to invert different Masing models and represent them as equivalent Iwan models. In this paper, the relationship is instead used to extract a non-parametric modal Iwan model from force-displacement data that has been obtained by applying QSMA on the nonlinear mode of interest. The modal model can then be numerically integrated to obtain the system's dynamic response to different loading conditions.

The following section of the paper gives an overview of the distribution function and the method of QSMA, followed by the proposed method of using QSMA to calculate the distribution function. Section 3 presents a 2D FE model of two cantilever beams clamped together by a single bolt. A non-parametric Iwan model is fit to the first bending mode of this structure. The dynamic analysis results are compared with the four-parameter Iwan model as well as the full FE model, showing that the proposed approach gives accurate results. A second case study is presented in Sec. 4, of the same assembly but with two bolts having different preload forces (or bolt torques). The non-parametric Iwan model is able to capture variations in damping and frequency due to the different preload forces, while the commonly used four-parameter model cannot, thus highlighting the simulation improvement offered by the proposed model.

2 Theory

2.1 The Iwan Model and the Distribution function

The nonlinear force due to friction is hysteretic in nature, i.e. it depends on current as well as past states of the system. The Iwan model [22] is a numerical model that can capture this hysteretic behavior. The restoring force due to an Iwan element can be written as

$$f_{\mathrm{nl}}(x,t,\tilde{\phi}) = \int_0^\infty k\tilde{\rho}(\tilde{\phi})[x(t) - \tilde{x}_{\mathrm{s}}(t,\tilde{\phi})]d\tilde{\phi} \tag{1}$$

where $x(t)$ is the imposed displacement, $\tilde{x}_{\mathrm{s}}(t)$ is the current displacement of the sliders, k is the stiffness of each Jenkins element, and $\tilde{\rho}(\tilde{\phi})$ is the population density of sliders having strength $\tilde{\phi}$. Note that $\tilde{\phi}$ here has units of force. Equation 1 can be written as the sum of the forces due to sliders that have slipped and the forces due to the sliders that remain stuck, given by Eq. 2.

$$f_{\mathrm{nl}}(x,t,\tilde{\phi}) = \int_0^{kx} \tilde{\phi}\tilde{\rho}(\tilde{\phi})d\tilde{\phi} + kx\int_{kx}^\infty \tilde{\rho}(\tilde{\phi})d\tilde{\phi} \tag{2}$$

Here, the first time on the right hand side is the force due to the sliders that have slipped when the imposed displacement is x, and the second term is the force due to the sliders that are stuck. Segalman [35] showed how the stiffness k can be eliminated from Eq. 2 by a change of variables,

$$\begin{aligned} \phi &= \frac{\tilde{\phi}}{k} \\ \rho(\phi) &= k^2\tilde{\rho}(k\phi) \end{aligned} \tag{3}$$

where ϕ is now the displacement at which $\rho(\phi)$ number of sliders slip. Due to this change of variables, Eq. 2 can be rewritten as

$$f_{\mathrm{nl}}(x,t,\phi) = \int_0^x \phi\rho(\phi)d\phi + x\int_x^\infty \rho(\phi)d\phi. \tag{4}$$

Thus, $\rho(\phi)$, known as the distribution function, completely characterizes the Iwan model. Taking a derivative of Eq. 4 with respect to the imposed displacement, x, results in Eq. 5

$$\frac{\partial F_{\text{nl}}}{\partial x} = x(t)\rho(x) + \int_0^\infty \rho(\phi)d\phi - x(t)\rho(x) \tag{5}$$

A second derivative of the nonlinear force with respect to x ultimately results in Eq. 6, thus giving a relation between the distribution function and the force-displacement data. Iwan [31] presented a similar result for the distribution function in terms of the stress-strain curve.

$$\begin{aligned} \frac{\partial^2 F_{\text{nl}}}{\partial x^2} &= -\rho(x) \\ \rho(\phi) &= -\left.\frac{\partial^2 F_{\text{nl}}}{\partial x^2}\right|_{x=\phi} \end{aligned} \tag{6}$$

Therefore, if the force-displacement relation is known, the underlying distribution function that defines the corresponding Iwan model can be calculated using Eq. 6. Segalman [35] proposed truncating the distribution function above and adding a dirac delta term at the point where macroslip occurs, i.e. when all sliders have slipped. The amplitude of the dirac delta is determined by the stiffness at initiation of macroslip. The method used for estimating this stiffness will be discussed in Sec. 2.3.

2.2 Overview of Quasi-Static Modal Analysis

Consider the Equation of Motion (EoM) of a multi degree-of-freedom (MDOF) nonlinear dynamic system, given by Eq. 7,

$$\mathbf{M}\ddot{\mathbf{x}} + \mathbf{C}_{\text{lin}}\dot{\mathbf{x}} + \mathbf{K}_\infty\mathbf{x} + \mathbf{f}_{\text{nl}}(x, t, \phi) = \mathbf{f}_{\text{ext}}(t) \tag{7}$$

where $\mathbf{C}_{\text{lin}}$ is the linear damping coefficient matrix, $\mathbf{K}_\infty$ is the linear stiffness matrix when the response amplitude is high enough to cause macroslip at the bolted interfaces, and $\mathbf{f}_{\text{ext}}(t)$ is the external force applied at the nodes. The displacement, velocity, and acceleration of

the DOFs are given by $\mathbf{x}, \dot{\mathbf{x}}, \ddot{\mathbf{x}}$ respectively. Linearizing Eq. 7 about $\mathbf{x} = 0$ and performing an eigen value analysis gives the natural frequencies, $\boldsymbol{\omega}_0$, and the mode-shapes, $\boldsymbol{\Phi}$ when all joints are stuck. If the nonlinear force-displacement relationship of the r^{th} mode is of interest, a static load is applied in the shape of mode r, so that it predominantly excites the r^{th} mode. The applied load must be $f_{\text{ext}} = \mathbf{M}\boldsymbol{\Phi}_r$, where $\boldsymbol{\Phi}_r$ is the low-amplitude linear mode-shape of the r^{th} mode [26]. This results in the following quasi-static problem:

$$\mathbf{K}_\infty \mathbf{x} + \mathbf{f}_{\text{nl}}(\mathbf{x}, \phi) = \boldsymbol{\beta}\mathbf{M}\boldsymbol{\Phi}_\mathbf{r}. \tag{8}$$

where $\boldsymbol{\beta}$, is the vector of monotonically increasing force levels, from zero to the level of interest. Equation 8 can be solved for $\mathbf{x}$ using a finite element package. Now, to retrieve the force-displacement relation of the r^{th} mode, the force applied to the structure and the displacement calculated need to be converted from the physical to the modal domain. This can be done using Eqs. 9 and 10.

$$\mathbf{f}_{\text{modal}} = \boldsymbol{\Phi}_r^{\text{T}} \boldsymbol{\beta}\mathbf{M}\boldsymbol{\Phi}_r = \boldsymbol{\beta} \tag{9}$$

$$q_r(\beta) = \boldsymbol{\Phi}_r^T \mathbf{M} x(\beta) \tag{10}$$

In this way, the force-displacement relation for the nonlinear mode of a structure, β versus $q_r(\beta)$, can be calculated by solving a quasi-static problem.

2.3 Extracting distribution function from backbone curve

Equation 6 gives the relationship between the distribution function and the force-displacement curve. It shows that the distribution function can be calculated by taking two derivatives of the nonlinear force, written as a function of the displacement, with respect to the displacement. However, QSMA gives the force at discrete values of displacement, not in some functional form that can be easily differentiated. Directly computing the numerical deriva-

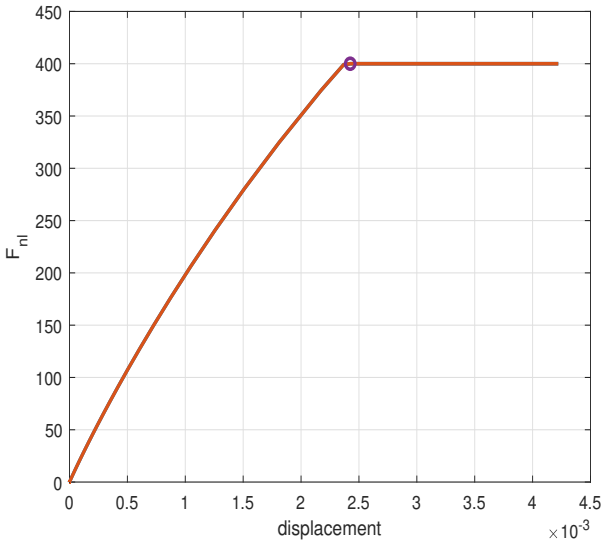

Figure 1: Example of force vs. displacement backbone curve highlighting the onset of macroslip

tive, for example by using the central difference method, gives inaccurate results since the QSMA backbone curve is noisy and taking a derivative further amplifies the noise. Therefore, some form of curve-fitting and mathematical post-processing is required. Additionally, the distribution function needs to be truncated at the macroslip displacement using a dirac delta function. Therefore, the macroslip displacement and the coefficient of the dirac delta term also need to be identified. A procedure for obtaining a discrete form of the distribution function from the force-displacement backbone curve has been explained below.

Estimating $\phi_{\max}$: Figure 1 gives an example of a backbone curve with the macroslip point circled. As can be seen, the slope of the force vs. displacement is zero when the Iwan element is in macroslip. The numerical derivative of the backbone curve is calculated and the displacement corresponding to numerical zero stiffness (up to computation accuracy) is stored as an estimate of $\phi_{\max}$.

Discretization of ϕ: The slider strength, ϕ, ranges from 0 to $\phi_{\max}$. For numerical computations, this range is divided into a set of discrete values at which the corresponding slider distribution, $\rho(\phi)$ is calculated. Segalman [35] proposed breaking up the interval $(0, \phi_{\max})$ into N intervals with the lengths forming a geometric series. Therefore, the spacing

between consecutive values of ϕ can be given by Eq. 11.

$$\triangle\phi_{\mathrm{m+1}} = \alpha\triangle\phi_{\mathrm{m}},\ \forall\ (m+1) < N \tag{11}$$

A value of N between 30 and 100 is typically sufficient to capture the nonlinearity in bolted joints. In Eq. 11, $\alpha = 1$ results in uniform spacing between consecutive points while $\alpha > 1$ results in the density of points decreasing as ϕ increases. The value of α must be chosen such that the density of points is higher in regions where the distribution function is changing rapidly. Generally, α is chosen to be slightly greater than 1 (typically 1.2) to ensure that the low-amplitude nonlinearity is accurately captured. Since the sum of intervals must equal ϕ_{max}, using the equation for the sum of a geometric series gives,

$$\triangle\phi_1 = \phi_{\mathrm{max}}\frac{\alpha - 1}{\alpha^N - 1}. \tag{12}$$

Any interval, $\triangle\phi_m$ can thus be written in terms of the initial interval, $\triangle\phi_1$, using Eqs. 11-12,

$$\triangle\phi_{\mathrm{m}} = \alpha^{m-1}\triangle\phi_1. \tag{13}$$

Therefore, Eqs. 12 and 13 can be used to obtain a vector of discrete values of the slider strength, $\boldsymbol{\phi}$.

Estimating $\rho(\phi)$ from the backbone curve: To calculate the distribution function using Eq. 6, first a piece-wise spline fit to the force-displacement data, i.e. β vs $q_r(\beta)$ was estimated in order to smooth out any noise in the backbone curve. The number of points per spline and the order of the polynomial were chosen depending on the number of data points available on the force-displacement curve and the shape of the curve. Typically, a 3^{rd}– 4^{th} order spline was found sufficient. Once the backbone curve has been fit, the distribution

function is evaluated for the slider strengths given by vector $\boldsymbol{\phi}$ using Eq. 14,

$$\rho_i = -\frac{\partial^2 S_{\mathrm{nl},i}}{\partial q^2}\bigg|_{q=\phi_i}, \forall i < N \tag{14}$$

where $S_{\mathrm{nl},i}(q)$ is the polynomial function of the spline when $q = \phi_i$. Thus, ρ_i is equals the density of sliders that slip at displacement ϕ_i. In this way, the discrete form of the distribution function can be obtained.

It must be noted that although the derivation for $\rho(\phi)$ in section 2.1 uses the nonlinear force f_{nl}, the total restoring force (i.e. $\mathbf{f}_{\mathrm{r}} = \mathbf{f}_{\mathrm{nl}} + K_\infty \mathbf{q}$) or the purely nonlinear component of the force (i.e. $\mathbf{f}_{\mathrm{nlr}} = \mathbf{f}_{\mathrm{r}} - K_0 \mathbf{q}$) can also be used since the linear stiffness term does not influence the second derivative of the force. K_0 here is the stiffness at low force amplitudes, also referred to as the linear "stuck" stiffness.

Estimating the Dirac delta stiffness: A Dirac delta function, $\delta(\phi - \phi_{\max})$, is added to the distribution function in order to allow the system to exhibit macroslip. The coefficient of the Dirac delta function is known as the Dirac delta stiffness, denoted by S. The value of S should be such that the total low-amplitude tangential stiffness estimated from the distribution function, denoted by $K_{\mathrm{T},\rho}$, must be equal to the initial slope of the backbone curve.

The expression for $K_{\mathrm{T},\rho}$ can be written as

$$K_{\mathrm{T},\rho} = \int_0^\infty \rho(\phi) d\phi. \tag{15}$$

For a discrete case, the integral would change to a summation as shown in Eq. 16,

$$K_{\mathrm{T},\rho} = \sum_{i=1}^{N-1} \rho_i(\phi_i) \triangle \phi_i + S \tag{16}$$

where N is the number of discretization points. The initial slope of the backbone curve, denoted by $K_{\mathrm{T,f}}$ can be calculated from the force and displacement vectors using finite

difference. This is set equal to Eq. 16, giving Eq. 17 that can be solved for S using the estimate of ϕ_{max} obtained as explained earlier.

$$K_{\mathrm{T,f}} = \frac{(\triangle f_{\mathrm{nl}})_i}{(\triangle q)_i}\bigg|_{i=1} = \sum_{i=1}^{N-1} \rho_i(\phi_i)\triangle\phi_i + S \tag{17}$$

It must be noted here that since the value of $\phi_{\max}$ estimated can only be as accurate as the interval between the discrete points on the backbone curve, choosing stiffness S using this method compensates for any minor errors in $\phi_{\max}$.

In this way, the distribution function for the Iwan model can be defined without the use of a finite set of parameters.

3 Numerical case study - Cantilever beam with a single bolt

The efficacy of the proposed method was tested on the two-dimensional Finite Element (FE) model constructed by Jewell et al. [59], shown in Fig. 2. The model consists of two steel beams, each 203 mm long and 6.35 mm thick, with fixed boundary condition applied at one end of the assembly. A 6.35 mm diameter bolt is modeled by applying a pressure load of 1.76×10^7 Pa on both faces of the beams over a 6.35 mm long section located 25.4 mm from the free end. Frictional contact between the beams is modeled, with the coefficient of friction $\mu = 0.6$. Friction is expected to be the only source of damping in the model. Further details about the model can be found in [59]. This section presents the results of fitting a non-parametric Iwan model to mode 1, the first bending mode of the stacked beam assembly, having a natural frequency of 198.23 Hz. First, the force vs displacement backbone curve was obtained by implementing the method of QSMA on the FE model, using the procedure documented in [59]. The load amplitude was specified in terms of the resulting vertical deflection at the free end. To extract the distribution function, the complete backbone curve

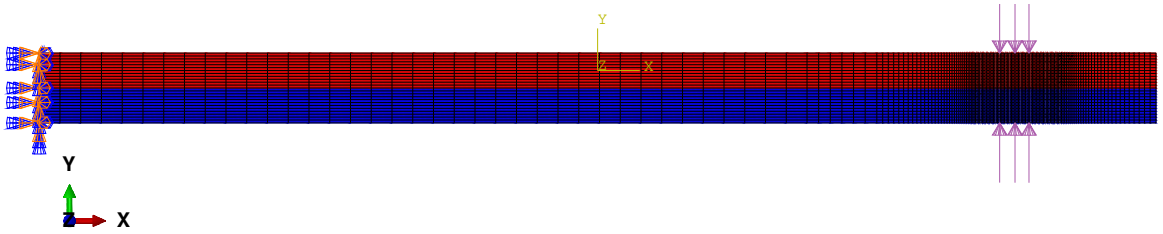

Figure 2: 2D FE model of the cantilever beam assembly

from zero displacement to macroslip is required. While a single quasi-static analysis over the entire range of corresponding load amplitudes can be performed, it was observed that doing so reduces the accuracy with which low-amplitude behavior is captured. Thus, two separate quasi-static analyses were performed - one resulting in a maximum tip deflection of 0.127 mm and the second, 0.698 mm. Figure 3 shows the two backbone curves obtained.

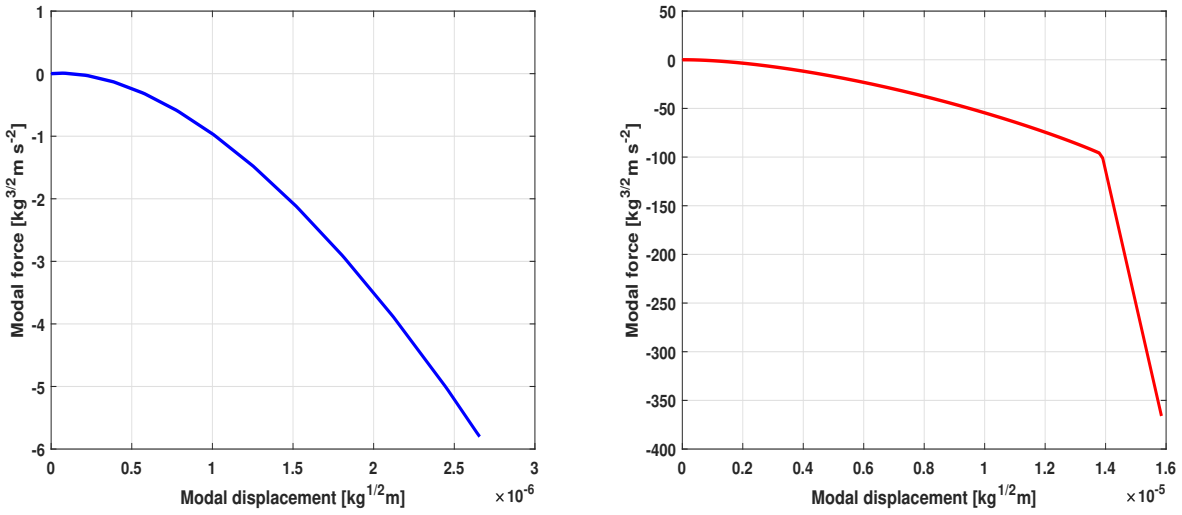

(a) Amplitude range from zero to 0.127 **mm tip deflection** **(b) Amplitude range from zero to** 0.698 **mm tip deflection**

Figure 3: Purely nonlinear component of the modal force (F_{nlr}) vs modal displacement obtained by performing QSMA on the cantilever beam assembly

The distribution function was then extracted from the two backbone curves using the procedure detailed in section 2.3. The low and high amplitude curves were processed separately and the resulting distribution functions were combined to obtain one that would be applica-

ble over the entire amplitude range. In both cases, the purely nonlinear component was fit to prevent the linear component from dominating the fit. To do so, the linear stiffness, K_∞, and the low-amplitude tangential stiffness, K_T, need to be estimated. The linear stiffness corresponds to the slope of the total restoring force vs. displacement curve in the macroslip regime, which can be calculated from the high-amplitude backbone curve. The tangential stiffness, on the other hand, can be calculated from the low-amplitude curve. Finite difference was used to estimate both the stiffness values. When fitting splines to the backbone curve, the number of points per spline and the highest order of the splines were chosen such that the error in the fit was minimum. For the low-amplitude curve, 3^{rd} order splines with 20 points per fit were found sufficient to fit the backbone curve. The step involving the calculation of macroslip displacement, $\phi_{\max}$, was omitted for the low-amplitude curve. The number of discretization points were set to 50 and $\alpha = 1.2$ was used to form the vector ϕ. The high-amplitude backbone curve was similarly processed, with a few changes. Since this curve includes the macroslip region, $\phi_{\max}$ could be calculated. 4^{th} order splines with 20 data points per spline were found more suitable to fit this curve. While the same number of discretization points were used, a values of α less than one ($\alpha = 0.9$) was concluded to be more suitable since the distribution function was found to rapidly increase with increase in amplitude. Figure 4 shows the distribution function obtained over the entire range of load amplitude from zero to macroslip by concatenating the distribution function extracted from the two backbone curves. As in the previous case study, the dirac delta stiffness was estimated using Eq. 17. Thus, a general, non-parametric Iwan model for the nonlinear mode under consideration was obtained.

It can be seen in Fig. 4 that the distribution function is U-shaped, first exponentially decreasing and then exponentially increasing with increase in slider strength, ϕ. Plotting the contact status gives some insight into why this happens. Figure 5 is a top-view of the contact patch on the bottom beam, showing the evolution of contact with increase in load amplitude. It must be noted here that the contact region is actually a line since the model

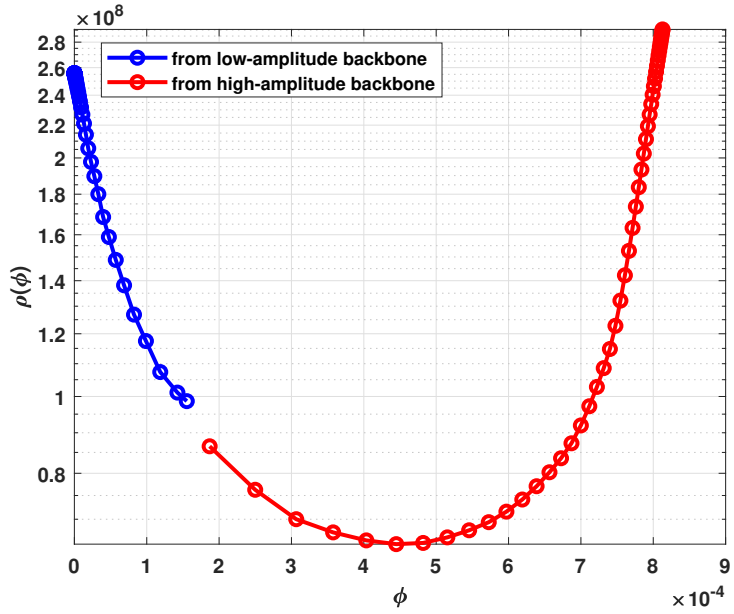

Figure 4: Distribution function obtained from QSMA over the entire amplitude range of interest.

is two-dimensional. However, the elements have been extruded to an arbitrary depth to be able to easily view the evolution of contact, thus appearing as an area of contact instead of a line. Figure 5 shows that slip initially begins to occur along the left edge while the right edge remains stuck. With increase in amplitude, however, the right edge also starts slipping, leading to a rapid increase in overall slip area. This corresponds to the exponential increase in the distribution function at high amplitude observed in Fig. 4. This also highlights the advantage of a non-parametric model - it is more flexible in capturing the observed dynamics since it is not limited to a finite set of parameters. The four-parameter Iwan model, on the other hand, is limited to distribution functions that exponentially decrease. In fact, there isn't a characeterized model existing (to the authors' knowledge) that is capable of fitting such a distribution function.

Next, the accuracy of the non-parametric Iwan model in estimating the dynamic behavior of the system was tested by analysing the free response of the structure to an initial displacement condition. The response computed by performing a transient analysis of the whole FE model was compared against that obtained by numerically integrating the non-parametric

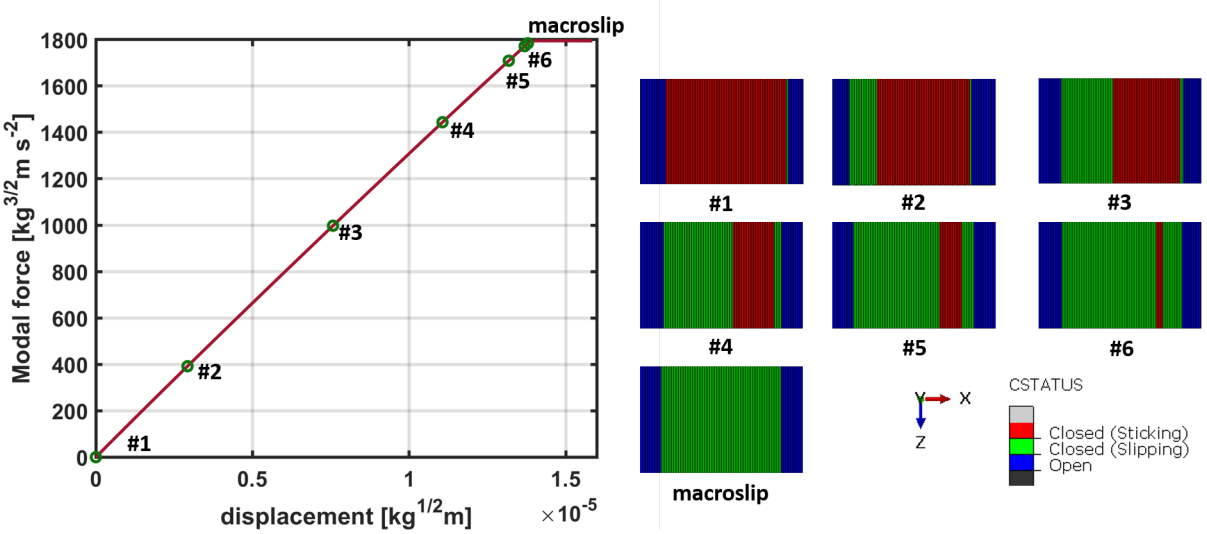

Figure 5: Top view of the bottom beam contact patch, showing the stuck and slipped elements, with the displacement that each frame corresponds to shown on the backbone curve

modal Iwan model. For the FE analysis, a static load was applied in the shape of the mode such that the deflection at the tip was 0.7 mm. The resulting deflection of the beam assembly was calculated and set as initial displacement condition for the transient analysis. An implicit dynamic integration with automatic time control was performed to simulate 0.5 s of the response. The step-size was not allowed to exceed 1×10^{-6} to minimize the numerical damping. This low value was still found to produce significant numerical damping, as will be discussed further when presenting the results. The response displacement at the tip, obtained through integration, was then scaled using the linear mode shape of the first mode. This results in an estimate of the modal response.

For the non-parametric model, the initial condition was replicated by applying an initial displacement equal to the modal response at time $t = 0$ s, calculated from the FE model. The Newmark-β method [44] was used to integrate the nonlinear equation of motion. The specifics of implementing the Newmark-β method have been described in [83] and have not been included here for brevity.

Figure 6 compares the modal response obtained from the FE model and the proposed non-parametric Iwan model, showing good phase agreement but a slight difference in amplitude

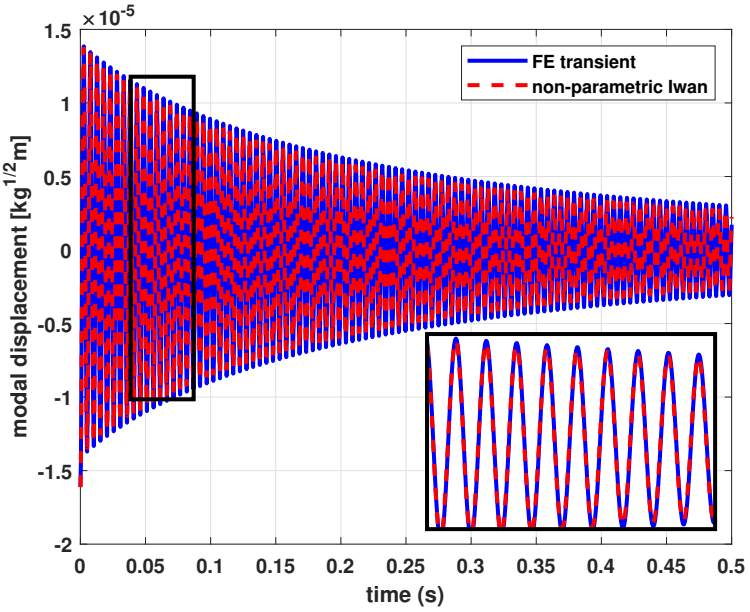

Figure 6: Modal displacement obtained by implicit dynamic integration of the FE model and Newmark-β integration of the non-parametric Iwan model

of the response. To observe this better, the instantaneous damping and frequency were estimated from the time response using the amplitude and phase fitting technique presented by Moldenhauer et al. [93]. Figure 7 shows the amplitude-dependent frequency and damping curves obtained. The results from QSMA have also been plotted as a reference. While the frequency is in good agreement throughout the domain, Fig. 7b shows that the damping calculated from the transient FE analysis, represented by dotted lines with circular markers, is offset from both the non-parametric Iwan and the QSMA results. This is due to the numerical damping introduced by the implicit integration. This also explains the deviation in amplitude observed in Fig. 6. After subtracting this numerical damping ($\xi = 2.68 \times 10^{-4}$), the FE analysis result (represented by dashed-dotted lines) agrees with the non-parametric Iwan model. It must be noted here that the non-parametric model additionally simulated 5 s of response to get a longer ring-down, which is why the dashed lines extend over a larger amplitude range in Fig. 7. This was done to verify that the instantaneous damping and frequency predicted by the model was accurate over a large range of response amplitudes.

Table 9 lists the time taken by the two methods to simulate 0.5 s of the dynamic response.

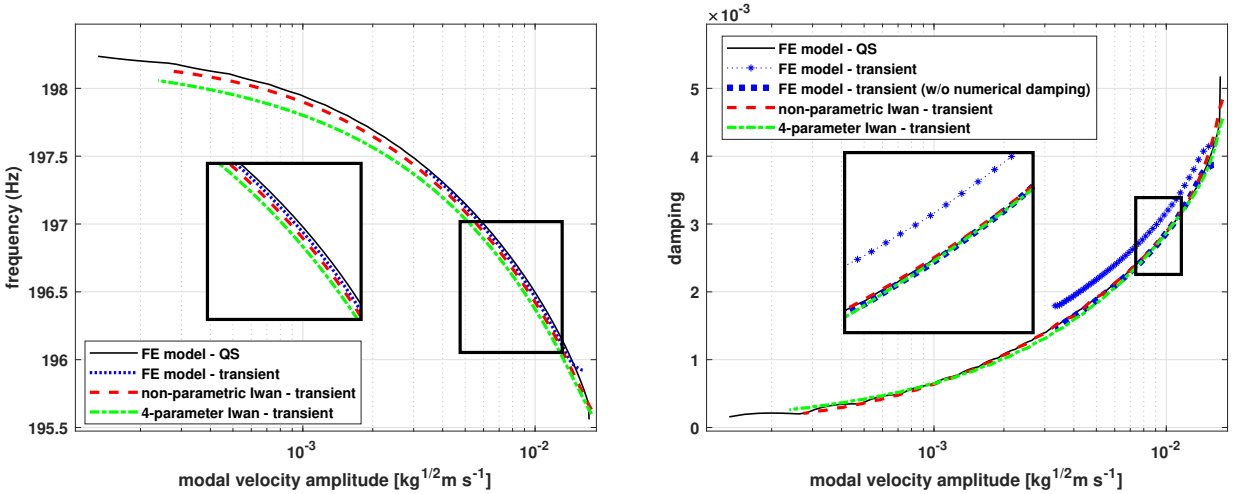

(a) Frequency vs modal velocity amplitude **(b) Damping vs modal velocity amplitude**

Figure 7: Comparing the instantaneous damping and frequency plotted against the modal velocity amplitude

Table 9: Time taken to simulate 0.5 s of response by the transient FE analysis and the non-parametric Iwan model using implicit dynamic integration

Method	Simulation time
Transient FE	1.468×10^5 s (≈ 40.7 h)
Newmark-β	2.604 s

The transient FE analysis is highly computationally expensive, taking nearly 41 hours to compute 0.5 s of the dynamic response. The non-parametric modal Iwan model, on the other hand, is significantly faster, taking less than 3 seconds for the dynamic simulation. The quasi-static analysis required to define the model takes an additional 380 s, resulting in an overall computation time of 383 s - orders of magnitude less than solving the whole FE model. Thus, it has been shown that the proposed general Iwan model provides a computational advantage over analysing the complete FE model without any significant loss in accuracy. It must be noted here that the approach proposed that the modes remain uncoupled and so one would have to verify this assumption for the system/loading of interest, as shown in [26].

A four-parameter Iwan model was also fit to compare its effectiveness in simulating the

system nonlinearity. To calculate the values of the four parameters, the distribution function of the non-parametric model was used. First, the macroslip displacement point, $\phi_{\max}$, is the same as in the non-parametric model. Next, the parameter χ can be estimated from the slider strength, ϕ, and the corresponding distribution, using the method of least squares. To do so, first consider the equation for the distribution function of the four-parameter Iwan model, given by Eq. 18. The first term in this equation represents the power-law distribution of the model in the microslip regime and the second term represents a Dirac delta function that truncates the distribution at macroslip. For the determination of χ, only the first term is relevant.

$$\rho(\phi) = R\phi^{\chi}[\mathrm{H}(\phi) - \mathrm{H}(\phi - \phi_{\max})] + S\delta(\phi - \phi_{\max}) \tag{18}$$

Taking a natural logarithm of Eq. 18 gives

$$\ln(\rho) = \ln(R) + \chi \ln(\phi). \tag{19}$$

Since $\phi, \rho(\phi)$ here are vectors, taking the difference between consecutive terms while treating R and χ as constants, and then rearranging gives Eq. 20.

$$\chi = [\triangle \ln(\phi)]^{\dagger}[\triangle \ln(\rho)] \tag{20}$$

Once the parameter χ is calculated, R can be found using Eq. 21, where ϕ^* is the point just before macroslip occurs and $\rho(\phi^*)$ is the corresponding distribution. In the case of the cantilever beam assembly considered here, since only the initial, power-law distribution can be captured by the 4-parameter model, ϕ^* corresponds to the point just before a definite upward trend in the distribution function of the non-parametric model is observed.

$$R = \frac{\rho(\phi^*)}{\phi^{*\chi}} \tag{21}$$

The parameter S can be obtained using the procedure for estimating the Delta stiffness detailed in Sec. 2.3. The parameters $[R, S, \chi, \phi_{\max}$ can be converted to their physically interpretable equivalents $[F_S, K_T, \chi, \beta]$ as shown in [35]. The resulting 4-parameter Iwan model for the cantilever beam assembly was found to be $[F_S,\ K_T,\ \chi,\ \beta] = [600.2\ \mathrm{N}/\sqrt{\mathrm{kg}},\ 7.786 \times 10^5\ \mathrm{s}^{-2},\ -0.367,\ 10.87]$. The distribution function for this 4-parameter model is shown in Fig. 8. The low-amplitude power-law behavior of the distribution is captured by the 4-parameter model but the exponential increase in distribution at high-amplitudes is not. This is because the distribution function of the four-parameter model is defined to be a single power of the slider strength, as seen in Eq. 18.

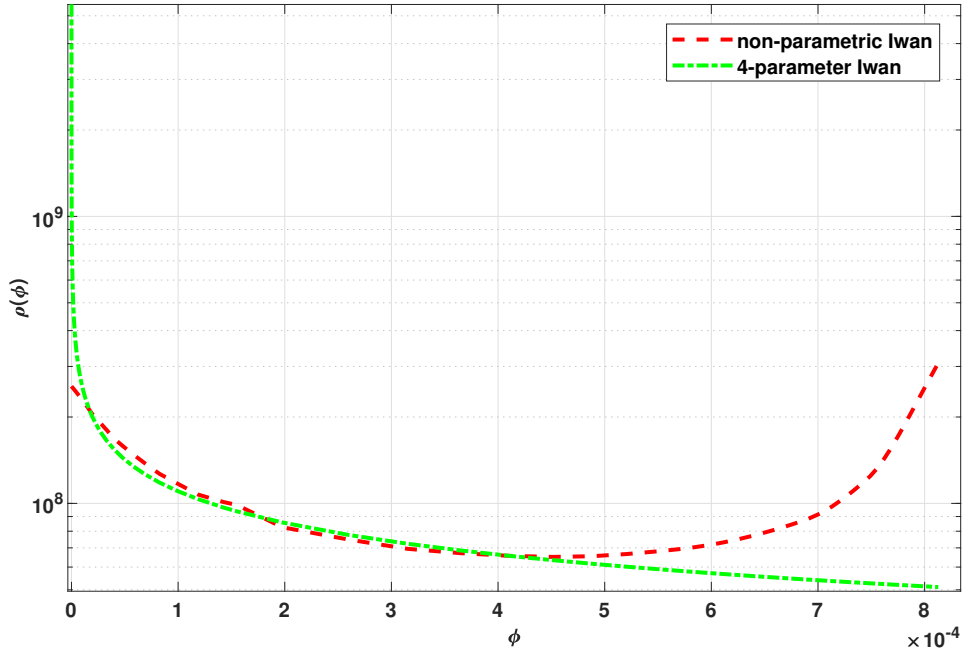

Figure 8: Distribution function of the 4-parameter Iwan model that represents the cantilever beam assembly, compared against that of the non-parametric Iwan model

Next, a transient dynamic analysis was performed to see how this difference in distribution function affects the 4-parameter model's ability to simulate the dynamic behavior of the system. The initial conditions and integration procedure used were identical to the non-parametric modal Iwan model. The time response obtained was post-processed to extract

the response amplitude, instantaneous damping and frequency. The resulting amplitude-dependant damping and frequency curves are given by the dash-dot lines in Fig. 7. In this case, the four-parameter model gives close enough results to the non-parametric model and the true solution. The damping curve nearly overlaps while the frequency shows minute differences at low amplitudes. Therefore, it appears that in this case, the four-parameter Iwan model can simulate the nonlinear dynamics even though it does not accurately capture the slip behavior.

4 Numerical case study - Cantilever beam with two bolts

The 2D FE model of the cantilever beam, used in the previous section, was modified to include two bolts with varying preload instead of a single bolt. The first bolt was modeled as a pressure load of 1.76×10^6 Pa applied on both the top and bottom surfaces over a length of 3.03 mm at a distance of 30.3 mm from the free end. For the second bolt, a pressure load of 1.76×10^7 Pa, 10 times higher than that on the first bolt, was applied over a length of 3.35 mm at a distance of 17.5 mm from the free end. Slip is first expected to occur along the region corresponding to the first bolt due to the lower pressure holding the surfaces together in this region. The first bending mode of the assembly was studied.

The method of QSMA was implemented to obtain the backbone curve. A single quasi-static analysis was not able to accurately capture the system behavior over the entire amplitude range, from zero to macroslip. Therefore, three separate quasi-static analyses were performed, each resulting in a maximum tip deflection of 0.0635 mm, 0.127 mm and 0.635 mm respectively. The three analyses effectively captured the three stages of the evolution of contact - slip at the first bolt interface, slip at the second bolt interface and the transition between the two. The linear stiffness, K_∞ and the low-amplitude tangential stiffness, K_T were obtained using the same procedure as in the previous case study (Sec. 3). Similar to the

case study presented in Sec. 3, the distribution function was calculated for each of the three backbone curves using the procedure described in Sec. 2.3, and then combined to obtain one that is applicable over the entire amplitude range. For the first two amplitude cases, 4^{th} order splines with 20 points per spline was used. The high amplitude case required 4^{th} order splines with 10 points per spline. As mentioned in Sec. 2.3, the number of points per spline depend on the density of data points available, i.e. the number of force amplitude values at which the displacement was evaluated using QSMA. For all three cases, 50 discretization points, with $\alpha = 1$, were used. The final distribution function obtained is shown in Fig. 9.

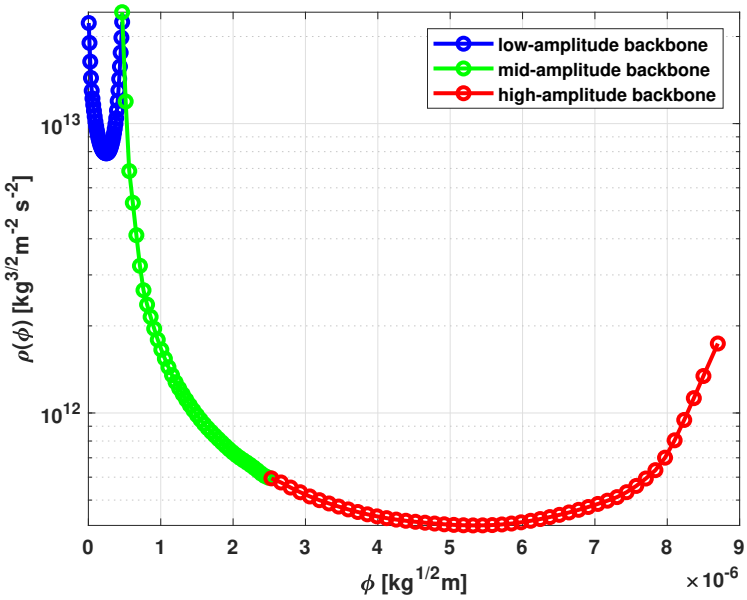

Figure 9: Distribution function for the 2D cantilever beam with two bolts, extracted from the force-displacement backbone curve obtained using QSMA

Similar to the previous case study, the accuracy of the non-parametric Iwan model was tested by comparing the amplitude-dependent frequency and damping predicted by it against the true solution. In this case, the true solution is estimated from the quasi-static force-displacement curve using the formulation detailed in [26]. The frequency and damping predicted by the non-parametric Iwan model can be similarly obtained by performing a quasi-static analysis. The resultant curves, given by the dashed lines in Fig. 11, show good agreement between the quasi-static results from the FE model and the non-parametric modal

Iwan model. A dynamic analysis was also performed on the non-parametric Iwan model by applying an impulsive force, simulated as half a sinusoid. The resulting time response was then post-processed to obtained the amplitude-dependent frequency and damping, using the technique described in [93]. The resultant frequency and damping curves are in good agreement with the true solution, as shown by the dotted lines in Fig. 11.

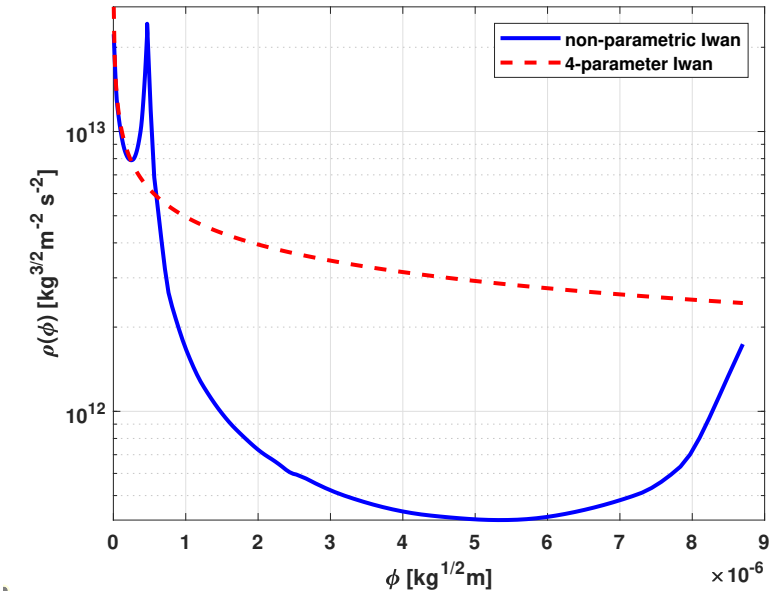

Figure 10: Distribution function of a four-parameter Iwan model fitted to the low-amplitude region of the 2D cantilever beam with two bolts

The four-parameter model's [35] ability to capture this nonlinear behavior was also tested. Since there isn't a single set of parameters that can produce the distribution function seen in Fig. 9, the model was fit to capture just the low-amplitude power-law behavior. The parameters were estimated from the distribution function of the non-parametric Iwan model using the same procedure as in Sec. 3, resulting in the four-parameter model, $[F_{\mathrm{S}}, K_{\mathrm{T}}, \chi, \beta] = [1903.1\mathrm{N}/\sqrt{\mathrm{kg}}, 8.04 \times 10^{-5}\mathrm{s}^{-2}, -0.3277, 1.0247]$. Figure 10 shows the resulting distribution function obtained. A transient, dynamic analysis was performed with the same impulsive force applied to the four-parameter model as to the non-parametric Iwan model. The resulting damping and frequency curves, seen in Fig. 11, indicate that the four-parameter model captures the low-amplitude nonlinearity well (i.e. when only the first

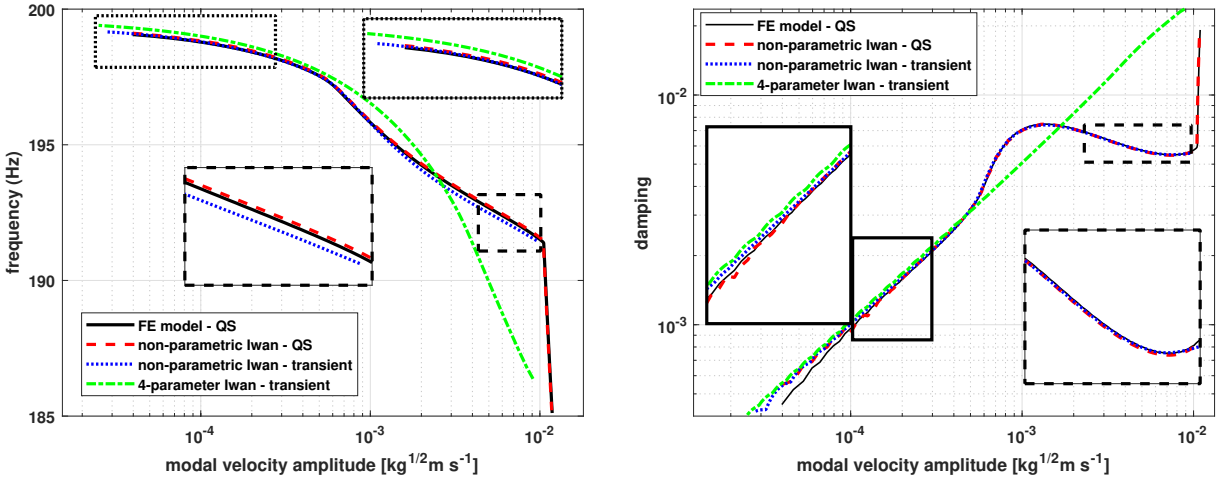

(a) Frequency vs modal velocity amplitude **(b) Damping vs modal velocity amplitude**

Figure 11: Comparing the instantaneous frequency and damping for the 2D cantilever beam with two bolts, obtained from the FE simulation (solid line), quasi-static analysis of the non-parametric modal Iwan model (dashed line), transient analysis of the non-parametric Iwan model (dotted line) and transient analysis of an equivalent four-parameter Iwan model (dashed-dotted line)

bolt region is slipping) but fails to simulate the higher amplitude behavior. On the other hand, the non-parametric model was not limited by a fixed definition of the distribution function and could therefore accurately capture the dynamic behavior over the entire amplitude range. Therefore, it Both the four-parameter model and the non-parametric model require the same computational power for dynamic integration since they use equivalent discretization and integration procedures.

5 Conclusions

This paper proposed a new, non-parametric form of the Iwan model in which the distribution function is directly extracted from the force-displacement backbone curve. QSMA is used to obtain the backbone curve of the nonlinear mode of interest. The distribution function can then be calculated from the second derivative of the restoring force with respect to displace-

ment. A procedure to implement this was presented. The proposed modeling approach offers two main advantages over the existing methods. Firstly, the accuracy of the model is not limited to the definition of the distribution function by a finite set of parameters. Secondly, it eliminates the need for computationally intensive optimization schemes, typically used for parameter identification in the standard Iwan element [26, 53].

Two case studies testing the non-parametric Iwan model were presented. First was the 2D FE model of a cantilever beam assembly with a line pressure applied near the free end to represent the preload due to a bolt. This case is interesting for two reasons. First, the contact behavior is such that the distribution function does not match the form of any existing parametric Iwan element. The non-parametric Iwan model was able to capture this contact behavior since the distribution function for the model was directly extracted from the backbone curve. Secondly, dynamic simulations of the full FE model which includes nonlinear contact and friction, are extremely expensive; simulating 0.5 s of response takes a few days. On the other hand, the only major computational costs involved in simulating the response of the non-parametric Iwan model are the quasi-static analyses to estimate the backbone curve and numerical integration of the non-parametric model EoM. This is significantly faster than integrating the full FE model, and the computational savings increase even more as the complexity of the FE model increases. An interesting observation in this case study was that even though the contact behavior exhibited could not be captured by existing Iwan models such as the four-parameter model, the frequency and damping estimated by the four-parameter model showed little error. Therefore, both the non-parametric and the four-parameter Iwan models gave acceptable results in this case.

In the second case, the 2D model was varied to include two closely-spaced bolts of varying preload. Here, the contact behavior was more complicated due to the overlap in the pressure cones of the two bolts. This case showed that in a structure with multiple closely-spaced bolts, if one of the bolts is loosened, the dynamic behavior can vary significantly. It was found that the non-parametric Iwan model was able to simulate the dynamic behavior while

the equivalent four-parameter model was not.

The proposed model has some limitations. Firstly, it is only applicable to systems that can be represented by a Masing model. Since a Masing model consists of Coulomb sliders, the normal force across the interface must remain constant. However, this may not always be the case [94, 95]. Moreover, this modeling approach also inherits the limitations of modal models, i.e. it is limited to cases where there is no coupling between the modes.

Paper IV: A New Approach to Model a System with Both Friction and Geometric Nonlinearity

This paper presents an approach for developing a reduced-order model to characterize the nonlinear dynamics of a structure comprising both friction and geometric nonlinearity. The Single-mode Implicit Condensation and Expansion (SICE) method can capture the resonant behavior of a geometrically nonlinear mode using QSMA. On the other hand, the modal Iwan model can be used to represent the hysteretic behavior of a mode exhibiting nonlinearity due to friction. This paper presents a new model, referred to here as the Iwan model with Geometric Nonlinearity (or the IGNL model), that combines a SICE-ROM with an Iwan model. It consists of an Iwan model with an additional spring-slider unit, where the slider has infinite strength and the spring consists of polynomial terms that define the SICE-ROM. The method of Quasi-Static Modal Analysis (QSMA) has been used to estimate the nonlinear force-displacement backbone curve that is required to identify the parameters of the IGNL model. Existing literature shows QSMA to be effective in estimating the force-displacement behavior of a nonlinear mode where the nonlinearity is due to friction or bending-stretching coupling, but not both simultaneously. This paper shows how QSMA can be applied by making certain adjustments to isolate the two forms of nonlinearity. Two case studies have been presented to test the efficacy of the IGNL model. The proposed method is shown to be significantly faster than performing dynamic simulations to estimate the amplitude-dependent frequency and damping behavior.

1 Introduction

The aircraft, spacecraft and automotive industries are increasingly making use of thin, curved panels in their structures for higher strength-to-weight ratios and lower fuel consumption. Such structures can exhibit geometric nonlinearities, caused by bending-stretching coupling under large deformations of the panels [2,3]. As a result, the structure experiences significant changes in stiffness at high load amplitudes, and the dynamic behavior cannot be captured by linear vibration theory. Additionally, these structures contain mechanical fasteners that are used to assemble the various parts together, making manufacturing and future maintenance convenient. The use of fasteners, however, results in changes in stiffness as well as significant damping due to frictional energy losses at the interfaces [4, 5]. The contact pressure at the interface is not uniform, with higher pressure closer to the bolted joint and lower pressure further away [15]. Therefore, at lower amplitudes, the edges of the jointed surfaces slip while the region closer to the bolt hole remains mostly stuck. This is called microslip. In the microslip regime, the stiffness of the joint decreases slightly, whereas the damping increases by orders of magnitude [17], as has been observed in several experimental studies [18–20]. The response of a structure at resonance, and, as a result, to random excitation, depends on the damping [21]. Thus, it is important to estimate the damping due to friction at the interfaces.

Simulating the dynamic response of a geometrically nonlinear structure using a high-fidelity Finite Element (FE) model is highly computationally expensive. Therefore, several reduced-order models have been developed as an alternative. A reduced-order model equation of motion for geometric nonlinearity will typically contain linear mass and stiffness terms along with additional higher-order polynomial stiffness terms, usually limited to quadratic and cubic terms. The polynomial coefficients can be estimated using static nonlinear solutions, as described in [63]. The methods that use static solutions can be classified as indirect, or non-intrusive evaluation methods, since they do not require manipulation of the nonlinear stiffness matrices in the FE package [64, 65]. Murayov and Rizzi [66] developed

one such method, known as the Enforced Displacement (ED) procedure. Here, the nonlinear FE model is constrained to take the shape of the linear mode of interest, and the reaction forces needed to do so are calculated by a static analysis. This is done over a range of displacement amplitudes, with the resultant force-displacement backbone curve being used to estimate the polynomial coefficients. In this method, both bending and stretching (i.e. axial or dual [64]) modes need to be included when defining the modal basis in order to capture the bending-stretching coupling. Alternatively, McEwan et al. [67] presented the Implicit Condensation (IC) method where a static force is applied in the shape of the mode of interest and the resulting displacement field is estimated using the nonlinear FE model. The displacement data is transformed from the physical to the modal space. Similar to the ED method, this can be done over a range of force amplitudes to estimate the nonlinear coefficients. In the IC method, however, the bending-stretching coupling is implicitly captured by applying a force instead of displacement. Thus, the axial modes do not need to be included in the basis. Hollkamp and Gordon [68] presented the Implicit Condensation and Expansion (ICE) method to recover the axial displacements or the corresponding stresses from the IC method. In both the ED and ICE methods, multiple modes can be considered simultaneously to account for modal coupling. Park and Allen [61] presented a single degree-of freedom ICE method, dubbed the SICE-ROM, where the nonlinear restoring force is approximated by a single, dominant mode. This ROM requires polynomial terms higher than just the third order, presumably to capture quasi-static coupling between the mode under consideration and all other modes. Park and Allen showed that the dynamics near a single mode of strongly nonlinear structures can often be represented by the SICE-ROM with minimal loss of accuracy.

Frictional systems are hysteretic in nature, meaning the response of the system is dependent on its current as well as past states. Therefore, unlike geometric nonlinearity that can be represented using polynomial-based ROMs, friction nonlinearity requires lumped, hysteretic models. These constitutive models can be incorporated into an FE model using

the whole-joint modeling approach, presented by Segalman [16]. In this approach, each side of the contact interface is treated as rigid and all its nodes are tied together to a single representative node. The appropriate hysteretic model is then applied between the representative nodes of the surfaces in contact. This approach is less computationally expensive that including a friction element between every pair on nodes in contact. However, in a structure with multiple joints, it is difficult to isolate the effect of each joint on the overall system dynamics, making the estimation of the parameters that describe the hysteretic model an arduous task. As an alternative, Segalman [25] proposed a modal approach in which each nonlinear mode can be represented by a single degree-of-freedom (SDOF) system, with the corresponding nonlinear restoring force given by a constitutive hysteretic model.

Gaul and Nitsche [29] reviewed different hysteretic models that can be used to capture the dynamics due to bolted joints. More recently, Mathis et al. [30] presented an extensive review of the different damping models and discussed the relation between them. Some of the models used for friction nonlinearity were originally developed to represent metal elastoplasticity [22, 27, 28]. The most commonly used hysteretic model among these is the Distributed-Element Model [22], also commonly referred to as the Iwan model . This model consists of an arrangement of linear spring and slider units, known as Jenkins elements. The sliders have varying strengths, resulting in a nonlinear force-displacement relationship. Since it is composed of Jenkins elements, the Iwan model falls under the category of Masing models [88,91]. This implies that the force-displacement curve of the Iwan model is symmetric about the origin and the complete hysteresis loop at any amplitude can be estimated, using Masing's rules [88], from the backbone curve calculated up to that amplitude. Lacayo and Allen [26] showed that the amplitude-dependent frequency and damping due to a Masing model can easily be calculated from the complete hysteresis loop, without the need to simulate the full dynamic response.

Both the SICE-ROM for geometric nonlinearity and the modal Masing model for friction nonlinearity require force-displacement data for identification. Various quasi-static methods

have been developed for estimating the force-displacement data. Festjens et al. [58] presented a method to study the nonlinearity due to bolted joints, in which a quasi-static distributed load was applied such that it represented the inertial loading when the structure vibrates in the mode of interest. The corresponding displacement can then be calculated using any finite element package. This was done over a range of load amplitudes to obtain the force-displacement curve. While Festjens et al. allowed the change of mode shapes in the nonlinear domain of the structure (i.e. near the bolted joints), Lacayo and Allen [26] proposed a simplification where they assumed the linear mode shape to be valid over the entire structure. This is called the method of Quasi-Static Modal Analysis, or QSMA. Its efficacy has been tested on various systems consisting of friction nonlinearity [12, 59, 60]. Further, Park and Allen [61] showed how QSMA could be successfully applied to estimate the force-displacement relationship for the nonlinear mode of a structure with geometric nonlinearity. Balaji and Brake [62] proposed a variation of QSMA, known as Rayleigh-Quotient based Nonlinear Modal Analysis (RQNMA), where they extended the concept of Rayleigh quotients to both conservative and non-conservative nonlinear systems, updating the mode shapes, and hence the applied static load, at each amplitude level.

The existing reduced-order modeling approaches consider either geometric or friction nonlinearity. For a structure exhibiting both forms of nonlinearity, one could use the ICE methods, thus ignoring the effect of friction, or use hysteretic models and ignore the effect of geometric nonlinearity. Both these approaches lead to a loss of accuracy. Alternatively, one could simulate the transient dynamic response of the full structure using a high-fidelity FE model. However, this is exceedingly computationally expensive. Kuether et al. [96] found that a cluster of 9 nodes and 432 cores, with 192 GB RAM per node, was required to simulate 0.25 s of dynamic response a high-fidelity 3D FE model of a structure with friction and geometric nonlinearity in 48 hours. This paper presents a reduced-order modeling technique for characterizing the nonlinear mode of a structure by combining the SICE-ROM with the modal Iwan Model to represent the nonlinearity arising from both friction and bending-

stretching coupling. The resulting ROM can be referred to as the Iwan model with Geometric Nonlinearity, or the IGNL model. The paper also presents an approach to identify the parameters of the IGNL model using QSMA. It shows how the effects of the two types of nonlinearity on the force-displacement behavior can be isolated, assuming the interactions between them are weak enough for superposition to hold. The IGNL model's ability to estimate the amplitude-dependent frequency and damping behavior of the nonlinear mode under consideration has also been presented. Finally, the paper shows that the proposed method is significantly faster than performing a dynamic simulation, and is more accurate than fitting just a SICE-ROM or a hysteretic model.

The next section provides theoretical background for QSMA, SICE-ROM and the Iwan Model. In Sec. 3, the proposed IGNL model is formulated and the method to estimate the frequency and damping from this model has been presented. Section 4 presents a simple numerical case study of a cubic spring with an Iwan element. This is followed by a more complex case study of the Tribomechadynamics Benchmark Structure [97], composed of a panel clamped at the ends using bolts, shown in Sec. 5. Finally, the conclusions are presented in Sec. 6.

2 Background

2.1 Overview of Quasi-Static Modal Analysis

Lacayo and Allen [26] showed that the method of Quasi-Static Modal Analysis (QSMA) can be used to calculate the force-displacement relation for a nonlinear mode of a jointed structure consisting only of friction nonlinearity. Park and Allen [61] further derived a similar relation for a single mode of a geometrically nonlinear structure. To understand how the method of QSMA is applied, consider a Finite Element (FE) model of a structure, the

Equations of Motion (EoM) for which can be written as

$$\mathbf{M}\ddot{\mathbf{x}} + \mathbf{C}\dot{\mathbf{x}} + \mathbf{K}\mathbf{x} + \mathbf{f}_{\text{nl}}(\mathbf{x}, \theta) = \mathbf{f}_{\text{ext}} \tag{1}$$

where $\mathbf{M}, \mathbf{C}, \mathbf{K}$ are the mass, damping and stiffness matrices, respectively, and $\mathbf{x}, \dot{\mathbf{x}}, \ddot{\mathbf{x}}$ are the displacement, velocity and acceleration vectors, respectively. The vector of nonlinear forces, $\mathbf{f}_{\text{nl}}(\mathbf{x}, \theta)$, is a function of displacement and the hysteretic variable, θ. The definition of this variable depends on the type of hysteretic model used. In the Iwan model, for example, it represents the state of the sliders that form the model. The equations can be linearized about some state of interest, to capture the behavior for small vibrations about that state. Without loss of generality, the equations above are assumed to be linearized about $x = 0$ to estimate the low-amplitude modal frequencies, $\boldsymbol{\omega}_0$, and linear mode-shapes, $\boldsymbol{\Phi}$, by performing an eigen-value analysis. Then, a static load is applied such that it excites only the r^{th} mode of the system. The applied load must be $f_{\text{ext}} = \mathbf{M}\boldsymbol{\Phi}_r$, where $\boldsymbol{\Phi}_r$ is the low-amplitude linear mode shape of the r^{th} mode of interest [26]. This results in the following quasi-static problem:

$$\mathbf{K}\mathbf{x} + \mathbf{f}_{\text{nl}}(\mathbf{x}, \theta) = \boldsymbol{\alpha}\mathbf{M}\boldsymbol{\Phi}_{\mathbf{r}}. \tag{2}$$

Equation 2 can be solved to obtain $\mathbf{x}$ for different force amplitude levels, $\boldsymbol{\alpha}$. Typically, the structure starts in equilibrium and $\boldsymbol{\alpha}$ is chosen to be monotonically increasing. This gives the initial loading behavior, also known as the backbone curve. Now, to retrieve the force-displacement relation of the r^{th} mode, the force applied to the structure and the displacement calculated need to be converted from the physical to the modal domain, using Eqs. 3 and 4.

$$\mathbf{f}_{\text{modal}} = \boldsymbol{\Phi}_r^{\text{T}}\boldsymbol{\alpha}\mathbf{M}\boldsymbol{\Phi}_r = \boldsymbol{\alpha} \tag{3}$$

$$q_r(\alpha) = \boldsymbol{\Phi}_r^T\mathbf{M}x(\alpha) \tag{4}$$

In this way, the force-displacement relation for the nonlinear mode of a structure, α versus $q_r(\alpha)$, can be calculated by solving a quasi-static problem. However, further post-processing is required to estimate the amplitude-dependent frequency and damping for the mode under consideration, as discussed in the following sections.

2.2 SICE-ROM for characterizing geometric nonlinearity

Park and Allen [61] derived a Reduced Order Model (ROM) for strongly nonlinear structures using QSMA, that has been briefly summarized here. The undamped SDOF EoM of the r^{th} mode was assumed to have the following form,

$$\ddot{q}_r + \omega_r^2 q_r + \theta_{\text{gnl}}(q_r) = \mathbf{\Phi}_r^{\text{T}} \mathbf{f}_{\text{ext}} \tag{5}$$

where $\theta_{\text{gnl}}(q_r)$ is the nonlinear restoring force approximated by the r^{th} mode only. This restoring force can be obtained from the quasi-static solution calculated using the method described in Sec. 2.1. Note here that this model form is not dependent on any hysteretic variable θ. Next, a polynomial can be used to approximate this restoring force function, given by Eq. 6,

$$\theta_{\text{gnl}}(q_r) = \sum_{j=2}^{m} k_j q_r^j, \tag{6}$$

where k_j is the j^{th} nonlinear stiffness coefficient and m is the highest order of the polynomial. Higher order polynomials are required for modes that exhibit strong static coupling. The coefficients, k_j, can be estimated from the quasi-static force-displacement data by applying the method of least squares, as elaborated in [61]. This approach minimizes the cost function, J, given by Eq. 7,

$$\min_{k_j} J = \frac{1}{S} \sum_{l=1}^{S} \frac{\left(\omega_r^2 q_{r,l} + \sum_{j=2}^{m} k_j (q_{r,l})^j - \alpha_l\right)^2}{\alpha_l^2} \tag{7}$$

where S is the number of sample points in the QSMA analysis, i.e. the length of the vector α. The resulting ROM is called the Single degree-of-freedom Implicit Condensation and

Expansion, or SICE-ROM. Once a ROM of this form is fit, the frequency behavior can be estimated using numerical continuation techniques, as discussed in Sec. 3.3. Park and Allen also showed three different case studies, where the SICE-ROM was used to successfully characterize the geometric nonlinearity of structures with varying complexity, thus verifying the method's capabilities. It must be noted that this ROM only accounts for static coupling between modes. In case of dynamic coupling, the SICE-ROM is unable to simulate the dynamic response accurately even when higher-order polynomials are used. In such a case the single-mode quasi-static backbone curve cannot be used to accurately predict the dynamic response. Additionally, since this is an SDOF ROM, it cannot capture any internal resonances in the Nonlinear Normal Mode (NNM). As discussed in [61], this can be an advantage in some applications, such as model updating. The method proposed in this work shares these limitations; it only estimates the behavior of a single, uncoupled mode.

2.3 Iwan Model for Friction Nonlinearity

In a built-up structure, hysteretic constitutive models are used to simulate the nonlinearity due to friction. The Distributed Element Model, developed by Iwan [22], is one such lumped, mathematical model. It consists of a series of elasto-plastic units, known as Jenkins elements, arranged as shown in Fig. 1a. The springs in all the elasto-plastic units are identical, while the sliders have varying yield levels. The restoring force calculations for such a model have been derived in [22], with a brief summary of the same included here.

By definition, each Jenkins element exhibits bi-linear behavior. During initial loading, an element may either lie in the region OA or AB of the plot shown in Fig. 1b, depending on its slip force. Thus, the force-displacement relation, in case of positive loading, for each element is given by Eq. 8,

$$\begin{aligned} f_i &= \frac{kx}{N}; \qquad \dot{x} > 0, 0 < kx/N \leq f_i^*/N \\ f_i &= \frac{f_i^*}{N}; \qquad \dot{x} > 0, kx/N > f_i^*/N \end{aligned} \tag{8}$$

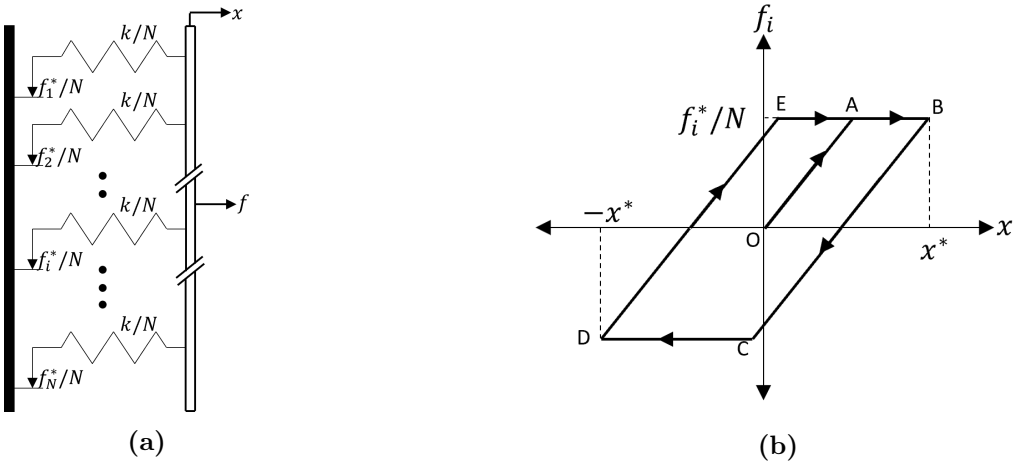

Figure 1: (a) Illustration of the Distributed Element (or Iwan) Model, and (b) The bi-linear force-displacement relationship of a Jenkins element

where k/N is the stiffness of each element, f_i^*/N is the yield force of each element, and N is the total number of elements. To calculate the force-displacement relation for the whole model, the number of elements that have yielded (or slipped) and those that are still stuck need to be considered separately. If n out of N elements have yielded (i.e. they have $kx/N > f_i^*/N$), their contribution to the total force can be given as

$$\sum_{i=1}^{n} \frac{f_i^*}{N} \tag{9}$$

while those that have not yet yielded, (i.e. they have $kx \leq f_i^*$) can be written as

$$\frac{k}{N} x(N-n) \tag{10}$$

The total force during initial loading can, therefore, be written as shown in Eq. 11.

$$f = \sum_{i=1}^{n} \frac{f_i^*}{N} + \frac{k}{N} x(N-n); \qquad \dot{x} > 0 \tag{11}$$

If the direction of loading is reversed, i.e. $\dot{x} < 0$, all the elements will switch to a stuck

state at the reversal point. As the reverse loading amplitude increases, the elements that did not yield during loading will remain unyielded. However, the elements that did yield during loading could have one of two states - either they will continue to be in a positive yield state or they will switch to a negative yield state. For an element that has already yielded in the positive direction to also yield in the negative direction, $k(x^* - x)$ must be greater than $2f_i^*$, where x^* is the displacement at which reversal occurs. Relationships similar to Eq. 8 can be written for the unloading case for each Jenkins element (see [22]). The total restoring force in the unloading direction can be given by

$$f_{\text{rev}} = \sum_{i=1}^{n'} \frac{-f_i^*}{N} + \sum_{i=n'}^{n} \left[\frac{f_i^*}{N} - \frac{k}{N}(x^* - x) \right] + \frac{k}{N} x(N-n); \qquad \dot{x} < 0,\ -x^* \leq x \leq x^* \tag{12}$$

where n' is the number of elements that have yielded in the negative direction. Note that the first term on the right-hand side of Eq. 12 corresponds to the Jenkins elements that lie in the region CD of Fig. 1b, the second terms corresponds to those that lie in the region BC and the final term corresponds to those that remain stuck and retrace their path along OA. For an infinite distribution of elements (i.e. N becomes very large), Eqs. 11 and 12 can be written in integral form instead of summations; this can be found in [22]. Note that in the integral form, a distribution function is defined that specifies the fraction of the total elements that yields at every force value. The DEM can take different forms, based on the distribution function specified. For example, the four-parameter Iwan model [35] implements a power-law distribution function and is commonly used to model friction nonlinearity due to bolted joints (and will be used in the case study presented in Sec. 4).

3 Proposed Approach

3.1 Iwan Model with Geometric Nonlinearity (IGNL model)

This paper proposes a modified form of the Iwan model that can capture both geometric and friction nonlinearity in a system. To do so, an element is added in parallel to the Jenkins elements, consisting of a nonlinear spring in series with a slider of infinite yield strength, i.e. $f^* = \infty$. The nonlinear spring corresponds to the SICE-ROM, defined to capture the geometrically nonlinear behavior. Since the slider associated with this nonlinear spring has infinite yield strength, it does not contribute to the hysteretic behavior exhibited by the Jenkin's elements. The IGNL model has been illustrated in Fig. 2.

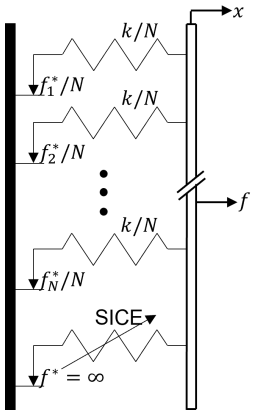

Figure 2: Illustration of the Iwan model with Geometric Nonlinearity, i.e. the IGNL model

The force-displacement relation for the added element can be given by

$$f_{\text{gnl}} = \sum_{j=2}^{m} k_j x^j; \qquad \forall \dot{x}, \forall x \tag{13}$$

where m is the order of the SICE-ROM and k_j is the j^{th} nonlinear stiffness coefficient. Since this nonlinear element is in parallel to the rest of the Jenkin's elements, its force contribution can be directly added to the total force-displacement relations described in Sec. 2.3. Thus, during initial loading, the force-displacement relation for the IGNL model, obtained by

appending Eq. 11, is given by Eq. 14.

$$f = \sum_{i=1}^{n} \frac{f_i^*}{N} + \frac{k}{N} x(N-n) + \sum_{j=2}^{m} k_j x^j; \qquad \dot{x} > 0. \tag{14}$$

Similarly, the force-displacement relation when the displacement direction is reversed can be given by modifying Eq. 12, resulting in

$$f_{\text{rev}} = \sum_{i=1}^{n'} \frac{-f_i^*}{N} + \sum_{i=n'}^{n} \Big[\frac{f_i^*}{N} - \frac{k}{N}(x^* - x)\Big] + \frac{k}{N} x(N-n) + \sum_{j=2}^{m} k_j x^j; \qquad \dot{x} < 0,\ -x^* \leq x \leq x^*. \tag{15}$$

In Eqs. 13 – 15, it can be seen that the nonlinear force due to the added element does not show any hysteretic behavior, just like the Jenkins elements that remain stuck. Therefore, the response of the added SICE element depends only on the current value of displacement and not it's history. This property helps separate geometric nonlinearity from friction nonlinearity when fitting the proposed ROM to a specific FE model, as will be shown in the subsequent section.

3.2 Identifying the IGNL Model Using QSMA

As discussed in Sec. 2.1, the method of QSMA can be used to obtain the force-displacement relation for the nonlinear mode of interest. Given a finite element model with both geometric and friction nonlinearity, the following procedure can be used to identify the IGNL model that can reproduce its nonlinear behavior, based on a few quasi-static simulations.

Consider the nonlinear mode r, the EoM for which can be written as

$$\ddot{q}_r + 2\zeta_{0,r}\omega_{0,r}\dot{q}_r + k_{\text{lin},r} q_r + \theta_{\text{nl}}(q_r, \theta) = \mathbf{\Phi}_r^{\text{T}} \mathbf{f}_{\text{ext}}, \tag{16}$$

where $k_{\text{lin},r}$ is the linear stiffness excluding the stiffness due to the IGNL element, $\zeta_{0,r}$ is the linear damping, $\theta_{\text{nl}}(q_r, \theta)$ is the nonlinear restoring force in the modal domain that is a

function of current displacement as well as previous states and is represented by Eqs. 14 and 15. The variables $q_r, \dot{q}_r, \ddot{q}_r$ are the nonlinear displacement, velocity and acceleration respectively. For the static case, the equation can therefore be reduced to

$$k_{\mathrm{lin},r} q_r(\alpha) + \theta_{\mathrm{nl}}(q_r, \theta) = \mathbf{\Phi}_r^{\mathrm{T}} \alpha \mathbf{M} \mathbf{\Phi}_r = \alpha. \tag{17}$$

The nonlinear restoring force, $\theta_{\mathrm{nl}}(q_r, \theta)$, comprises both geometric and frictional nonlinear effects. It can, therefore, be represented by the IGNL model. This means, during initial loading, the force-displacement relation (as per Eq. 14) can be given as

$$\theta_{\mathrm{nl}} = \sum_{i=1}^{n} \frac{\hat{f}_i^*}{N} + \frac{\hat{k}}{N} q_r (N - n) + \sum_{j=2}^{m} \hat{k}_j q_r^j; \qquad \dot{q}_r > 0, \forall q_r. \tag{18}$$

Note, here, that $\hat{f}_i^*, \hat{k}$ and $\hat{k}_j$ are the equivalent of f_i^*, k and k_j in the modal domain, since $\theta_{\mathrm{nl}}(q_r, \theta)$ is a modal force. Now, in order to identify the coefficients of the SICE-ROM, $\hat{k}_j$, the force due to geometric nonlinearity needs to be isolated from the frictional effects. This can be achieved by setting the yield strength of all the Jenkins elements to infinity, i.e. $n = 0$ in Eq. 18. In an FE software, this is equivalent to setting the friction coefficient, $\mu = \infty$. The quasi-static problem in the modal domain for this case can be written as

$$k_{\mathrm{lin},r} q_{r,\mathrm{stick}}(\alpha_{\mathrm{stick}}) + \theta_{\mathrm{nl,stick}}(\alpha_{\mathrm{stick}}) = \alpha_{\mathrm{stick}}, \tag{19}$$

where α_{stick} is the modal force amplitude, and $q_{r,\mathrm{stick}}(\alpha_{\mathrm{stick}})$ is the corresponding modal displacement calculated using QSMA. As discussed in Sec. 2.1, α takes discrete values over a range of force amplitudes to estimate the backbone curve. The nonlinear restoring force, $\theta_{\mathrm{nl,stick}}$ for this case can be written by substituting $n = 0$ in Eq. 18, resulting in

$$\theta_{\mathrm{nl,stick}} = \hat{k} q_{r,\mathrm{stick}} + \sum_{j=2}^{m} \hat{k}_j q_{r,\mathrm{stick}}^j; \qquad \dot{q}_{r,\mathrm{stick}} > 0, \forall q_{r,\mathrm{stick}}, \tag{20}$$

where $\hat{k}$ is equal to the sum of the stiffness values of all the linear springs in the IGNL model. Therefore, the total modal quasi-static force, α, according to Eq. 19, is a sum of the linear force, $(k_{\text{lin},r} + \hat{k})q_{r,\text{stick}}$, and the nonlinear force due to the SICE-ROM. The linear stiffness, $(k_{\text{lin},r} + \hat{k})$, must result in a frequency equal to the low-amplitude natural frequency of the r^{th} mode, $\omega_{0,r}$. Therefore,

$$k_{\text{lin},r} + \hat{k} = \omega_{0,r}^2 \tag{21}$$

The coefficients of the polynomial constituting the SICE-ROM, k_j, can then be calculated from the force-displacement data, i.e. $\boldsymbol{\alpha}_{\text{stick}}$ versus $\mathbf{q}_{r,\text{stick}}$, by applying the method of least squares described in Sec. 2.2. Note, again, that $\boldsymbol{\alpha}_{\text{stick}}$ and $\mathbf{q}_{r,\text{stick}}$ are vectors since QSMA is performed over a range of force amplitudes.

Next, the slider strengths of the Jenkins elements that capture the hysteretic behavior due to friction need to be identified. A second quasi-static analysis is considered, this time with the yield strengths of the Jenkins elements being f_i^*/N. In an FE model, this corresponds to setting a finite friction co-efficient, pre-determined based on the surface properties. Let $\boldsymbol{\alpha}_{\text{slip}}$ be the vector of applied quasi-static force values and $\mathbf{q}_{r,\text{slip}}$ be the corresponding displacement vector calculated using QSMA. This system obeys Eq. 17. Therefore,

$$k_{\text{lin},r}\mathbf{q}_{r,\text{slip}} + \boldsymbol{\theta}_{\text{nl}} = \boldsymbol{\alpha}_{\text{slip}}. \tag{22}$$

The vector $\boldsymbol{\theta}_{\text{nl}}$ in the above equation is composed of both geometric and friction nonlinearity. Subtracting Eq. 19 from Eq. 22 in order to isolate the nonlinear force due to friction gives,

$$k_{\text{lin},r}[\mathbf{q}_{r,\text{slip}} - \mathbf{q}_{r,\text{stick}}] + \boldsymbol{\theta}_{\text{nl}} - \boldsymbol{\theta}_{\text{nl,stick}} = \boldsymbol{\alpha}_{\text{slip}} - \boldsymbol{\alpha}_{\text{stick}}. \tag{23}$$

If a new vector of query points, $\mathbf{q}_r$, is defined over which both $\boldsymbol{\alpha}_{\text{stick}}$ and $\boldsymbol{\alpha}_{\text{slip}}$ are interpolated, Eq. 23 can be re-written as

$$\alpha_{\text{slip}}(q_r) - \alpha_{\text{stick}}(q_r) = \theta_{\text{nl}}(q_r) - \theta_{\text{nl,stick}}(q_r); \qquad \forall q_r. \tag{24}$$

Substituting Eqs. 18 and 20 in Eq. 24 gives

$$\alpha_{\text{slip}}(q_r) - \alpha_{\text{stick}}(q_r) = \sum_{i=1}^{n} \frac{\hat{f}_i^*}{N} + \frac{\hat{k}}{N} q_r (N-n) - \hat{k} q_r \qquad \dot{q}_r > 0, \forall q_r \tag{25}$$

$$= \theta_{\text{hnl}}(q_r) \tag{26}$$

The first two terms on the right-hand side of Eq. 25 are similar to the total nonlinear force due to the Iwan model, given by Eq. 11. The linear term, $\hat{k}q_r$ gets subtracted since it was included as part of the SICE-ROM in Eq. 20. Therefore, what remains is the restoring force due to the underlying DEM that captures the effect of friction in the response of the nonlinear mode. Typically, the strengths of the sliders, $\hat{f}_i^*$ are defined by a parametric distribution function. However, this paper assumes the nonlinear force due to the DEM is quasi-linear in nature, i.e. the right-hand side of Eq. 25 can be linearized at each value of q_r and represented by a constant stiffness and dissipation at that amplitude. Section 3.3 further elaborates on how this dissipation and stiffness can be calculated using Masing's rules.

3.3 Estimating amplitude-dependent frequency and damping from the IGNL model

Nonlinear Normal Modes [98], or NNMs, are commonly used to represent the frequency-energy dependence in strongly nonlinear systems, such as structures with geometric nonlinearity. Peeters et al. [72] presented a shooting and pseudo-arclength numerical continuation method to compute NNMs. In simple terms, the shooting method estimates the periodic solution to a nonlinear equation of motion for a particular set of initial conditions using numerical time integration methods. Numerical continuation is simultaneously used to march along the NNM branch. once the coefficients of the SICE-ROM have been estimated using the procedure described in Sec. 3.2, this shooting and continuation algorithm can be used to calculate the NNM of the SICE-ROM that constitutes the IGNL model. This NNM quan-

tifies the change in the modal natural frequency due to geometric nonlinearity as a function of modal displacement amplitude, and has been represented in this paper as $\omega_{\text{gnl}}(q_r)$. Since the element associated with the SICE-ROM in the IGNL model has infinite yield strength, it does not contribute to the damping of the overall system. Therefore, Eq. 20 can be written in quasi-linear form as

$$\theta_{\text{nl,stick}} = \omega^2_{\text{gnl}}(q_r) \times q_r. \tag{27}$$

On the other hand, Eq. 25 defines the hysteretic nonlinear force of the IGNL model. Since this nonlinearity is defined entirely by Jenkins elements, it behaves like a Masing Model [88,91]. Therefore, Masing's rules can be applied to calculate the complete hysteretic loop at each modal amplitude level. The stiffness and damping can be estimated from these hysteresis loops, as described by Lacayo and Allen [26]. First, the change in stiffness at each displacement amplitude is given by the slope of the secant line at that amplitude, expressed mathematically by Eq. 28.

$$dK_{\text{hnl}}(q_r) = \frac{\theta_{\text{hnl}}(q_r)}{q_r}, \tag{28}$$

where $\theta_{\text{hnl}}(q_r) = \alpha_{\text{slip}}(q_r) - \alpha_{\text{stick}}(q_r)$. The value of dK_{hnl} should be negative since the yielding of the Jenkins elements results in a loss of stiffness. Next, the area inside the loop equals the total energy dissipated at that amplitude level, represented as $D_{\text{IGNL}}(q_r)$. This area can be evaluated numerically using the trapezoid rule at each amplitude. Figure 3 shows the hysteresis loop calculated for a representative displacement q using Masing's rules, and the corresponding secant stiffness and dissipation.

Now, the amplitude-dependent behavior due to geometric nonlinearity (SICE-ROM) and hysteretic or friction nonlinearity (Masing model) need to be combined. From Eq. 28, $\theta_{\text{hnl}}(q_r) = dK_{\text{hnl}}(q_r) \times q_r$. Combining this with Eq. 27 gives

$$\theta_{\text{nl,stick}} + \theta_{\text{hnl}} = \omega^2_{\text{gnl}}(q_r) \times q_r + dK_{\text{hnl}}(q_r) \times q_r. \tag{29}$$

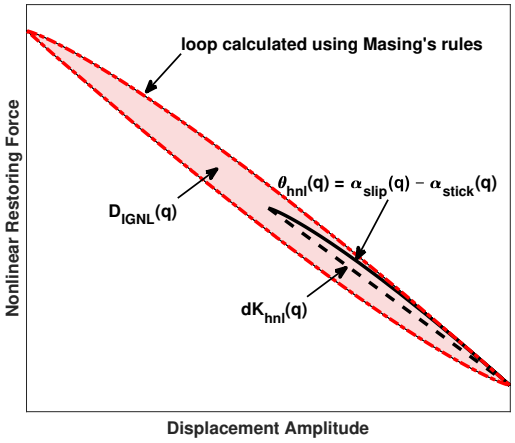

Figure 3: Illustrating the frequency and dissipation estimate due to hysteretic nonlinearity for amplitude q

Therefore, the total stiffness can be calculated using Eq. 30,

$$K_{\mathrm{IGNL}}(q_r) = (\omega_{\mathrm{gnl}}(q_r))^2 + dK_{\mathrm{hnl}}(q_r). \tag{30}$$

The natural frequency, ω_{IGNL} is then given by

$$\omega_{\mathrm{IGNL}}(q_r) = \sqrt{K_{\mathrm{IGNL}}(q_r)}. \tag{31}$$

To estimate the effective damping at each amplitude level from the dissipation, the analogy of a viscous damper is used, as shown by Lacayo et al. [57]. At each amplitude, an equivalent viscous damper oscillating at frequency ω_{IGNL} while dissipation energy D_{IGNL} gives damping ratio ζ_{IGNL}, according to Eq. 32,

$$\zeta_{\mathrm{IGNL}}(q_r) = \frac{D_{\mathrm{IGNL}}(q_r)}{2\pi q_{\mathrm{r}}^2(\omega_{\mathrm{IGNL}}(q_r))^2} + \zeta_{0,\mathrm{r}} \tag{32}$$

where $D_{\mathrm{IGNL}}(q_r)$ is calculated as the area inside the hysteresis loop at amplitude q_r.

In this way, the nonlinearity of the r^{th} mode can be characterized using the method of QSMA and the modified distributed element model. Note that an alternative to applying

Masing's rules would be to compute the complete hysteresis loop at each amplitude through QSMA itself. In this case, the force would need to be applied as an initial loading up to a positive amplitude followed by a reverse loading up to negative amplitude of the same magnitude and then a reloading back to the positive amplitude. However, Lengger and Wilner [99] show that the computational effort required to simulate the complete hysteresis loop at each amplitude make this method highly expensive.

4 Numerical Case Study - SDOF System with Cubic Spring and Iwan Element

To test the validity of the above-presented method, a single degree-of-freedom (SDOF) system with a parallel arrangement of a cubic spring and Iwan element was considered. The four-parameter Iwan model [35], commonly used to represent bolted joint nonlinearity, was used to define the distribution of the slider strengths seen in Fig. 2. The parameters of the system are listed in Table 10. The resulting system has a low-amplitude stuck frequency of 100 Hz. The cubic spring has a positive coefficient K_3, resulting in hardening behavior, i.e. the nonlinear stiffness due to this spring increases with increase in amplitude. The Iwan model, on the other hand, always exhibits softening behavior, i.e. it results in a decrease in stiffness with increasing amplitude. Thus, in this case study, the two nonlinearities can be understood to have opposing effects on the frequency.

As proposed in Sec. 3, two quasi-static analyses were performed. First, only the cubic spring was active, i.e. the Iwan element experienced no slip. This can be understood as replacing the Iwan element with a linear spring of stiffness K_{T} representing the total stiffness of all of the sliders, plus a linear spring K_∞ representing the stiffness of the Iwan joint when all sliders have slipped. Both of these are in parallel with the cubic spring. The low-amplitude linear frequency of the system equals the stuck frequency of 100 Hz. To estimate the force-displacement backbone curve, a linearly spaced force vector, $\mathbf{f}_{(\mathbf{nl},\mathbf{1})}$, from 1×10^{-4}

Table 10: Properties of the nonlinear SDOF system used in the numerical case study

Parameter	Value
Mass (m)	1 kg
Linear macroslip stiffness (K_∞)	1.316×10^5 N/m
Material damping (ξ_{lin})	1×10^{-4}
Cubic spring stiffness (K_3)	5.396×10^{10} N/m^3
Iwan model [$F_\text{s}, K_\text{T}, \chi, \beta$]	[10000 N,2.632×10^5 N/m,-0.8,2]

N to 5000 N was defined. Note that a cubic spring results in symmetric force-displacement curves in the positive and negative loading directions. Therefore, only the positive loading curve is sufficient to fully identify the geometric nonlinearity exhibited. The displacement at each force value was then calculated by solving Eq. 33. Since this is a cubic equation, the roots could be calculated using Cardano's formula. However, the results presented here were obtained by solving the equation implicitly using the Newton-Raphson iteration scheme [44], so that the same numerical method could also be used when the Iwan model is considered in the subsequent quasi-static analysis. The resulting nonlinear displacement is represented here as $\mathbf{x_1}$. The dashed-dotted curve in Fig. 4a shows the force-displacement behavior obtained.

$$(K_\infty + K_\text{T})\mathbf{x_1} + K_3\mathbf{x_1^3} = \mathbf{f_{(nl,1)}} \tag{33}$$

In the second case, the complete system, including the four-parameter Iwan model, was considered. The nonlinear displacement, given by $\mathbf{x_2}$, was calculated by solving Eq. 34,

$$K_\infty\mathbf{x_2} + K_3\mathbf{x_2^3} + \mathbf{f_j}(\mathbf{x_2}, \phi) = \mathbf{f_{(nl,2)}} \tag{34}$$

where $\mathbf{f_j}(\mathbf{x_2}, \phi)$ is the nonlinear restoring force due to the Iwan model, given by Eq. 35.

$$f_\text{j}(x_2, \phi) = \int_0^\infty \rho(\phi)[x_2 - x_\text{s}(\phi)]d\phi \tag{35}$$

Here, $x_s(\phi)$ is the slider displacement, ϕ is the strength of the slider, and $\rho(\phi)$ is the density of sliders that have strength ϕ. Now, similar to case 1, Eq. 34 can be solved for x_2 using the Newton-Raphson scheme. To do so, the integral in Eq. 35 needs to be discretized. This was done using the method outlined in [35], with a total of 100 discretization points or sliders. The resultant backbone curve for case 2 is given by the solid line in Fig. 4a.

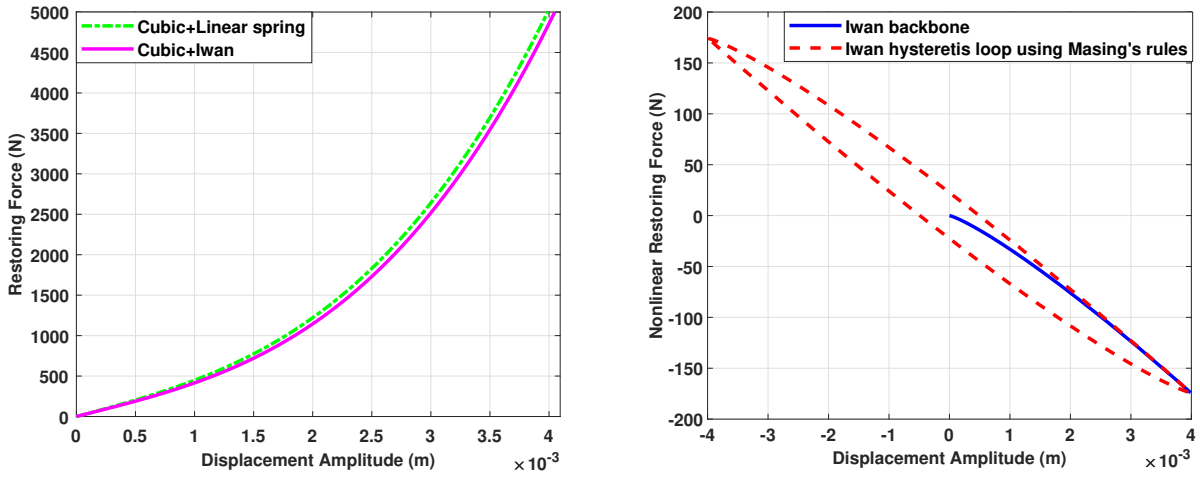

(a) (b)

Figure 4: (a) Force-displacement curve $\mathbf{f}_{(nl,1)}$ with all sliders stuck, i.e. when the cubic spring is in parallel with a linear spring (dashed-dotted curve), and curve $\mathbf{f}_{(nl,2)}$ when the cubic spring is in parallel with the Iwan element (solid curve), (b) The restoring force purely due to the Iwan element, obtained by subtracting the dashed-dotted curve from the solid curve in (a) (solid line) and the hysteresis loop at maximum amplitude, calculated using Masing's rules (dashed line)

As described in Sec. 3.2, the nonlinear restoring force purely due to the Iwan model can be obtained by subtracting the restoring force when only the cubic spring is active (i.e. case 1) from the restoring force obtained when both the cubic spring and the Iwan element are active (i.e. case 2). However, since the quasi-static analyses were performed by solving for the nonlinear displacement, the restoring force for case 2 was first interpolated linearly over the nonlinear displacement obtained for case 1, using Eq. 36,

$$f^*_{(nl,2)_i} = f_{(\mathrm{nl},2)_{i-}} + (x_{1_i} - x_{2_{i-}}) \left[\frac{f_{(\mathrm{nl},2)_{i+}} - f_{(\mathrm{nl},2)_{i-}}}{x_{2_{i+}} - x_{2_{i-}}} \right], \ \forall i \in [1, N] \tag{36}$$

where N is the length of the vector $\mathbf{x_1}$, $i+$ is the index of the first element of $f_{(\mathrm{nl},2)}$ that is greater than or equal to $f_{(\mathrm{nl},1_\mathrm{i})}$ and $i-$ is the index of the first element of $f_{(\mathrm{nl},2)}$ that is less than $f_{(\mathrm{nl},1_i)}$. The nonlinear restoring force purely due to the Iwan model, $\mathbf{f}_{\mathrm{nl,Iwan}}$ was then obtained using Eq. 37. Figure 4b shows this nonlinear force as a function of displacement.

$$\mathbf{f}_{\mathrm{nl,Iwan}} = \mathbf{f}^*_{(\mathrm{nl},2)} - \mathbf{f}_{(\mathrm{nl},1)} \tag{37}$$

Next, the amplitude-dependent frequency and damping were calculated from these backbone curves using the method outlined in Sec. 3.3. The effect of cubic spring alone on the frequency was estimated using the pseudo-arclength continuation method [72]. For the Iwan model, Masing's rules were applied to $\mathbf{f}_{\mathrm{nl,Iwan}}$ to estimate the complete hysteresis loop at every displacement amplitude. The dashed line in Fig. 4b shows the hysteresis loop calculated at the maximum amplitude. The area inside the hysteresis loop at each amplitude gave the dissipation due to the Iwan model at that amplitude, while Eq. 28 was used to calculate the loss of stiffness at that amplitude. Finally, the overall nonlinear frequency and damping was then calculated using Eqs. 30-32.

The complete system's dynamic response to non-zero initial conditions was simulated to verify the quasi-static results. The displacement and state of the sliders at the end of the quasi-static analysis were used to define the initial conditions of the dynamic analysis. This means the initial displacement was set equal to the highest value of $\mathbf{x}_2$. A total of 100 sliders, or discretization points, were used, similar to the quasi-static analysis, and the initial positions of these sliders were set equal to the final positions calculated in the quasi-static analysis. The initial velocity and acceleration of the SDOF system was set to zero. The Newmark-β method [44] was used to integrate the nonlinear differential equations. Since this is an implicit integration technique, a Newton-Raphson iteration scheme must be used to converge to a solution at each time step. Shetty and Allen [83] provide the equations necessary to implement the Newmark-β method for an SDOF system with a single Iwan

element. In the case presented here, the equations for the residue function, η_{NR}, and gradient, θ_{NR}, of the Newton-Raphson scheme need to be modified, with an additional term included to account for the cubic spring. Equations 38 and 39 describe the modified residue and gradient,

$$\eta_{\mathrm{NR}} = m\ddot{x}_{n+1} + C_{\mathrm{lin}}\dot{x}_{n+1} + K_{\infty}x_{n+1} + F_{\mathrm{nl}}(x_{n+1}, \boldsymbol{\phi}_{n+1}) + K_3 x_{n+1}^3 - F_{\mathrm{ext}}(t_{n+1}) \tag{38}$$

$$\theta_{\mathrm{NR}} = m + C_{\mathrm{lin}}\gamma_{\mathrm{nb}}\triangle t + [K_{\infty} + K_{\mathrm{nl}} + 3K_3 x_{n+1}^2]\beta_{\mathrm{nb}}(\triangle t)^2 \tag{39}$$

where $(n+1)$ represents the current time step, n represents the previous time step and $\triangle t$ is the step size. The nonlinear force due to the Iwan model, $F_{\mathrm{nl}}(x, \boldsymbol{\phi})$ and the corresponding stiffness $K_{\mathrm{nl}}(x, \boldsymbol{\phi})$ depend on the current displacement x and position of the sliders $\boldsymbol{\phi}$, a 100×1 vector, and are calculated for every iteration using the equations derived in [35]. The constants β_{NB} and γ_{NB} are pre-defined based on whether a constant or linear acceleration between time steps is assumed. Further details can be found in [83]. Figure 5 shows the evolution of displacement over time obtained after integration.

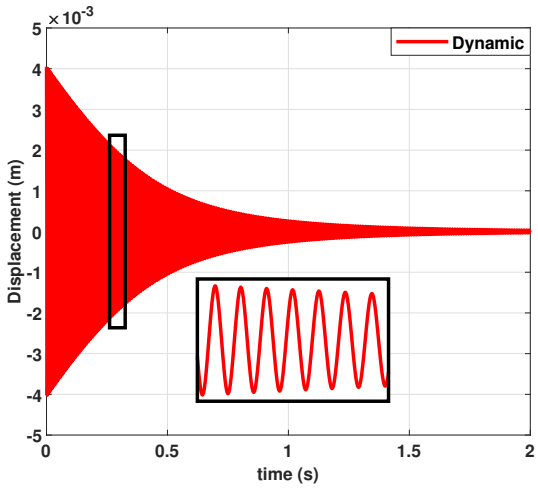

Figure 5: The dynamic response (displacement vs time) for the SDOF model with a parallel arrangement of cubic spring and Iwan element

This dynamic response was then post-processed using the Hilbert transform [89] to estimate the amplitude-dependent frequency and damping. Figure 6a compares the amplitude-

dependent frequency from the dynamic analysis (dashed line) against the IGNL model (solid line). The dashed-dotted line in Fig. 6a, $\omega_{n,3}(X)$, was obtained by using the pseudo-arclength continuation method to calculate the nonlinear normal mode (NNM) of the SDOF system with just a cubic spring. As can be seen, the Iwan element causes significant change in frequency, especially at lower displacement amplitudes. Note here that both the dynamic analysis result (dashed line) and the final quasi-static result (solid line) eventually converge to the linear frequency value of 100 Hz at very low amplitudes, beyond the left edge of Fig 6a. There is good agreement between the true dynamic response and the IGNL model prediction at lower displacement amplitudes, with near zero error as seen in Fig. 6b. The error in frequency increases with amplitude, with a maximum error of 2.96%. While it is possible that the the proposed quasi-static method is less accurate as the level of nonlinearity increases at high amplitudes, it must be noted that the accuracy of the dynamic result itself is sensitive to the time-step used for the Newmark-β integration. As the frequency of oscillation of the system increases, the time-step must be decreased to mitigate integration error. For the results presented, a time-step $\triangle t = 1 \times 10^{-6}$s was used. Despite such a small step-size, it can be seen in Fig. 6a that the frequency estimated by the dynamic analysis at the highest amplitude is even higher than that due to just the cubic spring (dashed-dotted line). This is not realistic, though, since the cubic spring provides an upper bound to the expected hardening behavior.

Figure 7a plots the amplitude-dependent damping calculated from the dynamic analysis (dashed line) and the proposed method (solid line). Note that a traditional reduced order model, such as a SICE model, would not be able to predict the nonlinearity in the damping that is observed here, so one would have to assume a damping ratio based on material damping ($\zeta = 1 \times 10^{-4}$ in this case) or past experience. At low amplitudes, the proposed method gives an error of about 10%. This error decreases, and then increases, as the amplitude increases. The dotted line in this figure was obtained by calculating the damping as a function of the secant frequency estimated using Masing's rules instead of the final frequency estimate

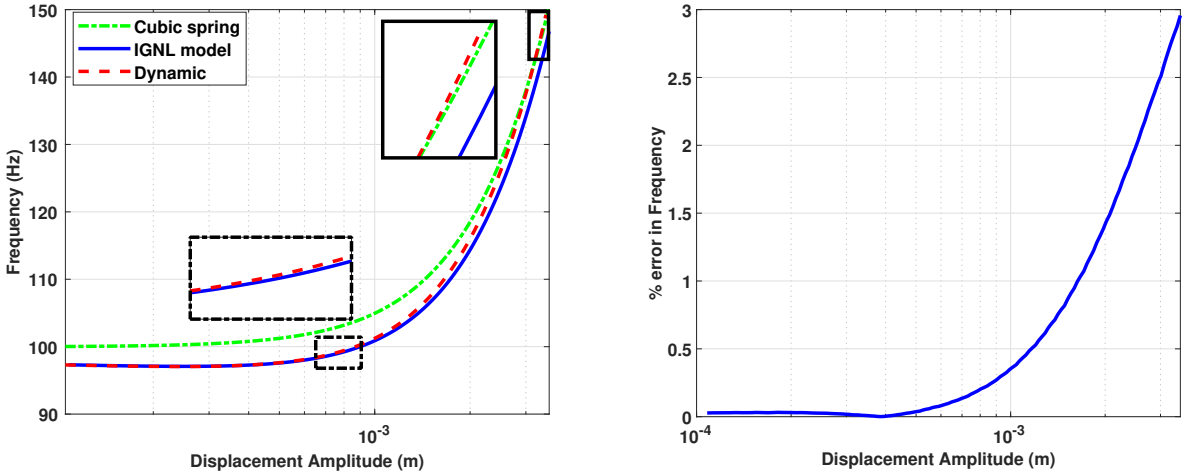

(a) (b)

Figure 6: (a) Comparing the amplitude-dependent frequency estimated using the proposed method (solid curve) and by performing a dynamic analysis (dashed curve) when $K_3 = 5.396 \times 10^10$ N/m^3 (positive). The dashed-dotted curve is the amplitude-dependent frequency change only due to the cubic spring, calculated using pseudo-arclength continuation. (b) The percentage error in frequency estimated using the proposed method, when compared to the dynamic results.

of the full IGNL model. As the amplitude increases, the dotted line significantly deviates from the dashed and solid lines. To explain this, consider Eq. 32, used to calculate the damping ratio from dissipation. The damping ratio at each amplitude is inversely proportional to the frequency at that amplitude. As the amplitude increases, the hardening effect of the cubic spring strongly influences the overall frequency, and this significant increase in frequency causes the damping ratio to decrease despite the dissipation increasing. This is why using the secant frequency gives inaccurate damping ratios at higher amplitudes and it is essential to account for the actual instantaneous frequency of the full IGNL model.

Performing the dynamic analysis for this nonlinear SDOF system using the Newmark-β method with a time-step of $1 \times 10^{-6} s$ took $634.68 s$ of processor time on an Intel(R) Core(TM) i7 CPU 950 @ 3.07GHz. On the other hand, the two quasi-static analyses and application of Masing's rules took $0.345 s$, while the pseudo-arclength continuation algorithm to estimate the frequency of the cubic spring took about $20 s$, resulting in a total simulation time of

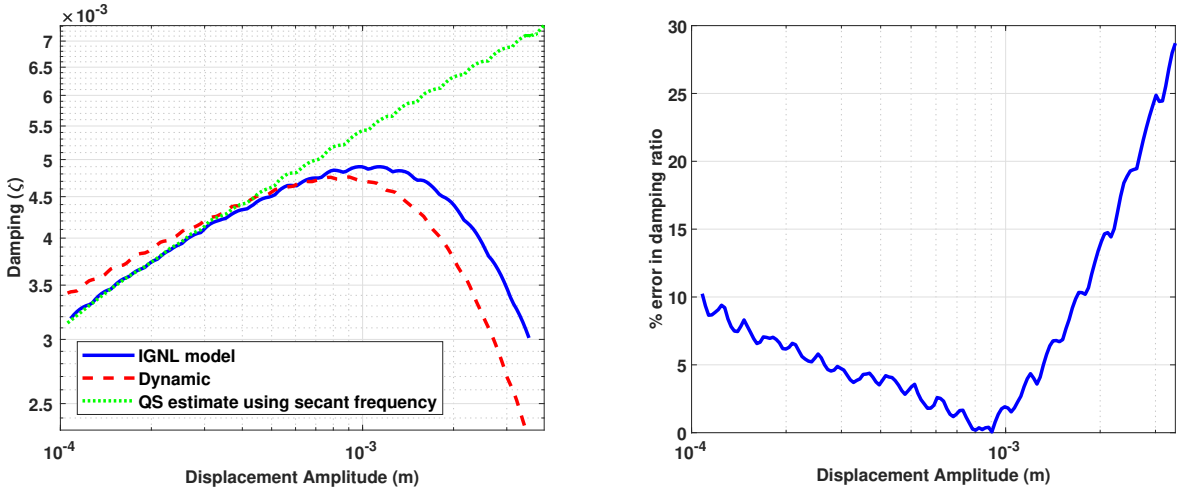

(a) (b)

Figure 7: (a) Comparing the amplitude-dependent damping estimated using the proposed method (solid curve) and by performing a dynamic analysis (dashed curve) when $K_3 = 5.396 \times 10^10$ N/m^3 (positive). The dashed-dotted curve represents the quasi-static estimate when using the secant frequency to calculate the damping ratio from the dissipation. (b) Percentage error in damping between the solid and dashed curves in (a)

20.345s. Thus, the proposed method is nearly 30 times faster than performing dynamic simulations to characterize the nonlinear behavior of the system.

A second case with negative cubic stiffness was considered, to evaluate the accuracy of the proposed method when both the cubic spring and the Iwan element exhibit softening behavior. A value of $K_3 = -5.395 \times 10^8$ N/m^3 was used, keeping all other parameters the same. The amplitude-dependent frequency and damping were estimated by following the exact same procedure as the one used for the positive cubic stiffness case. Figure 8a shows that the frequency estimated using the proposed method is in very good agreement with the dynamic results, with a maximum error of 0.41% at the highest amplitude. Figure 8b shows that the predicted amplitude-dependent damping is also in good agreement with the dynamic results. In fact, the proposed quasi-static method gives better results in this case than in the case of positive cubic stiffness. One reason for this could be that the proposed method is more effective when the Iwan, or friction, nonlinearity is the dominant form of

nonlinearity. When the cubic spring stiffness is positive, the hardening effect dominates the overall system nonlinearity and opposes the Iwan element by reducing the number of sliders that can slip. On the other hand, the negative cubic stiffness results in softening behavior that assists, or amplifies the effect of, the Iwan element. Additionally, when the cubic spring stiffness is positive, the strong nonlinearity results in excitation of higher harmonics which may violate the quasi-linear assumptions used in the proposed method. On the other hand, the nonlinearity with negative cubic stiffness is less severe, obeying those assumptions.

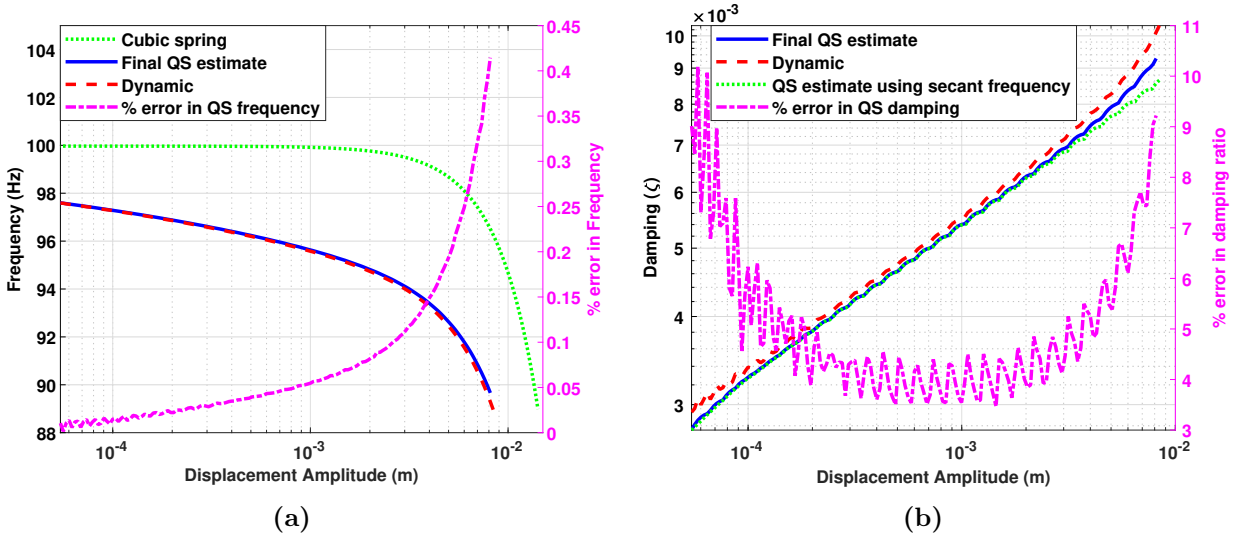

Figure 8: (a) Amplitude dependent frequency (left axis) and percentage error in the frequency (right axis) when $K_3 = -5.395 \times 10^8$ N/m^3, and (b) the corresponding amplitude-dependent damping (left axis) and percentage error in damping (right axis)

5 Application to the Tribomechadynamics Benchmark Structure

Krack et al. [100] proposed a challenge - to perform a blind prediction of the dynamic behavior of a system with geometric and friction nonlinearity, referred to, here, as the Tribomechadynamics (or TMD) benchmark structure. A 3D CAD model of this structure is

shown in Fig. 9. It consists of four main parts - a thin panel, a monolithic support comprising two pillars and a rear plate, and two blades. The panel is 1.5 mm thick, and is clamped between the blades and the support pillars via screws and washers. The surface of the support that is in contact with the panel has an inclination of about 1.1°. Thus, the panel has some curvature when assembled. The bolted connections that clamp the panel to the support introduce friction nonlinearity in the structure, whereas the clamped panel itself exhibits geometric nonlinearity due to transverse deflection causing in-plane stresses (i.e bending-stretching coupling). The support is designed to be mounted to a shaker through a fixture along the rear plate. This structure was designed to be representative of real-world, industrial systems such as aircraft wing panels. The presence of both forms of nonlinearities makes this a challenging structure to study. Kuether et al. [96] found that it can take nearly 56 hours to simulate 0.25 s of dynamic response of a 3D FE model of the structure, using an HPC cluster with 9 nodes and 432 cores. This highlights the potential of a more computationally efficient approach, like the one presented here.

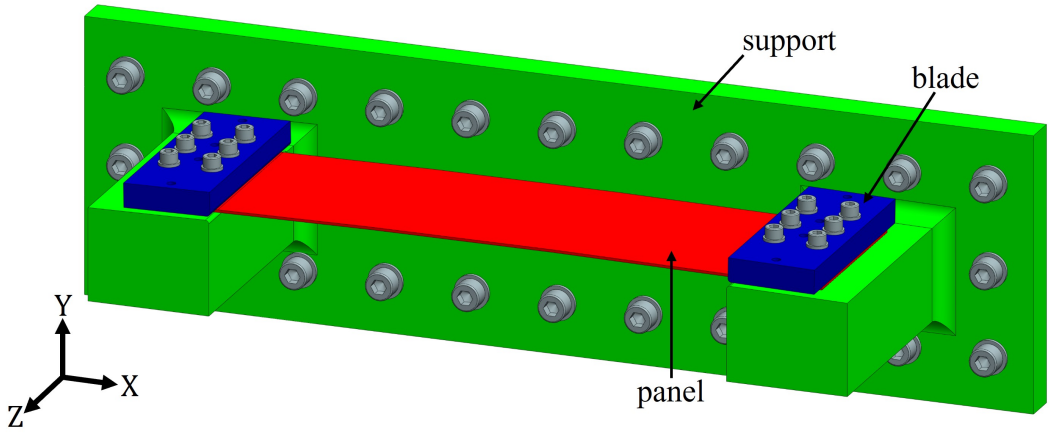

Figure 9: CAD model of the benchmark structure

The main aim of the challenge was to predict the nonlinear frequency and damping of the first bending mode of the system as a function of the displacement amplitude. To do so, first a suitable FE model needs to be created. Even quasi-static analyses of 3D FE models containing contact can be highly computationally expensive. For example, Wall et al. [56]

found that a 3D model of two beams with held together using two lap joints required a minimum of 6 hours to perform a quasi-static analysis, with the solve-time climbing up to 48 hours if the contact surfaces were not initially flat. Therefore, a 2D FE model of the TMD structure was created to characterize its nonlinearity. Certain approximations were made to model the 3D structure in 2D. First, the bolt preload was simulated by applying a pressure load along a line of length equal to the washer diameter. According to the model specifications, the fasteners clamping the panels at the ends are ISO 4762 - M6 screws, with a tensile strength of 800 MPa, and yield strength of $0.8 \times 800 = 640$ MPa. The applied preload is 90% of the yield strength. With a pitch diameter (d_p) of 5.35 mm and core diameter (d_c) of 4.773 mm for the M6 coarse series, the stress area can be calculated as $\pi(d_\mathrm{p}d_\mathrm{c})^2/16 = 20.1$ mm^2. Therefore, the applied preload equals 11578 N. The line pressure applied in the FE model was assumed to be an average of the total pressure acting along the depth of the support (or along the Z-axis), i.e. an average of the preload force acting on the area covered by the three washers and zero force acting on the rest of the area. Since the washers have a diameter of 12 mm, a pressure of 20.68 MPa was applied over a length of 12 mm. Note that the 2D FE model assumes unit thickness along the Z-axis. Second, it was estimated that the stiffness arising due to the cantilever nature of the support-fixture arrangement is large enough for the support to be assumed to behave as a rigid structure. Therefore, fixed translational and rotational boundary conditions were applied at all the nodes along the bottom edge of the support. This assumption was verified by creating a 3D model and comparing the linear frequencies for the two different boundary conditions [101]. Next, a Coulomb friction model, with a friction coefficient $\mu = 0.6$, was implemented to model the interface interactions. Three-node linear (CPE3 in Abaqus) plane strain elements were used to mesh all the parts. Initially, a mesh size of 1 mm was used near all the contact regions. After running a modal and quasi-static nonlinear analysis, this was refined further to better capture slip at the interfaces, reducing the size to $0.2 - 0.5$ mm. Five elements were used across the thickness of the panel. The mesh was gradually made coarser further away from

the contact regions, with a maximum mesh size of 3 mm. The panel was modeled as flat and the application of line pressure in the preload step resulted in its curvature, as would be the case experimentally. Figure 10 shows the 2D FE model that was created. The magnified version of the left-hand side contact interface shows the fine mesh that was used to capture the slip behavior at the interface. It also shows the panel modeled as flat with the support being at an angle, resulting in a gap between the two before the preload was applied. Note that the same mesh was replicated on the right-hand side interface.

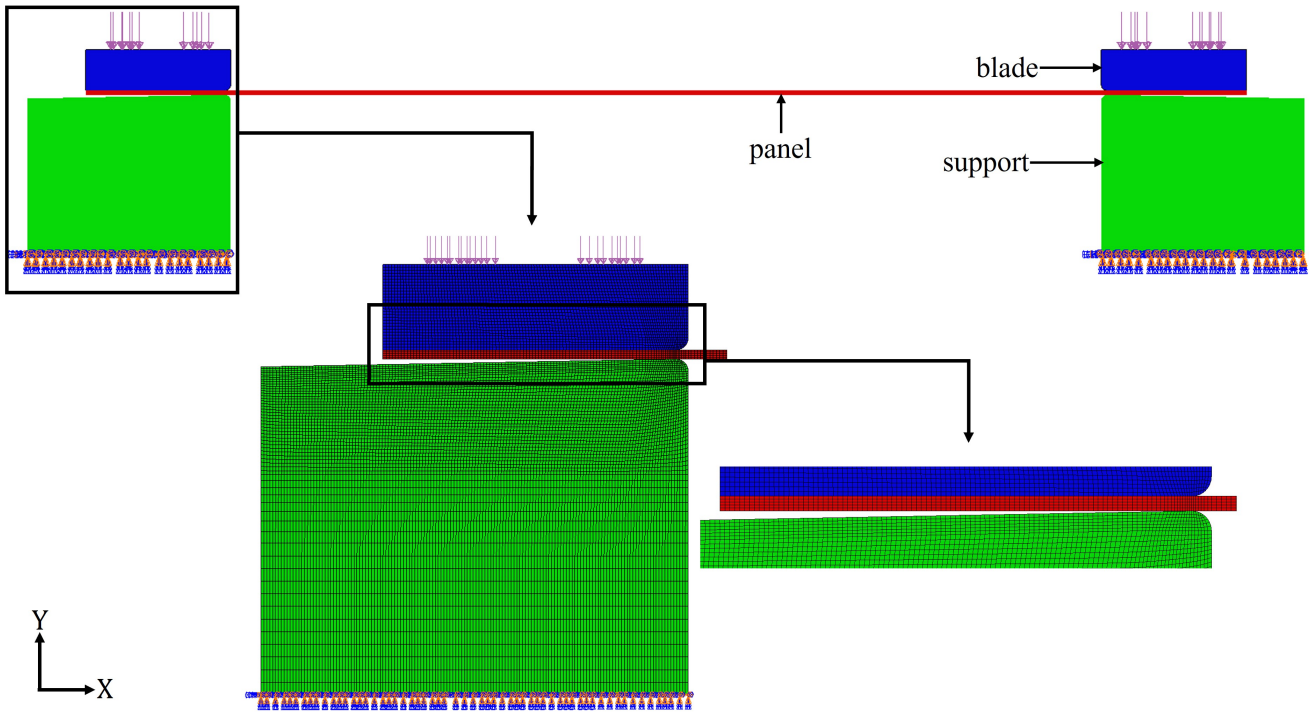

Figure 10: 2D FE model of the TMD structure, with a magnified version of the left-hand side interface showing the mesh density at contact

Figure 11 outlines the procedure used to estimate the amplitude-dependent frequency and damping for the TMD structure from the 2D FE model. The first step was a preload analysis, where the pressure applied resulted in 1) a negative bending moment on the panel and, 2) complete contact between the panel and the top surface of the support. This step estimated the contact pressure at the interfaces and the curvature of the panel when assembled. Step 1 was then followed by a linear modal analysis, step 2, estimating the linear frequencies and

mode shapes of the first 15 modes. The linear frequency of mode 1 was found to be 118.12 Hz.

Step 3 was the main, quasi-static step, where concentrated loads were applied to load the FE model in the shape of mode 1. The mode shape calculated in step 2 was used to define the concentrated loads. Three separate quasi-static analyses - referred to, here, as A, B and C - were performed. For analysis A and B, the contact type at all interfaces was changed to not allow any slip between interfaces (i.e. $\mu = \infty$). In Abaqus, this corresponds to selecting the contact type as 'Rough' when defining the tangential behavior of the interaction property. In analysis A, the load was applied along the negative Y-axis, i.e. opposing the curvature of the panel. On the other hand, in analysis B, the load was applied along the positive Y-axis. Both these analyses are required to fully characterize the geometric nonlinearity since the curvature of the panel results in unsymmetric behavior along the positive and negative loading directions. On the other hand, analysis C had frictional contact with $\mu = 0.6$, same as the preload step. There is no difference in the loading of analyses B and C; the only difference is in the friction at the surfaces. A version of the modified Riks method [102] was used to solve the quasi-static step in all analyses. This method is suitable for highly nonlinear structures since it can capture any geometric instabilities when computing the force-displacement curve. In the modified Riks method, the scale of the loading is also solved for, using arclength continuation. Since the panel deflects by approximately 1.15 mm at the center by the end of the preload step, the maximum displacement at the center of the panel for stopping the quasi-static analysis was set to be 4.2 mm, resulting in a deflection approximately 3 mm (i.e. twice the thickness of the panel) in the quasi-static step.

Figure 12 shows the quasi-static force-displacement curves from analyses A and B. As anticipated, the curve is not symmetric in the positive and negative directions due to the curvature of the panel. The contribution of each mode to the displacement at the center of the panel was also plotted to check for static coupling between the modes. The displacement at the panel center due to mode r can be given as $x_{r,c} = \Phi_{r,c}^T q_r$, where c equals the node

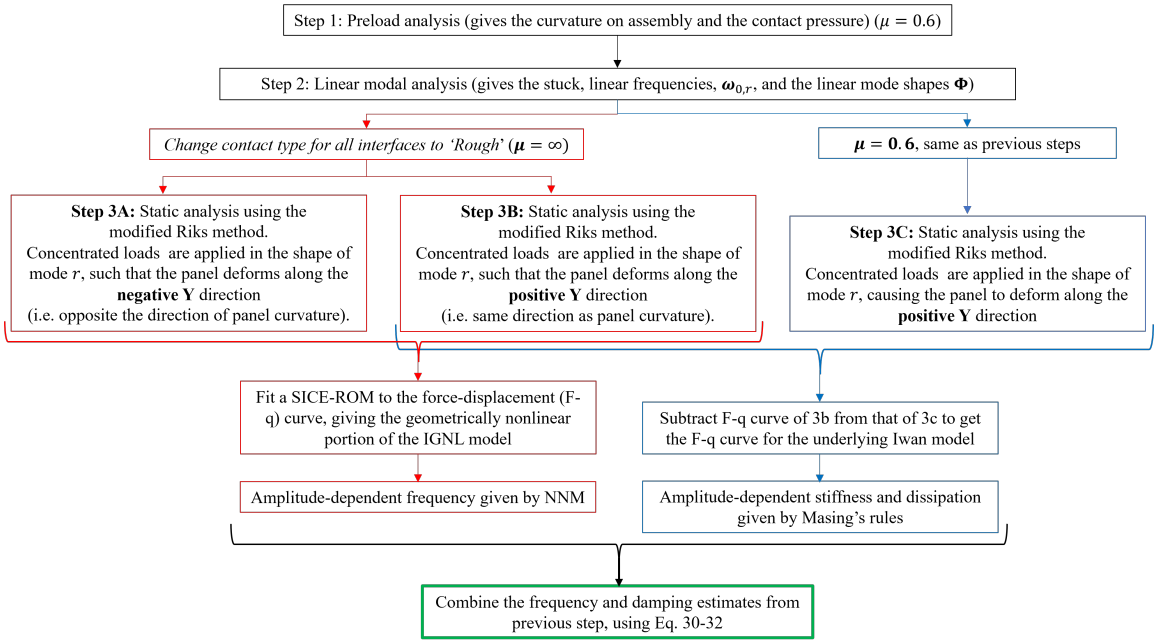

Figure 11: Flowchart summarizing the steps involved in estimating the amplitude-dependent nonlinearities from a full FE model using the proposed quasi-static approach and the IGNL model

index corresponding to the panel center. Figure 13a shows the contribution of modes 1, 3, 5 and 7, the first four dominant modes. It can be seen that the third mode shows maximum static coupling to mode 1. The maximum displacement due to mode 3 was 0.306 mm, which is only 9.6% of the displacement due to mode 1. Therefore, the SICE-ROM was fit only to mode 1 and static coupling was neglected.

Third to seventh order SICE-ROMs were considered. As seen in Fig. 13a, the 3^{rd} order ROM did not accurately fit the low-amplitude softening observed during negative loading. Additionally, higher order ROMs were able to capture the force-displacement behavior at high amplitudes better. Note that the 6^{th} and 7^{th} order fits have not been included in Fig. 13a for clarity. Figure 13b shows the amplitude-dependent frequency due to the SICE-ROMs of varying order, obtained by the arclength continuation method described in Sec. 3.3. The softening behavior between 0.5 mm and 1 mm corresponds to the low-amplitude softening observed in the negative loading direction in Fig. 13a. Additionally, it can be seen that the SICE-ROMs of odd order show more softening that those of even order. As the order of the

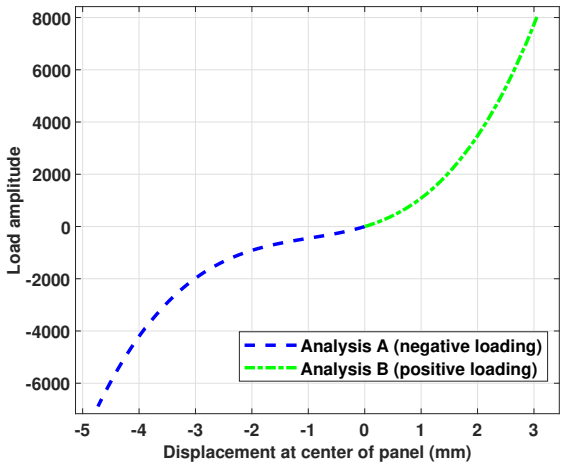

Figure 12: Quasi-static response when no slip allowed at interfaces. The load amplitude is plotted against the displacement of the center of the panel, as calculated using FEA.

ROM increases, the difference between the NNMs significantly decreases, with the NNMs from the 5^{th} and 7^{th} order ROMs nearly overlapping. Therefore, the 5^{th} order SICE-ROM was used in the IGNL model.

On the other hand, analyses B and C were considered to characterize the friction nonlinearity of the mode, with their respective force-displacement curves shown in Fig. 14a. The force estimated from analysis B was subtracted from that of analysis C to isolate the effect of friction. The resulting nonlinear restoring force due to friction is plotted against the displacement of the panel center in Fig. 14b. Masing's rules were then applied to estimate the change in stiffness and dissipation due to friction. Finally, the results of Masing's rules were combined with the NNM estimated by the 5^{th} order SICE using the method described in Sec. 3.3. Figure 15a compares the amplitude-dependent frequency of the final IGNL model with the NNM of the 5^{th} order SICE. At low displacement amplitudes, the frequency of the IGNL model is lower than the SICE-ROM, due to the decrease in stiffness as a result of friction. As the amplitude increases, the hardening behavior due to geometric nonlinearity dominates, leading to an overall increase in frequency. While the effect of friction on the frequency is small, its effect on the overall damping is significant, as seen in Fig. 15b. Note that the

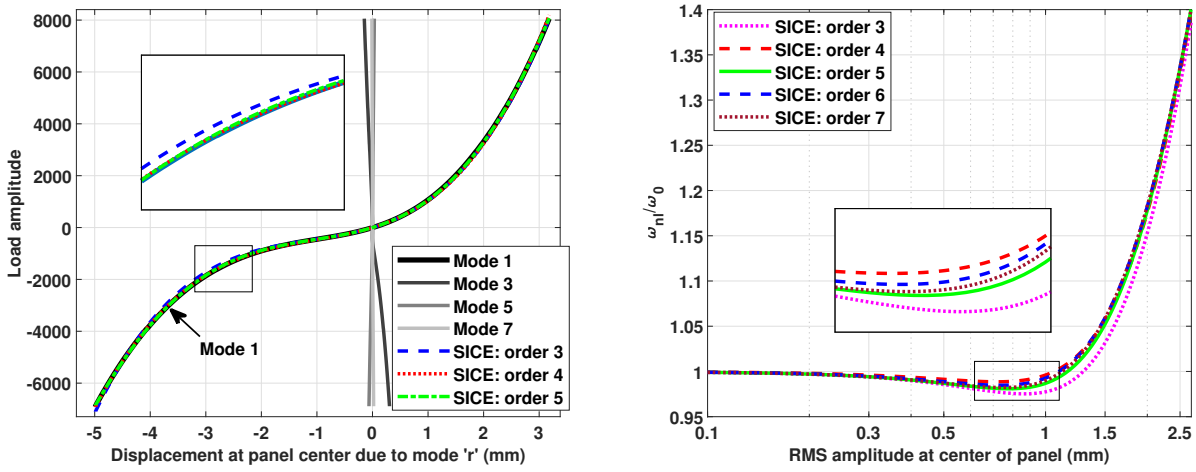

(a) (b)

Figure 13: (a) Quasi-static response of the four most dominant modes, when the load is applied in the shape of mode 1. The X-axis represents the contribution of each dominant mode to the displacement at the center of the panel, and the Y axis represents the load amplitude. The dashed, dotted and dashed-dotted lines show the 3rd, 4th and 5th order SICE polynomial fits respectively; (b) The frequency estimated by the SICE-ROMs of order 3-7 plotted against the root-mean-square (RMS) amplitude of the center of the panel. The frequency is non-dimensionalized by dividing by the linear frequency of mode 1, i.e. 118.12 **Hz.**

damping between 0.1 mm and 0.3 mm contains noise, likely due to the size of the mesh. An even finer mesh would be needed to capture slip at low amplitudes more accurately.

Table 11 shows the time taken to complete the above analysis on an Intel(R) i7-4790K CPU running at 4 GHz using 7 processors. The preload step required significant computational effort since the curvature of the panel was calculated in this step by the application of the preload force. The quasi-static analysis with infinite friction and negative loading, i.e. analysis A, required smaller increments at low amplitudes in comparison to analysis B, resulting in greater computational time. After completion of the quasi-static analysis, some post-processing is required to extract the force-displacement data from the output files. This process took longer than the quasi-static analysis itself, as shown in Table 11. Overall, the simulation took approximately 6 hours, which is significantly faster than performing a dynamic analysis [96]. Note that efforts are underway to implement some of these

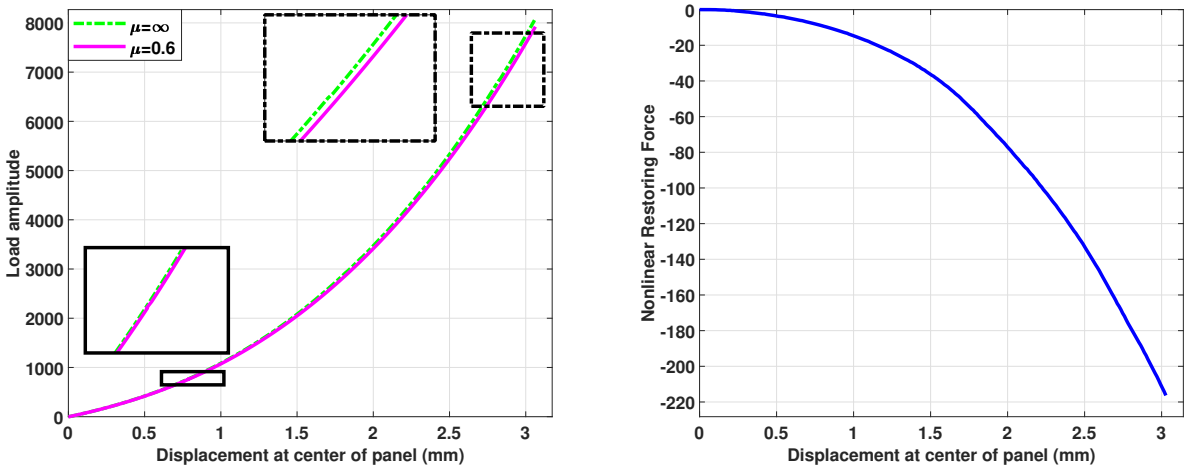

(a) (b)

Figure 14: (a) Force-displacement curve from analysis B (dashed-dotted curve), i.e. when the coefficient of friction is infinity, and from analysis C (solid curve), i.e. when the coefficient of friction is 0.6**; (b) The restoring force purely due to friction, obtained by subtracting the dashed-dotted curve from the solid curve in (a)**

steps in Python or directly within the FEA package to further reduce the computational effort required.

One of the assumptions made in the proposed method is that the system obeys Masing's rules. This was verified for the TMD model by applying Masing's rules to the force-displacement curve due to negative loading. For a hysteretic system that obeys Masing's rules, the above results should be valid even in the negative loading direction. For example, if the cubic spring in the case study presented in Sec. 4 was replaced by a higher-order SICE-ROM that showed unsymmetric behavior in the positive and negative loading directions, the quasi-static identification approach used in Sec. 4 could be performed for either positive or negative loading, giving identical results. For the TMD model, this was tested by performing quasi-static analysis C with negative instead of positive loading. The nonlinear force from analysis A was then subtracted to check if the resulting nonlinear force-displacement curve is symmetric about the origin to the force-displacement curve from the positive loading case (plotted in Fig. 14b). Figure 16a shows the two quasi-static curves to be subtracted, and

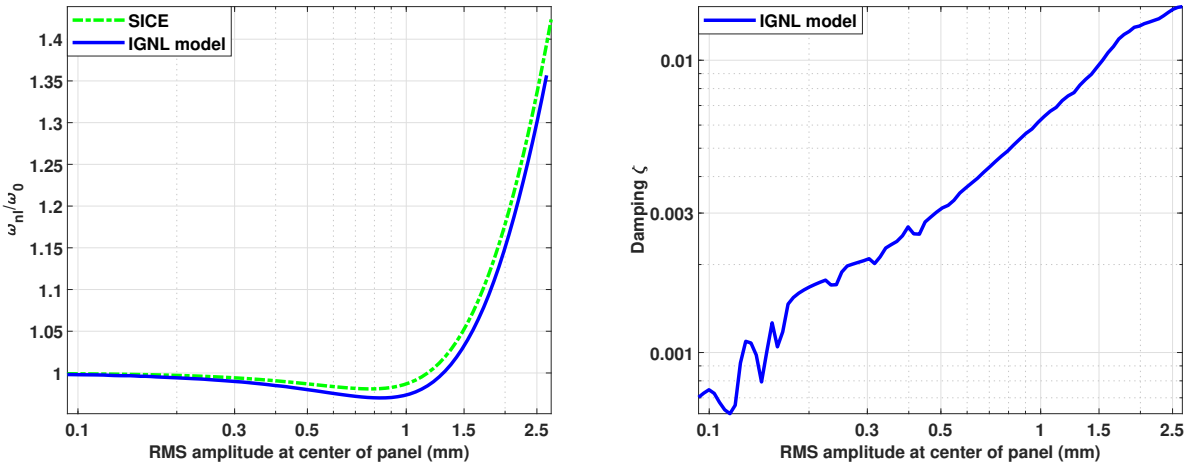

(a) (b)

Figure 15: (a) Non-dimensional frequency vs. RMS amplitude of the center of the panel, estimated from the 5^{th} order SICE (dashed-dotted line) and from the full IGNL model (solid line); (b) Damping vs. RMS amplitude estimated by applying Masing's rules to the IGNL model

Fig. 16b compares the nonlinear force after subtraction against that obtained from positive loading. Note that, on subtraction, the restoring force due to friction in case of negative loading is in the second quadrant. However, in Fig. 16b, the curve has been mirrored about the origin by multiplying both the force and displacement vectors by -1 in order to easily compare it with the positive loading case. It can be seen that the curves from the positive and negative loading cases do not overlap. On studying the contact status, it was found that no slip occurs at the interfaces until the panel, which is concave at the start of the quasi-static step, deforms to a convex curvature. This explains why the frictional force is negligible up to a displacement value of 1.28 mm in Fig. 16b. Moreover, even after the onset of slip, the backbone curves obtained from positive and negative loading have different slopes, indicating different rates of slip. This implies that the hysteretic behavior of the FE model under consideration deviates from that due to a Masing model.

Nevertheless, Masing's rules were applied to the force-displacement curve from the negative loading case to estimate the bounds of the amplitude-dependent frequency and damping

Table 11: Time taken to estimate the frequency and damping of the TMD 2D FE model using QSMA and the IGNL model

Analysis	**Simulation time**
Preload Analysis	3912 s ($\approx$ 65 min.)
Linear Modal Analysis	3 s
QSMA - Analysis A	2069 s ($\approx$ 35 min.)
QSMA - Analysis B	1009 s ($\approx$ 17 min.)
QSMA - Analysis C	1413 s ($\approx$ 24 min.)
Post-processing QSMA output	$(3 \times 4080) = 12240$ s ($\approx$ 3.4 h)
Frequency and damping computation	63 s
Total time taken	**5.75 h**

using the IGNL model. As seen in Fig. 17a, in case of negative loading, friction has a negligible effect on the frequency. In an actual cycle of vibration the system would pass through both positive and negative displacements, and the natural frequency would represent an average of both. Therefore, once can expect that the positive loading case provides a lower bound for the frequency and the negative loading case can be understood as the upper bound. Figure 17b shows the damping estimated from the negative and positive loading cases. The damping in the negative loading case up to RMS amplitude of 0.5 mm is numerical, since no slip occurs at the interfaces up to this point. Beyond 0.5 mm, the damping increases, but is less than the damping obtained from the positive loading case. Considering that the actual damping is due to the energy dissipated as the system moves through both positive and negative displacements, the true damping can be expected to lie between the two values estimated using the positive and negative loading curves.

6 Conclusions

This paper presented a novel reduced-order modeling approach to predict the amplitude-dependent frequency and damping of a system comprising geometric and friction nonlinearity. A numerical case study of an SDOF system with a cubic spring and Iwan element in parallel

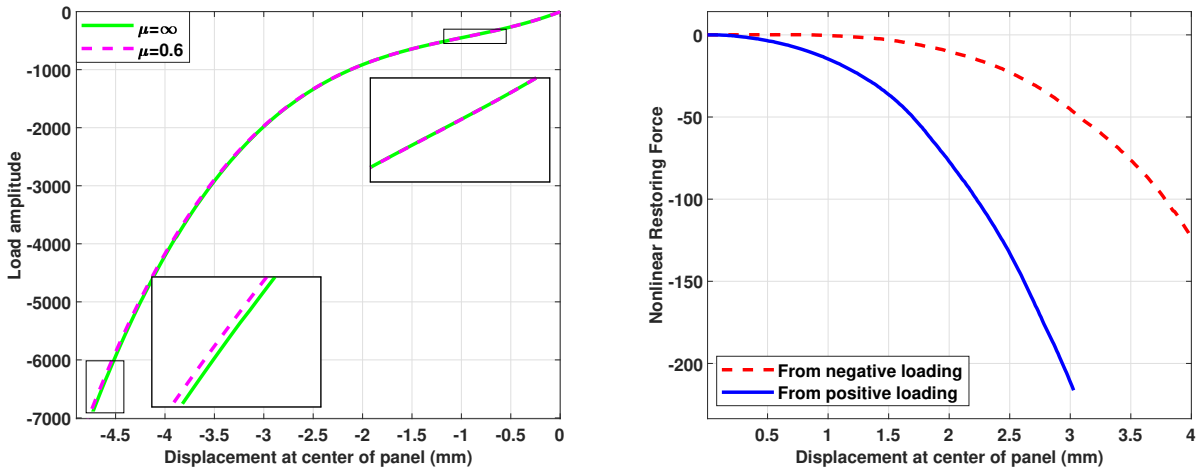

(a) (b)

Figure 16: (a) Force-displacement curve for negative loading when $\mu = \infty$ (dashed-dotted line), and when $\mu = 0.6$ (solid line); (b) Comparing the hysteretic nonlinear force from Eq. 23 obtained from the negative loading case (dashed line) and the positive loading case (solid line). Note that the dashed line is originally in the second quadrant, but the signs of the force and displacement vectors have been reversed to be able to visually compare it with the positive loading case.

was considered to test the accuracy and speed of the proposed approach. A maximum error of 2.96% in frequency and 25% in damping was observed, with the error being highest at larger amplitudes. The proposed method was found to be nearly 30 times faster than simulating the dynamic response of the system. A 2D FE model of a structure with a thin panel clamped at the ends using mechanical fasteners was considered. The paper showed how the interaction properties of the FE model can be varied to isolate the geometric and friction nonlinearities. For this 2D model, preload analysis took about 1 hour and the three quasi-static analyses that were used took about 0.5 hours each. This represents the minimum computations that could be performed to fit an IGNL model to the measurements, assuming Masing's rules are applicable. Moreover, the IGNL model can be used to speed up further simulations of the system rather than integrating high-fidelity models. However, it was observed that the hysteretic behavior of the TMD model deviated from that due to a Masing model, adding significant uncertainty to the frequency and damping predictions. Alternatively, quasi-static

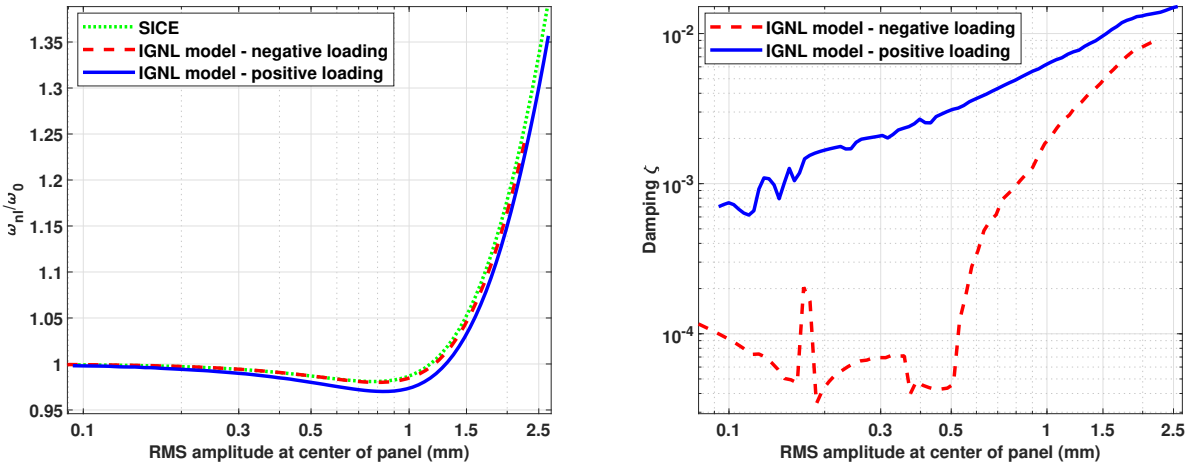

(a) (b)

Figure 17: (a) Non-dimensional frequency vs. RMS amplitude of the center of the panel, estimated from the 5^{th} order SICE (dashed-dotted line) and from the full IGNL model (solid line); (b) Damping vs. RMS amplitude estimated by applying Masing's rules to the IGNL model

simulations could have been performed for a complete cycle by applying loading, unloading and reloading forces. This would have to be repeated at each amplitude of interest to characterize the behavior without using Masing's rules. The simulation of each hysteresis loop would approximately take an additional $0.5 \times 2 = 1$ hour. Therefore, if the hysteresis loops at N number of force amplitude values are required, the additional computation time would be N hours. While this could improve the accuracy of the IGNL model, it must be noted that the model is inherently Masing in nature and wouldn't be able to capture non-Masing behavior accurately. Regardless, the proposed approach provides a range for the nonlinear frequency as well as damping by taking into account both geometric and friction nonlinearity, something that cannot be done by existing reduced-order models. In the future, other, non-Masing hysteretic models can be considered instead of the Iwan model, to further improve the accuracy and flexibility of the proposed approach.

Bibliography

[1] Singiresu S. Rao. *Mechanical Vibrations*. Prentice Hall, Upper Saddle River, N.J, 5th ed edition, 2011.

[2] S. Woinowsky-Krieger. The Effect of an Axial Force on the Vibration of Hinged Bars. *Journal of Applied Mechanics*, 17(1):35–36, April 2021.

[3] I. S. Raju, G. Venkateswara Rao, and K. Kanaka Raju. Effect of longitudinal or inplane deformation and inertia on the large amplitude flexural vibrations of slender beams and thin plates. *Journal of Sound and Vibration*, 49(3):415–422, December 1976.

[4] E. J. Richards and D. J. Mead. *Noise and Acoustic Fatigue in Aeronautics*. Chichester, United Kingdom: John Wiley & Sons Ltd, London New York Sydney Toronto, 1st edition edition, 1968.

[5] E.E. Ungar. The Status of Engineering Knowledge Concerning the Damping of Built-up Structures. *Journal of Sound and Vibration*, 26(1):141–154, 1973.

[6] Ramji Kamakoti and Wei Shyy. Fluid–structure interaction for aeroelastic applications. *Progress in Aerospace Sciences*, 40(8):535–558, November 2004.

[7] Enis T. Turgut. An Analysis of the Effect of Non-Payload Weight on Fuel Consumption for a Wide-Bodied Aircraft. *ANADOLU UNIVERSITY JOURNAL OF SCIENCE AND TECHNOLOGY A - Applied Sciences and Engineering*, 18(1):59–59, March 2017.

[8] Sin-Young Lee, Kang-Ho Ko, and Jang Moo Lee. Analysis of Dynamic Characteristics of Structural Joints Using Stiffness Influence Coefficients. *Journal of Mechanical Science and Technology*, 12(14):1319–1327, 2000.

[9] Emily A. Jewell, Matthew S. Allen, and Robert Lacayo. Predicting Damping of a Cantilever Beam With a Bolted Joint Using Quasi-Static Modal Analysis. In *Volume 8: 29th Conference on Mechanical Vibration and Noise*, page V008T12A019, Cleveland, Ohio, USA, August 2017. ASME.

[10] M. Eriten, A. A. Polycarpou, and L. A. Bergman. Physics-Based Modeling for Fretting Behavior of Nominally Flat Rough Surfaces. *International Journal of Solids and Structures*, 48(10):1436–1450, May 2011.

[11] A. Fantetti, L. R. Tamatam, M. Volvert, I. Lawal, L. Liu, L. Salles, M. R. W. Brake, C. W. Schwingshackl, and D. Nowell. The Impact of Fretting Wear on Structural Dynamics: Experiment and Simulation. *Tribology International*, 138:111–124, October 2019.

[12] Mitchell Wall, Iman Zare, and Matthew S Allen. Predicting S4 Beam Joint Nonlinearity Using Quasi-Static Modal Analysis. In *38th International Modal Analysis Conference (IMAC XXXVIII)*. Springer International Publishing, February 2020.

[13] Nidish Narayanaa Balaji, Wei Chen, and Matthew R. W. Brake. Traction-based multi-scale nonlinear dynamic modeling of bolted joints: Formulation, application, and trends in micro-scale interface evolution. *Mechanical Systems and Signal Processing*, 139:106615, May 2020.

[14] Daniel J Segalman. An Initial Overview of Iwan Modeling for Mechanical Joints. Technical Report SAND2001-0811, 780307, Sandia National Lab. (SNL-NM), Albuquerque, NM (United States), March 2001.

[15] L. Gaul and J. Lenz. Nonlinear Dynamics of Structures Assembled by Bolted Joints. *Acta Mechanica*, 125(1):169–181, 1997.

[16] D. J. Segalman. Modelling Joint Friction in Structural Dynamics. *Structural Control and Health Monitoring*, 13(1):430–453, 2006.

[17] J. Lenz and L. Gaul. The Influence of Microslip on the Dynamic Behavior of Bolted Joints. In *Proceedings of the International Modal Analysis Conference (IMAC XXIII)*, pages 248–254, Nashville, TN, 1995.

[18] David O. Smallwood, Danny Lynn Gregory, and Ronald G. Coleman. Damping Investigations of a Simplified Frictional Shear Joint. Technical Report SAND2000-1929C, Sandia National Lab. (SNL-NM), Albuquerque, NM (US);Sandia National Labs., Livermore, CA (US), 2000.

[19] Brandon J. Deaner, Matthew S. Allen, Michael J. Starr, Daniel J. Segalman, and Hartono Sumali. Application of Viscous and Iwan Modal Damping Models to Experimental Measurements From Bolted Structures. *Journal of Vibration and Acoustics*, 137(2):021012, 2015.

[20] Daniel R. Roettgen and Matthew S. Allen. Nonlinear Characterization of a Bolted, Industrial Structure Using a Modal Framework. *Mechanical Systems and Signal Processing*, 84:152 – 170, 2017.

[21] Eric E. Ungar. Energy Dissipation at Structural Joints; Mechanisms and Magnitudes:. Technical report, Defense Technical Information Center, Fort Belvoir, VA, 1964.

[22] W. D. Iwan. A Distributed-Element Model for Hysteresis and Its Steady-State Dynamic Response. *Journal of Applied Mechanics*, 33(4):893–900, December 1966.

[23] R. Bouc. A Mathematical Model for Hysteresis. *Acustica*, 21:16–25, 1971.

[24] Yi-Kwei Wen. Method for Random Vibration of Hysteretic Systems. *Journal of the Engineering Mechanics Division*, 102(2):249–263, 1976. Publisher: ASCE.

[25] Daniel Joseph Segalman. A Modal Approach to Modeling Spatially Distributed Vibration Energy Dissipation. Technical Report SAND2010-4763, 993326, Sandia National Lab., Albuquerque, NM, 2010.

[26] Robert M. Lacayo and Matthew S. Allen. Updating structural models containing nonlinear Iwan joints using quasi-static modal analysis. *Mechanical Systems and Signal Processing*, 118:133–157, March 2019.

[27] P. R. Dahl. A Solid Friction Model:. Technical report, Defense Technical Information Center, Fort Belvoir, VA, May 1968.

[28] K. C. Valanis. A Theory of Visco-Plasticity Without a Yield Surface, Part I: General Theory. *Archives of Mechanics*, 23:535, 1971. Publisher: ARCHIVES OF MECHANICS.

[29] L. Gaul and R. Nitsche. The Role of Friction in Mechanical Joints. *Applied Mechanics Reviews*, 54(2):93–106, March 2001.

[30] Allen T. Mathis, Nidish N. Balaji, Robert J. Kuether, Adam R. Brink, Matthew R. W. Brake, and D. Dane Quinn. A Review of Damping Models for Structures With Mechanical Joints1. *Applied Mechanics Reviews*, 72(4):040802, July 2020.

[31] W. D. Iwan. On a Class of Models for the Yielding Behavior of Continuous and Composite Systems. *Journal of Applied Mechanics*, 34(3):612–617, September 1967.

[32] D. Dane Quinn and Daniel J. Segalman. Using Series-Series Iwan-Type Models for Understanding Joint Dynamics. *Journal of Applied Mechanics*, 72(5):666–673, August 2004.

[33] K. Y. Sanliturk and D. J. Ewins. Modelling Two-Dimensional Friction Contact and its Application Using Harmonic Balance Method. *Journal of Sound and Vibration*, 193(2):511–523, June 1996.

[34] Y. Song, C. J. Hartwigsen, D. M. McFarland, A. F. Vakakis, and L. A. Bergman. Simulation of dynamics of beam structures with bolted joints using adjusted Iwan beam elements. *Journal of Sound and Vibration*, 273(1):249–276, May 2004.

[35] Daniel J. Segalman. A Four-Parameter Iwan Model for Lap-Type Joints. *Journal of Applied Mechanics*, 72(5), 2005.

[36] M. R. W. Brake. A Reduced Iwan Model That Includes Pinning for Bolted Joint Mechanics. *Nonlinear Dynamics*, 87(2):1335–1349, 2017.

[37] Marc P. Mignolet, Pengchao Song, and X. Q. Wang. A Stochastic Iwan-Type Model for Joint Behavior Variability Modeling. *Journal of Sound and Vibration*, 349:289–298, August 2015.

[38] Robert M. Lacayo and Matthew S. Allen. Towards an Understanding of the Transient Behavior of the Five-Parameter Iwan-Type Model. In Gaetan Kerschen, Matthew R.W. Brake, and Ludovic Renson, editors, *Nonlinear Structures & Systems, Volume 1*, Conference Proceedings of the Society for Experimental Mechanics Series, pages 117–120, Cham, 2021. Springer International Publishing.

[39] Yikun Li and Zhiming Hao. A Six-Parameter Iwan Model and Its Application. *Mechanical Systems and Signal Processing*, 68-69:354–365, February 2016.

[40] Nathan M. Newmark. A Method of Computation for Structural Dynamics. *Journal of the Engineering Mechanics Division*, 85(3):67–94, July 1959. Publisher: American Society of Civil Engineers.

[41] Hans M. Hilber and Thomas J. R. Hughes. Collocation, dissipation and [overshoot] for time integration schemes in structural dynamics. *Earthquake Engineering & Structural Dynamics*, 6(1):99–117, 1978. _eprint: https://onlinelibrary.wiley.com/doi/pdf/10.1002/eqe.4290060111.

[42] J. Crank and P. Nicolson. A practical method for numerical evaluation of solutions of partial differential equations of the heat-conduction type. *Advances in Computational Mathematics*, 6(1):207–226, December 1996.

[43] J. Chung and G. M. Hulbert. A Time Integration Algorithm for Structural Dynamics With Improved Numerical Dissipation: The Generalized- Method. *Journal of Applied Mechanics*, 60(2):371–375, June 1993.

[44] Robert D. Cook, David S. Malkus, Michael E. Plesha, and Robert J. Witt. *Concepts and Applications of Finite Element Analysis*. John Wiley & Sons, New York, 2007.

[45] A. E. Charalampakis and V. K. Koumousis. On the response and dissipated energy of Bouc–Wen hysteretic model. *Journal of Sound and Vibration*, 309(3):887–895, January 2008.

[46] T. S. Low and W. Guo. Modeling of a Three-Layer Piezoelectric Bimorph Beam with Hysteresis. *Journal of Microelectromechanical Systems*, 4(4):230–237, December 1995. Conference Name: Journal of Microelectromechanical Systems.

[47] H. Yoshioka, J. C. Ramallo, and B. F. Spencer. "Smart" Base Isolation Strategies Employing Magnetorheological Dampers. *Journal of Engineering Mechanics*, 128(5):540–551, May 2002. Publisher: American Society of Civil Engineers.

[48] Greg C. Foliente. Hysteresis Modeling of Wood Joints and Structural Systems. *Journal of Structural Engineering*, 121(6):1013–1022, June 1995. Publisher: American Society of Civil Engineers.

[49] Kejian Guo, Xingang Zhang, Hongguang Li, Hongxing Hua, and Guang Meng. A New Dynamical Friction Model. *International Journal of Modern Physics B*, 22(08):967–980, March 2008. Publisher: World Scientific Publishing Co.

[50] Fayçal Ikhouane, Víctor Mañosa, and José Rodellar. Dynamic properties of the hysteretic Bouc-Wen model. *Systems & Control Letters*, 56(3):197–205, March 2007.

[51] Fayçal Ikhouane, Jorge E. Hurtado, and José Rodellar. Variation of the Hysteresis Loop with the Bouc–Wen Model Parameters. *Nonlinear Dynamics*, 48(4):361–380, March 2007.

[52] Xudong Zhu and Xilin Lu. Parametric Identification of Bouc-Wen Model and Its Application in Mild Steel Damper Modeling. *Procedia Engineering*, 14:318–324, 2011.

[53] David A. Najera-Flores and Robert J. Kuether. A Study of Whole Joint Model Calibration Using Quasi-Static Modal Analysis. *Journal of Vibration and Acoustics*, 142(5), June 2020.

[54] Melih Eriten, Mehmet Kurt, Guanyang Luo, D. Michael McFarland, Lawrence A. Bergman, and Alexander F. Vakakis. Nonlinear system identification of frictional effects in a beam with a bolted joint connection. *Mechanical Systems and Signal Processing*, 39(1):245–264, August 2013.

[55] Benjamin J. Moldenhauer, Aabhas Singh, Phil Thoenen, Daniel R. Roettgen, Benjamin R. Pacini, Robert J. Kuether, and Matthew S. Allen. Influences of Modal Coupling on Experimentally Extracted Nonlinear Modal Models. In Gaetan Kerschen, M. R. W. Brake, and Ludovic Renson, editors, *Nonlinear Structures and Systems, Volume 1*, Conference Proceedings of the Society for Experimental Mechanics Series, pages 189–204, Cham, 2020. Springer International Publishing.

[56] Mitchell Wall, Matthew S. Allen, and Robert J. Kuether. Observations of modal coupling due to bolted joints in an experimental benchmark structure. *Mechanical Systems and Signal Processing*, 162:107968, January 2022.

[57] Robert M. Lacayo, Brandon J. Deaner, and Matthew S. Allen. A Numerical Study on the Limitations of Modal Iwan Models for Impulsive Excitations. *Journal of Sound and Vibration*, 390:118–140, 2017.

[58] Hugo Festjens, Gaël Chevallier, and Jean-luc Dion. A Numerical Tool for the Design of Assembled Structures Under Dynamic Loads. *International Journal of Mechanical Sciences*, 75:170–177, October 2013.

[59] Emily Jewell, Matthew S. Allen, Iman Zare, and Mitchell Wall. Application of quasi-static modal analysis to a finite element model and experimental correlation. *Journal of Sound and Vibration*, 479:115376, August 2020.

[60] Iman Zare and Matthew S. Allen. Adapting a Contact-Mechanics Algorithm to Predict Damping in Bolted Joints Using Quasi-Static Modal Analysis. *International Journal of Mechanical Sciences*, 189:105982, January 2021.

[61] Kyusic Park and Matthew S. Allen. Quasi-Static Modal Analysis for Reduced Order Modeling of Geometrically Nonlinear Structures. *Journal of Sound and Vibration*, 502:116076, June 2021.

[62] Nidish Narayanaa Balaji and Matthew R. W. Brake. A quasi-static non-linear modal analysis procedure extending Rayleigh quotient stationarity for non-conservative dynamical systems. *Computers & Structures*, 230:106184, April 2020.

[63] D. J. Segalman and C. R. Dohrmann. A Method for Calculating the Dynamics of Rotating Flexible Structures, Part 1: Derivation. *Journal of Vibration and Acoustics*, 118(3):313–317, July 1996.

[64] Marc P. Mignolet, Adam Przekop, Stephen A. Rizzi, and S. Michael Spottswood. A review of indirect/non-intrusive reduced order modeling of nonlinear geometric structures. *Journal of Sound and Vibration*, 332(10):2437–2460, May 2013.

[65] Robert J. Kuether, Brandon J. Deaner, Joseph J. Hollkamp, and Matthew S. Allen. Evaluation of Geometrically Nonlinear Reduced-Order Models with Nonlinear Normal Modes. *AIAA Journal*, 53(11):3273–3285, November 2015.

[66] Alexander A Muravyov and Stephen A Rizzi. Determination of nonlinear stiffness with application to random vibration of geometrically nonlinear structures. *Computers & Structures*, 81(15):1513–1523, July 2003.

[67] M. I. Mcewan, J. R. Wright, J. E. Cooper, and A. Y. T. Leung. A Combined Modal/Finite Element Analysis Technique for the Dynamic Response of a Non-Linear Beam to Harmonic Excitation. *Journal of Sound and Vibration*, 243(4):601–624, June 2001.

[68] Joseph J. Hollkamp and Robert W. Gordon. Reduced-Order Models for Nonlinear Response Prediction: Implicit Condensation and Expansion. *Journal of Sound and Vibration*, 318(4):1139–1153, December 2008.

[69] R. M. Rosenberg. Normal Modes of Nonlinear Dual-Mode Systems. *Journal of Applied Mechanics*, 27(2):263–268, June 1960.

[70] M. Peeters, G. Kerschen, and J. C. Golinval. Dynamic testing of nonlinear vibrating structures using nonlinear normal modes. *Journal of Sound and Vibration*, 330(3):486–509, January 2011.

[71] Jean-Philippe Noël, L. Renson, C. Grappasonni, and G. Kerschen. Identification of nonlinear normal modes of engineering structures under broadband forcing. *Mechanical Systems and Signal Processing*, 74:95–110, June 2016.

[72] M. Peeters, R. Viguié, G. Sérandour, G. Kerschen, and J. C. Golinval. Nonlinear Normal Modes, Part II: Toward a Practical Computation Using Numerical Continuation Techniques. *Mechanical Systems and Signal Processing*, 23(1):195–216, January 2009.

[73] Aabhas Singh, Matthew Allen, and Robert Kuether. Multi-mode Quasi-static Excitation for Systems with Nonlinear Joints. In *Proposed for presentation at the International Modal Analysis Conference (IMAC) XXXIX held February 8-11, 2021 in Orlando, FL, US.* US DOE, December 2020.

[74] Ali H. Nayfeh. *Introduction to Perturbation Techniques*. John Wiley & Sons, New York, 2011.

[75] Hartono Sumali and Rick A. Kellogg. Calculating Damping from Ring-Down Using Hilbert Transform and Curve Fitting. Technical Report SAND2011-1960C, Sandia National Lab., Albuquerque, NM, 2011.

[76] Malte Krack, Lars Panning-von Scheidt, and Jörg Wallaschek. On the computation of the slow dynamics of nonlinear modes of mechanical systems. *Mechanical Systems and Signal Processing*, 42(1-2):71–87, 2014.

[77] Nicoli M. Ames, James P. Lauffer, Michael D. Jew, Daniel Joseph Segalman, Danny Lynn Gregory, Michael James Starr, and Brian Ray Resor. Handbook on dynamics of jointed structures. Technical Report SAND2009-4164, 1028891, Sandia National Lab., Albuquerque, NM, 2009.

[78] Alexander H. Haslam, Gaurav Chauda, Nalik Kenia, Esther S. Rufat-Meix, Matthew S. Allen, Robert M. Lacayo, Malte Krack, and Matthew R. W. Brake. Nonlinear System Identification for Joints Including Modal Interactions. In Gaetan Kerschen, editor, *Nonlinear Dynamics, Volume 1*, Conference Proceedings of the Society for Experimental Mechanics Series, pages 79–99, Cham, 2019. Springer International Publishing.

[79] Walter C. Hurty. Dynamic analysis of structural systems using component modes. *AIAA Journal*, 3(4):678–685, 1965.

[80] Roy R Craig and Mervyn C C Bampton. Coupling of Substructures for Dynamic Analyses. *AIAA Journal*, 6(7):1313–1319, 1968.

[81] J Ginsberg. *Mechanical and Structural Vibrations: Theory and Applications*. John Wiley and Sons, Inc., New York, NY, 2001.

[82] L. E. Goodman. Contributions of continuum mechanics to the analysis of the sliding of unlubricated solids. In *AMD Symposium Series of the ASME Applied Mechanics Division*, volume 39, pages 1–12, 1980.

[83] Drithi Shetty and Matthew Allen. Fast Simulation of a Single Degree-of-Freedom System Consisting of An Iwan Element Using the Method of Averaging. *Journal of Vibration and Acoustics*, 142(5):051107, October 2020.

[84] Mohammed Ismail, Fayçal Ikhouane, and José Rodellar. The Hysteresis Bouc-Wen Model, a Survey. *Archives of Computational Methods in Engineering*, 16(2):161–188, June 2009.

[85] Matthew Oldfield, Huajiang Ouyang, and John E. Mottershead. Simplified Models of Bolted Joints Under Harmonic Loading. *Computers & Structures*, 84(1):25–33, December 2005.

[86] Matthew S. Allen, Joe Schoneman, Wesley Scott, and Joel Sills. Application of Quasi-Static Modal Analysis to an Orion Multi-Purpose Crew Vehicle Test. In Chad Walber, Patrick Walter, and Steve Seidlitz, editors, *Sensors and Instrumentation, Aircraft/Aerospace, Energy Harvesting & Dynamic Environments Testing, Volume 7*, Conference Proceedings of the Society for Experimental Mechanics Series, pages 65–75, Cham, 2021. Springer International Publishing.

[87] Matthew R. W. Brake. *The mechanics of jointed structures*. Springer Science+Business Media, New York, NY, 2017.

[88] Paramsothy Jayakumar. *Modeling and identification in structural dynamics*. Report or Paper, California Institute of Technology, Pasadena, CA, May 1987. Issue: 87-01 Number: 87-01 Publisher: California Institute of Technology.

[89] Michael Feldman. Non-Linear System Vibration Analysis Using Hilbert Transform–I. Free Vibration Analysis Method 'Freevib'. *Mechanical Systems and Signal Processing*, 8(2):119–127, March 1994.

[90] G M Jenkins. Analysis of the stress-strain relationships in reactor grade graphite. *British Journal of Applied Physics*, 13(1):30–32, January 1962.

[91] G Masing. Self-stretching and hardening for brass. In *Proceedings of the 2nd International Congress for Applied Mechanics*, pages 332–335, Zurich, Switzerland, 1926.

[92] Daniel J. Segalman and Michael J. Starr. Inversion of Masing models via continuous Iwan systems. *International Journal of Non-Linear Mechanics*, 43(1):74–80, January 2008.

[93] Benjamin Moldenhauer, Aabhas Singh, Matthew Allen, and Daniel Roettgen. Extensions to a method for characterizing instantaneous frequency and damping of nonlinear systems. In *Proceedings of the Society for Experimental Mechanics Series*, Orlando, Florida, 2021.

[94] Adam R. Brink, Robert J. Kuether, Matthew D. Fronk, Bryan L. Witt, and Brendan L. Nation. Contact Stress and Linearized Modal Predictions of As-Built Preloaded Assembly. *Journal of Vibration and Acoustics*, 142(5), May 2020.

[95] T. Dreher, M. R. W. Brake, B. Seeger, and M. Krack. In situ, real-time measurements of contact pressure internal to jointed interfaces during dynamic excitation of an as-

sembled structure. *Mechanical Systems and Signal Processing*, 160:107859, November 2021.

[96] Robert J. Kuether, David A. Najera, Jonel Ortiz, Moheimin Y. Khan, and Paul R. Miles. 2021 Tribomechadynamics Research Challenge: Sandia National Laboratories High-Fidelity FEA Approach, February 2022. presented at 40th International Modal Analysis Conference (IMAC-XL).

[97] Malte Krack, Christoph Schwingshackl, and Matthew R Brake. The Tribomechadynamics Research Challenge. In *40th International Modal Analysis Conference (IMAC-XL)*, page 3, February 2022.

[98] G. Kerschen, M. Peeters, J. C. Golinval, and A. F. Vakakis. Nonlinear Normal Modes, Part I: A Useful Framework for the Structural Dynamicist. *Mechanical Systems and Signal Processing*, 23(1):170–194, January 2009.

[99] Michael Lengger and Kai Willner. Application of Quasi-Static Modal Analysis to the Tribomechadynamics Benchmark System, July 2021. presented at Tribomechadynamcis Research Conference.

[100] Malte Krack and Johann Gross. *Harmonic Balance for Nonlinear Vibration Problems*. Mathematical Engineering. Springer International Publishing, Cham, 2019.

[101] Drithi Shetty, Kyusic Park, Courtney Payne, and Matthew S. Allen. Predicting Nonlinearity in the TMD Benchmark Structure Using QSMA and SICE. In *Nonlinear Structures & Systems, Volume 1*, pages 281–287, Cham, February 2022. Springer International Publishing. Series Title: Conference Proceedings of the Society for Experimental Mechanics Series.

[102] E. Riks. An incremental approach to the solution of snapping and buckling problems. *International Journal of Solids and Structures*, 15(7):529–551, January 1979.